1-1-2003

The age, stratigraphy, and tectonic provenance of clastic deposits in the western Bikou terrane, southwestern Qinling Mountains, China

Peter Alexander Druschke
University of Nevada, Las Vegas

THE AGE, STRATIGRAPHY, AND TECTONIC PROVENANCE OF CLASTIC DEPOSITS IN THE WESTERN BIKOU TERRANE, SOUTHWESTERN QINLING MOUNTAINS, CHINA

by

Peter Alexander Druschke

Bachelor of Science
Sonoma State University,
1999

A thesis submitted in partial fulfillment
of the requirements for

Master of Science Degree
Geoscience Department
College of Sciences

Graduate College
University of Nevada, Las Vegas
December, 2003

UNLV

Thesis Approval

The Graduate College
University of Nevada, Las Vegas

September 19, 2003

The Thesis prepared by

Peter A. Druschke

Entitled

The Age, Stratigraphy, and Tectonic Provenance of Clastic Deposits in the Western Bikou Terrane, Southwestern Qinling Mountains, China

is approved in partial fulfillment of the requirements for the degree of

Master of Science in Geoscience

Examination Committee Chair

Dean of the Graduate College

Examination Committee Member

Examination Committee Member

Graduate College Faculty Representative

1017-53

ABSTRACT

The Age, Stratigraphy, and Tectonic Provenance of Clastic Deposits in the Western Bikou Terrane, Southwestern Qinling Mountains China

by

Peter Alexander Druschke

Dr. Andrew Hanson, Examination Committee Chair
Associate Professor of Geology
University of Nevada, Las Vegas

The Qinling Mountains of central China are the product of Late Paleozoic to Triassic collision between the North China Plate and the South China Plate. Located within the southwestern Qinling Mountains is the Bikou terrane, a low grade metamorphic assemblage of igneous and clastic sedimentary rocks located adjacent to the northern margin of the South China Plate. The age and tectonic setting of clastic deposits within the Bikou terrane have long been controversial, with age estimates ranging from Lower Proterozoic to Late Paleozoic, and tectonic provenance theories ranging from subduction arc to continental rift.

The southeastern portion of the Bikou terrane is composed of a metamorphosed volcanic arc with minor marine volcaniclastic sediments, known as the Bikou Group, previously dated by SHRIMP U-Pb zircon and conventional U-Pb as Late Proterozoic in age (approximately 845 to 760 Ma). Separated by a NE/SW striking fault, the

northwestern Bikou terrane consists of a turbidite dominated sedimentary basin known as the Hengdan Group.

The Hengdan basin comprises a 10 to 15 km thick succession of coarsening upward, volcaniclastic sand-rich submarine fan deposits. Paleocurrent data obtained during this study from deposits within the Hengdan Group indicate a south to north transport direction (i.e., from the direction of the Bikou arc). In order to provide stronger correlatetion between the Hengdan Group and the Bikou Group, SHRIMP U-Pb analyses of detrital zircon recovered from tuffaceous sandstone in the Hengdan Group was performed. Results indicate a provenance age range of roughly 845 to 705 Ma. The Bikou-arc overlapping age distribution and paleocurrent data suggest that the Bikou arc was the primary source for volcaniclastic deposits within the Hengdan basin. The detrital zircon data also suggest that the Bikou volcanic arc was active for an approximate 140 m.y. interval, nearly double the duration previously recognized.

Comparison of the Hengdan basin with a number of well-known forearc basins and rift to drift successions disfavors continental rift provenance interpretations. The voluminous thickness of immature, volcaniclastic deposits, and the coarsening upward sedimentary trend within the Hengdan Group is characteristic of forearc sedimentation. Similarly, the detrital zircon population within the Hengdan Group is characterized by short transport, arc derived, single-cycle zircons, also indicating a probable forearc basin setting. These new data contradict theories that South China occupied an intra-cratonic setting within the supercontinent Rodinia during 850-700 Ma. Instead, it supports an alternate theory that the northern and western margins of the South China Plate composed a continent-ocean subduction system in the Late Proterozoic.

TABLE OF CONTENTS

LIST OF FIGURES

ACKNOWLEDGEMENTS

I would like to thank the members of my committee, Drs. Andrew Hanson, Wanda Taylor, Terry Spell and Helen Neill for their support and guidance, as well as Drs. Yan Quanren and Wang Zongqi of the Chinese Academy of Geological Sciences. Special thanks to Weiquan Dong for help in translating key papers from Chinese, and Joe Kula for his assistance in processing SHRIMP data. Thanks also to Dr. Joe Wooden of the Stanford/USGS SHRIMP Laboratory for advice and helpful discussions, as well as my friends, family, and colleagues at the University of Nevada Las Vegas. This project has received generous financial support from the Geological Society of America Student Grant Foundation, the UNLV Bernada French Scholarship Fund, as well as a New Investigator Award and SITE Grants administered by UNLV awarded to Dr. Andrew Hanson, and a University of Nevada International Studies Travel Grant. Additional travel and living expenses were covered by a Chinese National Science Foundation grant awarded to Dr. Yan Quanren of the Chinese Academy of Geological Sciences.

CHAPTER 1

INTRODUCTION

The Qinling Mountain belt of central China represents the Middle Paleozoic to Triassic collisional suturing of the North China Block and South China Block (Fig. 1), which together form the cratonic nucleus of East Asia (Zhang et al., 1984). The Qinling Mountains contain evidence of a long and complex collisional history, including island arc and possible micro-plate accretion, multiple subduction complexes, multiple metamorphic events, and both thin-and thick-skinned thrusting (Zhai et al., 1998). Much research has been conducted in recent years on the formation of ultra-high pressure metamorphic rocks within the eastern Qinling (Dabie) Mountains during the Mesozoic (Xu et al., 1992; Ames et al., 1993, 1996; Hacker et al., 1995, 2000; Rowley et al., 1997; Webb et al., 1999; Ratschbacher et al., 2000; Grimmer et al., 2002; Oberhansli et al., 2002) but the earlier pre-Mesozoic tectonic history recorded in the geology of the Qinling Mountains is still poorly understood.

The Qinling Mountains and the adjacent North and South China cratons also record evidence of a complex Precambrian history, including possible arc magmatism, rifting, and formation of passive continental margins persisting from the Late Proterozoic through the Early Paleozoic. Precambrian arc volcanism and volcaniclastic basin formation along the north margin of the South China Block (Yangtze craton) have been

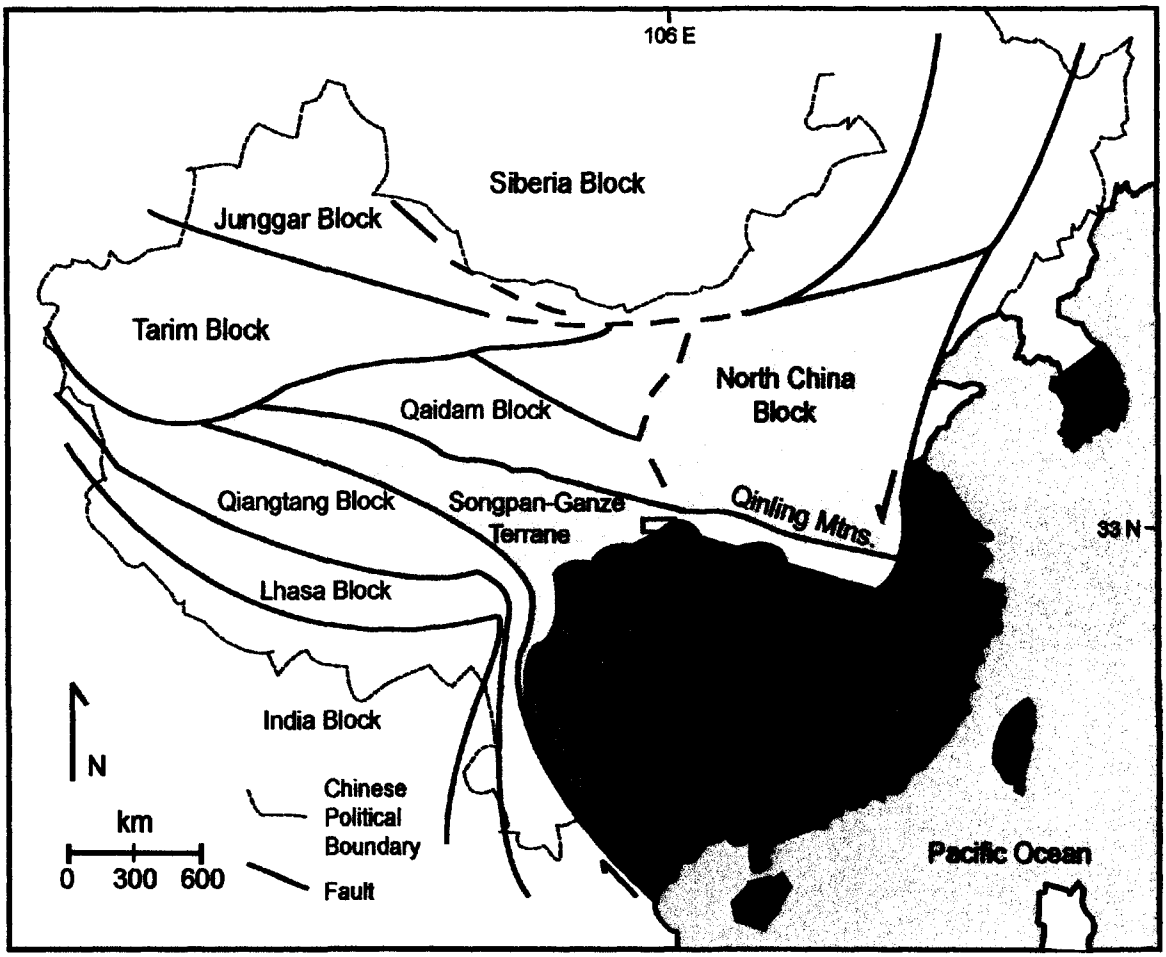

Figure 1. Plate tectonic map of China, highlighting the North and South China Blocks, the Qinling orogen, and the Songpan-Ganze terrane (modified from Watson et al., 1987).

interpreted to record a prior suturing and breakup of Rodinia during the Middle to Late Proterozoic (Li et al., 1995, 1999, 2002; Li, 1999). Others have interpreted these same volcano-sedimentary complexes to represent a continental subduction setting during the same time interval (Gao et al., 1990; Zhou et al., 2002a, 2002b; Yan et al., 2003).

Xia and others (1996a) have interpreted the Precambrian rifting of South China and collision with North China in the Late Paleozoic to Mesozoic to represent a Precambrian to Mesozoic Wilson Cycle. However, significant debate continues about the age of

volcanism and basin formation, as well as pre-Mesozoic plate reconstructions for much of East Asia based on geological correlations and paleomagnetism. Unraveling the Precambrian history of the Qinling Mountains has been hampered by problems with geochronological control and conflicting tectonic interpretations (Yan, pers. comm., 2002).

Located in the southwestern Qinling Mountain belt near the junction of Sichuan, Shaanxi and Gansu Provinces is the Bikou terrane, a discrete, fault-bounded block comprising a complex of meta-volcanic and meta-sedimentary rocks (Fig. 2). Although controversy exists as to the exact age and tectonic setting of the Bikou terrane, it is widely believed to represent a Meso/Neoproterozoic arc complex situated on or adjacent to the northern margin of the South China Plate. Interpretations of the tectonic setting of the Bikou terrane have included an island arc or continental arc relating to the Middle to Late Proterozoic collision of the North and South China Plates (Pei, 1989; Tao, 1993; Qin et al., 1994; Wei, 1995), and/or their Late Proterozoic rifting (Xia et al., 1996b; Qiang, 1999). The Bikou terrane has also been interpreted to represent a micro-plate that accreted to the South China Plate during the Paleozoic (Xia et al., 1996b; Yin and Huang, 1996)

A fault-bounded subunit of the Bikou terrane, the Hengdan Group, is a thick volcaniclastic turbidite succession metamorphosed to lower greenschist facies (Wei, 1995) that composes the northwestern half of the Bikou Terrane. The Hengdan Group has been generally regarded as contemporaneous in age and closely associated with the meta-volcanic sequence of the Bikou Group, although workers support differing conclusions as to whether the Hengdan Group represents a forearc (Pei, 1992; Qin et al.,

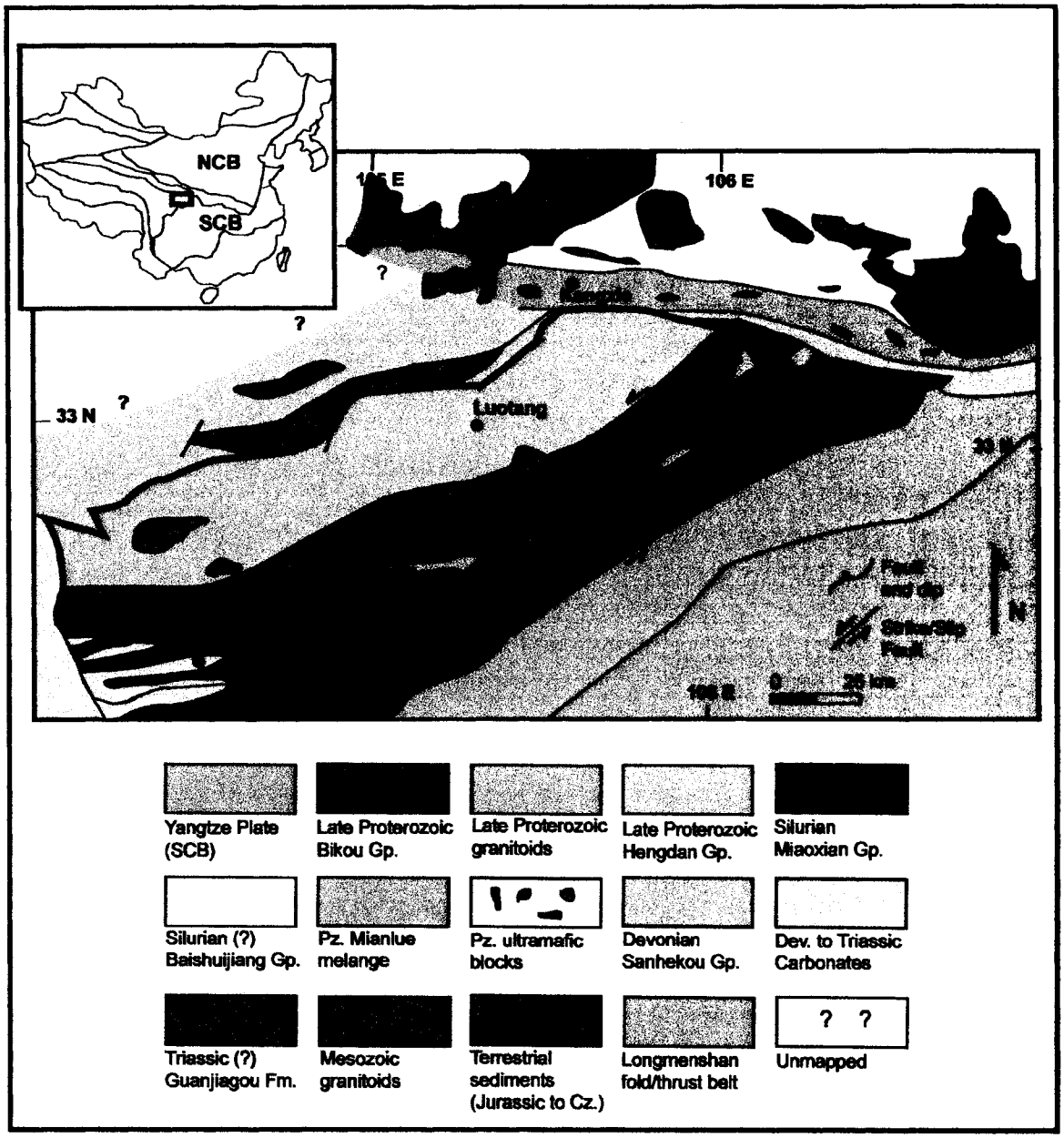

Figure 2. Geologic map of the Bikou terrane (outlined in bold) and vicinity (modified from Yan and others, 2002).

1992, 1994; Tao, 1993; Yan et al., 2002) or rift basin setting (Lu et al., 1996, 1997; Xia et al., 1996a; Qiang, 1999). Lu and others (1996, 1997) have inferred through stratigraphic correlation with nearby recognized Paleozoic units that the Hengdan Group is actually

Silurian to Devonian in age or younger. No dating of volcanic rocks within the Hengdan Group had been previously performed, although dates of metamorphosed volcanic units in the Bikou Group by K-Ar, conventional zircon U-Pb, and Rb-Sr systems indicated a wide spread of Middle to Late Proterozoic ages (Pei, 1989; Qin et al., 1992; Tao, 1993; Wei, 1995).

Bounding the northern margin of the Bikou terrane is the Mianlue mélange, which is a recently recognized Late Paleozoic accretionary complex (Xu et al., 1994). Within the western Qinling Mountains, the Mianlue mélange is generally regarded as the boundary between the North and South China Plates (Meng and Zhang, 1999, 2000). The complex includes greenschist facies metamorphic rocks, MORB blocks (Li et al., 1996, Xu et al., 1998), and sedimentary blocks containing Early Carboniferous age fossils (Feng et al., 1996).

Given the poor age control, and the fact that other presumed Precambrian terranes within the Qinling Mountains have recently been shown to be much younger (Ames et al., 1993; Lerch et al., 1995; Zhai et al; 1998), Druschke et al., (2002), Hanson et al., (2002), and Yan et al., (2002), proposed a model for the southwest Qinling Mountains that speculated on a possible Paleozoic tectonic history for the Bikou terrane. To further test this hypothesis, ion microprobe dating of reworked tuff in the Hengdan Group and volcanic rock of the Bikou Group was performed as part of this study to better constrain the tectonic history of the region. Our previous research had tested the hypothesis that the Mianlue mélange, Hengdan basin, and Bikou arc together composed a Late Paleozoic to Early Mesozoic convergent margin built upon the north margin of the South China

Plate, related to the Late Paleozoic to Triassic collision of the North and South China Plates (Druschke et al., 2002; Hanson et al., 2002; Yan et al., 2002).

However, given the possible Proterozoic age of the Bikou terrane, and position at the northern margin of the South China Plate, understanding the tectonic history of the Bikou terrane could also prove important for reconstructing the Precambrian history of South China. Recently, a number of new theories have been advanced concerning the position of the South China micro-plate with respect to the super-continent Rodinia. One such theory proposes that South China may in fact be the "missing link" between Australia and Laurentia (Fig. 3), by correlating possible rift related volcanism across Australia and South China at 750 Ma (Li et al., 1995, 1999). A new Neoproterozoic (ca 750 Ma) paleomagnetic pole for South China produced by Evans and others (2000) suggests that the "missing link" theory is plausible. However, other paleomagnetic studies conflict with this conclusion (Zhang and Piper, 1997; Piper, 2000). It is therefore crucial to understand the age and tectonic setting of deposits along the northern margin of South China in order to evaluate Rodinia reconstructions with conflicting positions for South China.

At the heart of this problem lie a number of volcanic arc/volcaniclastic basin terranes, including the Bikou terrane, situated along the northern and western margin of the South China Plate. Recent ion probe dating has revealed that many of these terranes share overlapping Late Proterozoic ages (ca. 850-720 Ma) (Gao et al., 1996; Li et al., 1999; Zhou et al., 2002a, 2002b; Yan, pers. comm.). However, there is still considerable debate as to whether these terranes represent convergent or divergent margins, thus complicating efforts to evaluate the South China Plate's position relative to the supercontinent Rodinia.

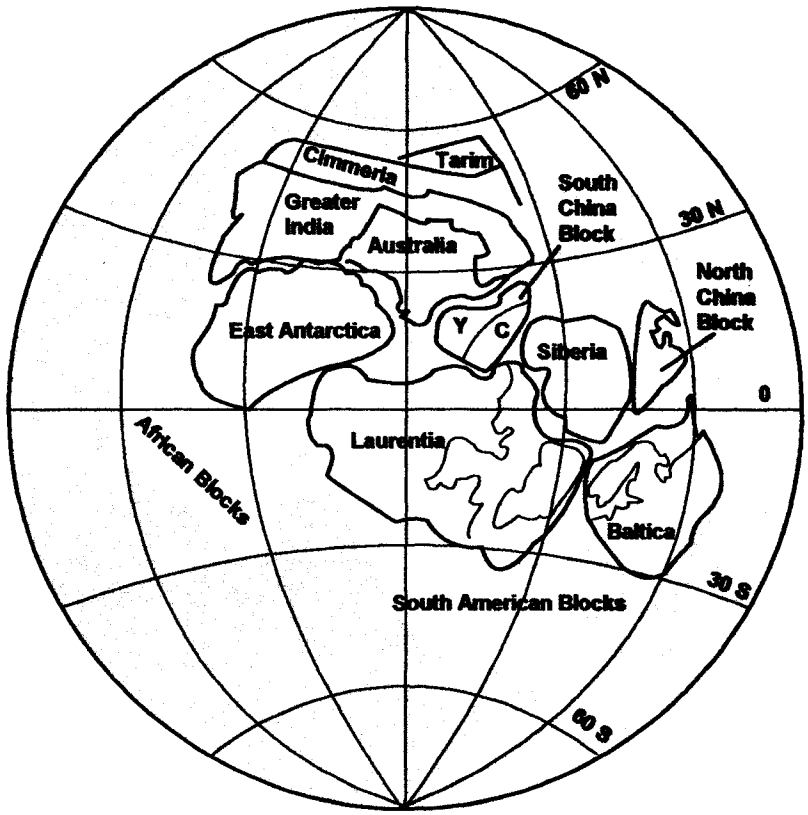

Figure 3. Plate reconstruction for Rodinia circa 800 Ma illustrating the "missing-link" position for South China (from Li et al., 1999).

This study addresses the disparate hypotheses of age and tectonic setting of the Bikou terrane. Recent tectonic provenance studies have paid little attention to voluminous volcaniclastic deposits contained within the Hengdan Group or within the Bikou Group itself, although recent sedimentological studies have likewise revealed evidence used to argue both rift and arc related provenance. Lacking however from many recent studies focusing on the tectonic setting of the Bikou terrane has been a detailed comparison of the basin stratigraphy and related volcanic assemblages to proto-oceanic rift troughs such as the Red Sea, well-studied rift to drift sequences along the Atlantic margin, or

numerous well-studied forearc basin systems throughout the world. Such comparison is essential for correctly deducing tectonic provenance.

The focus of this study was to provide a detailed description of the basin-scale stratigraphy of the Hengdan Group, and to evaluate rift and forearc hypotheses based on comparison with modern and ancient analogs. This study also provides new age control by applying detrital U-Pb zircon microprobe dating on volcaniclastic units within the Hengdan Group. As no previous dating of the Hengdan Group had been performed, geochronology is essential for testing the hypothesis that the Bikou Group and Hengdan Group are genetically and temporally related. By establishing a correlation between the Bikou and Hengdan Groups, and determining the tectonic provenance of the Hengdan basin, this study attempts to create a new perspective and new method for testing tectonic provenance theories for the Bikou terrane. The recognition of the plate tectonic provenance of the Bikou terrane may then be used to evaluate reconstructions and tectonic models for South China.

CHAPTER 2

BACKGROUND AND PREVIOUS WORK

Regional Overview: The Qinling Mountains

The Qinling belt is a prominent east-west trending mountain range that occupies a central location within eastern and central China, geographically dividing the Yellow River plains of northern China from the Sichuan basin and Yangtze River plains to the south. Arising near the eastern coast of China, the Qinling Mountains stretch nearly 800 km toward the northeastern corner of the Tibetan Plateau, and are on average approximately 150 km wide in north/south extent. Continuing westward along the northern edge of the Tibetan Plateau, the Kunlun and Qilian Mountains form a cogenetic extension of the Qinling Mountains, which together compose a nearly 2,000 km long orogenic belt (Sun et al., 2000). Geologically, the Qinling Mountains have been divided into four distinct tectonic subdivisions. They are: (1) Precambrian basement of the North and South China Plates, frequently involved in thick-skinned thrusting or basement uplift structures; (2) the Qinling metamorphic complex consisting mainly of multi-phase metamorphosed arc related rocks of Ordovician to Triassic age; (3) marginal basins comprised largely of thrust and fold belt deformed flysch, and; (4) folded and uplifted Jurassic and younger foreland deposits (Hsu et al., 1987).

Today, the Qinling Mountains are generally recognized to be the product of inter-continental collision, brought on by the closure of the Paleo-Tethys Ocean during the Mesozoic (Sengor, 1985; Hsu et al., 1987). The Qinling Mountains however display a long and complex history, recording not only the Paleozoic to Triassic collision of North and South China, but also ensuing regional collisions which have built east Asia, culminating with the India-Asia collision which continues to this day (Zhang et al., 1984, 1989; Webb et al., 1999; Ratschbacher et al., 2000).

The Late Paleozoic through Triassic Qinling Orogeny

In the eastern portion of the Qinling Mountains (Dabie sub-range) lies a suite of ultra-high pressure metamorphic rocks including micro-diamond and coesite bearing eclogites. This assemblage is believed to have formed during the collision of the North and South China micro-plates, and partial subduction of the South China plate to a depth of 120 km (Xu et al., 1992). This collision was subsequently dated as Lower Triassic by U-Pb dating of zircon within the ultra-high pressure belt (Ames et al., 1993, 1996). Paleomagnetic studies previously carried out by Zhao and Coe (1987) also indicated that North and South China collided during the Triassic, and that the South China Plate underwent an approximate 70-degree clockwise rotation prior to final suturing.

Nie and others (1994), inferred that the original mountain belt produced during this collision would have rivaled the modern Himalayas in height, and up to 4 to 6 million km^3 of material was unroofed following collision to expose the crustal levels seen within the eastern Qinling today. The sediment thus produced was largely shed westward, filling the Songpan-Ganze basin southwest of the central Qinling Mountains, with

Triassic turbidite deposits up to 15 km thick. Zhou and Graham (1996) further interpreted that the diachronous east to west closure implied by the paleomagnetic data (Zhao and Coe, 1987) allowed for sediment unroofed from the eastern Qinling to be transported westward and accumulate on a trapped sliver of oceanic crust within the closing paleo-Tethyan sea-way, which they dubbed a "remnant ocean basin." Detrital zircon studies have shown a large Proterozoic aged zircon component in the Songpan-Ganze flysch, which has been interpreted as having a South China Plate provenance (Bruguier et al., 1997).

Debate continues, however, upon the exact timing of the North/South China collision, with theories calling for either Late Paleozoic (Devonian or Carboniferous) or Triassic collision. Evidence exists of an Ordovician to Silurian island arc along the south margin of the North China Plate displaying southward subduction and Devonian metamorphic overprinting, leading to the theory that the North and South China Plate collision occurred by the Carboniferous (Lerch et al., 1995). A model based on this hypothesis holds that Triassic metamorphism within the Qinling Mountains resulted from renewed deformation after the initial collision of the North and South China Plates (Xue et al., 1996), possibly due to the collision of the Southeast Asian micro-plate with South China.

Similarly, a study of the rare-earth element signatures of Paleozoic clastic strata contained within the Qinling Mountains reveal sediment source area changes during the Silurian-Devonian (Gao et al., 1995). Fossil evidence of rapid faunal shifts during the same interval also occurred, implying close proximity or connection between North and South China at that time (Yin and Huang, 1996). Isotopic Pb analyses of over 30 granitoid intrusions ranging from Neoproterozoic to Devonian in age on the North and

South China Blocks revealed that although the isotopic signature of North and South China granitoids was distinctly different prior to the Devonian, homogeneity following the Devonian suggests Paleozoic suturing (Zhang et al., 1997). U-Pb and $^{40}Ar/^{39}Ar$ dating of metamorphism within the north-central Qinling Mountains has also revealed Silurian to Devonian arc magmatism, with a widespread Carboniferous metamorphic event (Zhai et al., 1998). In contrast, Zhai and others (1998) concluded that pre-Triassic metamorphism was the result of island arc accretion and amalgamation, terminating with a Triassic continental collision.

Other diverse evidence points to an Early Triassic age for suturing of the North and South China micro-plates. A recent paleomagnetic study performed by Yang and Besse (2001), reaffirms that North and South China displayed independent motion prior to the Triassic, but display identical apparent polar wander paths from the Jurassic onward. The study also confirms clockwise rotation of South China as a whole, rather than more minor fault block rotation along post Triassic localized faults. U-Pb dating of a 400 km long presumed synorogenic granitoid belt within the southern Qinling Mountains reveals a 205 to 220 m.y. range, further suggesting Triassic suturing of North and South China (Sun et al., 2002).

Located directly to the north of the Bikou terrane within the southwest Qinling Mountains, the Late Paleozoic Mianlue mélange of Xu and others (1994), has been inferred by Meng and Zhang (1999, 2000) to represent the final Late Paleozoic to Triassic closure of the paleo-Tethys prior to suturing of the North and South China plates. Evidence of Late Devonian to Early Carboniferous fossil bearing chert (Feng et al., 1996;

Wang et al., 1999) and limestone blocks included in a tectonic mélange with pillow basalt, gabbro, serpentenite, and greenschist imply that an ocean basin was opened within the south Qinling during the Late Paleozoic, and had closed by the time of Triassic North-South China Plate collision (Du et al., 1998a, 1998b).

While generally considered to be strong evidence of the closure of an ocean basin during the Late Paleozoic, some features of the Mianlue mélange remain enigmatic. Although the presence of MORB blocks have been widely reported (Li et al., 1996; Lai et al., 1997; Xu et al., 1998, 2000), the presence of arc-derived volcanic rocks within the mélange indicate that the subduction complex was involved with an unidentified volcanic arc (Lai et al., 1997; Xu et al., 2000), or possibly formed in a back-arc setting. Although Triassic metamorphic overprinting is present in the rocks of the Mianlue mélange, (Li et al., 1996) few Late Carboniferous or Permian volcanic rocks have been uncovered to prove that the ocean basin persisted until the Triassic.

Post Triassic Tectonic History of the Qinling Mountains

Apart from the timing of collision and final suturing of the North and South China Plates, recent work within the Qinling Mountains has also focused on the complexity of faulting, folding, and exhumation of ultra-high pressure metamorphic rocks. Wang and others (2003), hypothesize that a pair of crystalline basement indentors on the northern margin of the South China Plate caused a zone of maximum shortening within the sedimentary and volcanic-arc terranes of the central Qinling orogen. The zone of maximum shortening led to large-scale lateral strike-slip displacement of young accreted terranes and marginal basins caught between the cratons. Lateral extrusion and

transtension is similarly theorized to have caused the unroofing of the Dabie ultra-high pressure metamorphic rocks. A number of recent studies have inferred that the Bikou terrane appears to be a basement block that underwent westward lateral displacement, with bounding faults displaying appropriate shear sense indicators (Burchfiel et al., 1995; Wang and Burchfiel, 1998; Wang et al., 2001) (Fig. 4). This theory also helps to explain many complex fault patterns within the Qinling orogen that appear to juxtapose distinct tectonic units of various ages and settings.

During the Jurassic and Cretaceous, the Qinling orogen was reactivated due to the collision of continental blocks that formed the ancestral Tibetan Plateau (Qiantang and Lhasa blocks) to the southwest, transtension associated with Pacific Plate subduction to the east, and collision of the Southeast Asian micro-continent to the south (Hacker et al., 1995; Webb et al. 1999; Ratschbacher et al., 2000; Grimmer et al., 2002). Widespread Cretaceous volcanism and Cretaceous resetting of detrital apatite found in Triassic and Jurassic foreland basin deposits appear to confirm reheating in the Qinling Orogen due to Late Mesozoic transtension (Grimmer et al., 2002). Extension/ transtension appears responsible for widespread magmatism and granite intrusion in the Cretaceous and early Cenozoic (Ratschbacher et al., 2000). These diverse tectonic events combined to create transtensional and extensional deformation within the Qinling orogen, the reactivation of strike-slip faults, and the activation of dip-slip and normal faults that facilitated further unroofing of ultra-high pressure rocks in the eastern Qinling Mountains.

Reactivation of many structures within the Qinling Mountains also occurred with the Himalayan orogeny, and portions of the Qinling Mountains have experienced Eocene to recent faulting and uplift as a result (Hacker, 1995; Ratschbacher et al., 2000; Webb,

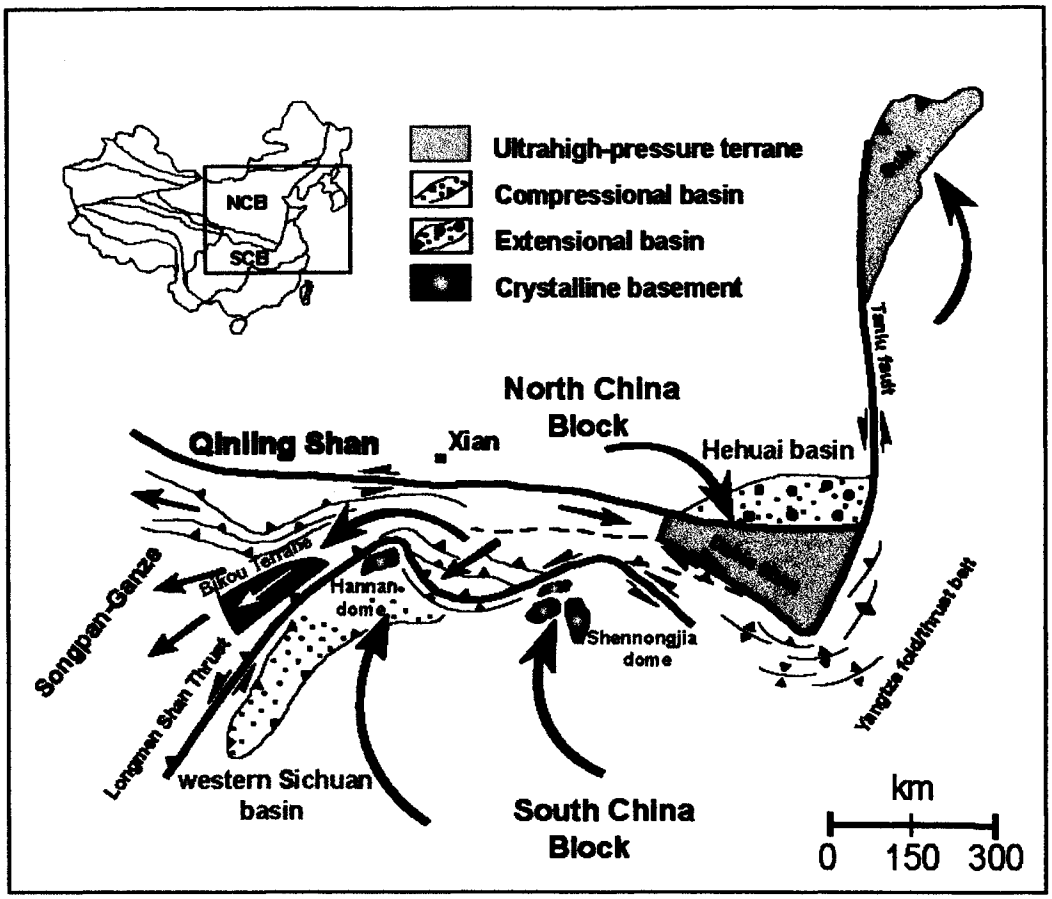

Figure 4. Schematic illustration of the Mesozoic Qinling orogen, detailing how two cratonic promontories on the north margin of the South China Plate may have created a zone of maximum shortening within the central Qinling Mountains. The Bikou terrane (in black) was translated westward as a result of escape tectonics (modified from Wang et al., 2002).

1999). Thermochronological studies of mineralization along faults in the Longmenshan Mountains immediately to the southwest of the southern Qinling Mountains (and the Bikou terrane) indicate reactivation in the Neogene to recent (Arne et al., 1997). Studies of active, east-west trending faults within and along the Qinling orogen have revealed that South China continues to undergo approximately 4 mm of left lateral movement relative to northern China/Mongolia per year (Zhang et al., 1995). The study also

uncovered evidence of active fault partitioning and counterclockwise rotation of blocks within the eastern Qinling Mountains.

Precambrian History of Central China

Compared with the Phanerozoic history of the North and South China blocks, the Precambrian history of central China is still poorly understood. The North China Plate contains evidence of Late Archean greenstone belts along its southern margin (Kroner et al., 1988), as well as remnants of crustal fragments exceeding 3 Ga in age (Liu et al., 1992). The South China Plate, once widely thought to be younger than the North China Plate, has recently also yielded evidence of older than 3 Ga Archean nuclei (Qiu et al., 2000).

Recent paleomagnetic data recovered from ca. 600 Ma glacial rocks on the North China and South China Plates has cast doubt on the Chinese Wilson Cycle theory. Paleomagnetic data suggest that the two plates lay on opposing sides of Australia at that time (Piper and Zhang, 1997; Zhang and Piper, 1997). With no biostratigraphic evidence and little stratigraphic evidence of a Precambrian North-South China link, their position relative to each other is largely speculative. Of the two micro-plates, the South China Plate has been the subject of more study in recent years, and due to a sparsity of data, the North China Plate is absent from many Rodinia reconstructions.

The South China Plate is composed of two separate micro-plates, the Yangtze in the west/northwest, and the Cathaysian in the east/southeast (Fig. 5). The two micro-plates sutured during the Middle to Late Proterozoic to form the modern South China Plate, although the exact timing of this event, like many others in the region is still subject to

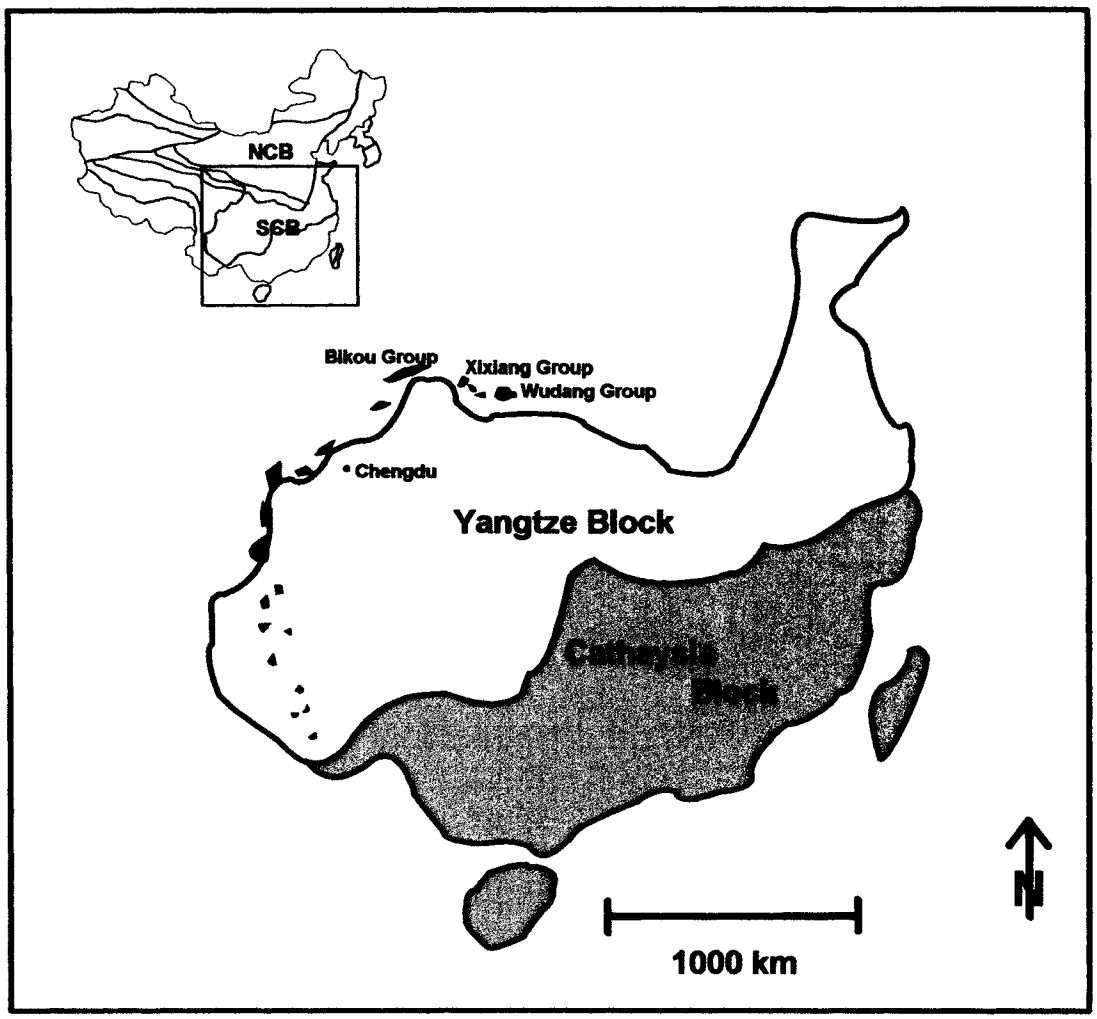

Figure 5. Map of the South China Plate and the Yangtze and Cathaysia Block sub-plates. Outlined areas indicate locations of confirmed Late Proterozoic volcanic terranes (locations from Gao et al., 1996; Zhou et al., 2002a, 2002b).

debate. Recent ion-microprobe dating has revealed a 1.3 to 1.0 Ga metamorphic event in the Sibao orogen separating the Yangtze and Cathaysian cratons, which has been interpreted to represent the suturing of South China, as well as the regional assembly of Rodinia (Li et al., 2002). However, studies of 0.8 Ga meta- sedimentary, arc related rocks in southeast China have been interpreted by others to represent Neoproterozoic

suturing of the Yangtze and Cathaysia micro-plates to form South China (Gu et al., 2002). Studies of arc volcanic rocks within the Cathaysia block also suggest Neoproterozoic suturing between 820 and 870 Ma (Zhao and Cawood, 1999), with a similar age for synorogenic granitoids within the suture zone (Li, 1999).

Much recent attention has also been given to Middle to Late Proterozoic volcano-sedimentary terranes that ring the northern and western margins of the South China Plate, commonly exposed as basement uplifts within the southern Qinling Mountains and eastern Tibetan Plateau. The majority of these terranes are highly deformed due to the complex regional tectonic history, but are commonly composed of bimodal volcanic rocks, and volcaniclastic turbidite deposits (Zhang et al., 1996). During the Neoproterozoic, the northern and western margins of the South China Plate underwent rifting to form a passive margin that persisted through the Early Paleozoic (Gao et al., 1996), but the exact timing of this event is poorly constrained due to lack of biostratigraphy, sparse or unreliable geochronology, and disagreement over the tectonic provenance of many Precambrian rock units.

It has been proposed that the volcano-sedimentary terranes of the northern and western margins of South China represent a complex history of subduction and collision to form Rodinia between 1.0 Ga and 800 Ma, followed by break-up between 800 and 700 Ma (Gao et al., 1990; Zhang et al., 1996), or collision at 1.1 Ga., and break-up at 850 Ma (Zhou et al., 1999). Xia and others (1996a, 1996b) hypothesized that volcano-sedimentary terranes along the north margin of the South China plate record protracted extension or a series of extensional events from 1.45 Ga to final break-up at

approximately 700 Ma, a period of 750 million years. Li and others (1995, 1999) hypothesize that ca. 830 Ma mafic and ultramafic dike swarms in South China correlate to similar aged dike swarms in Australia, and represent initiation of Rodinia break-up at 820 Ma. The authors also hypothesize that the Neoproterozoic volcanic terranes ringing much of the western and northern boundary of the South China plate represent a pre-rift mantle plume.

In sharp contrast with the rift hypothesis for the Neoproterozoic South China fringing terranes, a number of recent studies suggest that these terranes are in fact evidence of a long-lived continental arc. Zhou and others (2002a) hypothesize that large mafic intrusions along the northern margin of South China are the product of continental arc magmatism, due to the enrichment of large ion lithophile and light REE, and depletion of high field-strength elements. The authors also reported new zircon U-Pb ion-microprobe dates of two mafic intrusions with crystallization ages of 819 $\pm$ 10 Ma and 782 $\pm$ 12 Ma. Previous workers had concluded that these same mafic intrusions represented flood basalts erupted in an extensional setting based largely on Sr and Nd isotopic data (Xia et al., 1996b).

Zhou and others (2002b) also examined gneissic, amphibolite facies metamorphic complexes along the western margin of the South China Plate, and concluded that they were the product of either continental arc magmatism or island arc accretion. Also reported were ion-microprobe dates from zircon ranging from 764 $\pm$ 9 Ma, to 864 $\pm$ 8 Ma, with metamorphic overgrowths of 150 to 180 Ma, which were interpreted as Mesozoic reheating possibly due to collision and exhumation during assembly of the ancestral Tibetan Plateau. The combined evidence of Neoproterozoic subduction along

the north and west margins of South China simultaneously lead Zhou and others (2002b) to infer that South China flanked Rodinia at least until 760 Ma.

Recent protolith studies within the eastern Qinling (Dabie) Mountains also indicate the existence of Neoproterozoic volcanic assemblages along the northeast margin of the South China Plate. The Dabie ultrahigh-pressure terrane is considered to be the northern margin of the South China Plate in the eastern Qinling Mountains, and U-Pb microprobe dating of intensely deformed eclogites and orthogneisses indicate a 780 Ma protolith age (Ames et al., 1993, 1996; Rowley et al., 1997). However, until recently, most protolith structures were believed to have been completely overprinted. Oberhansli and others (2002) identified zones within the ultrahigh-pressure terrane that preserved a layered sequence of pillow basalt, felsic to intermediate volcanic breccias and flows, volcaniclastic sandstone, chert, and volcanic ash, similar to Neoproterozoic sequences seen elsewhere along the north and northwest margin of the South China Plate. However, Ames and others (1996) hypothesize that the Dabie terrane represents a separate micro-plate, and is discrete from the South China Plate due to crustal isotopic variations.

Within the north margin of South China is evidence of Neoproterozoic dike swarms that display primitive REE characteristics, and are also hypothesized to be rift-related in provenance. Recent studies have located basic dike swarms in the Wudang area along the north-central margin of the South China Plate that display rift-provenance geochemistry, and were dated using Sm-Nd as 764 $\pm$ 164 Ma (Zhou et al., 1999; Zhang and Zhou, 1999). Yan and others (pers. comm., 2003) report the existence of small mafic dike swarms intruding the Bikou terrane, also displaying rift provenance geochemistry. These dike swarms were dated using the $^{40}Ar/^{39}Ar$ method, and range from 660 $\pm$ 2 Ma,

to 650 ± 4 Ma (unpublished data), overlapping the published ages of the Wudang dike swarms of Zhou and others (1999), within error. While the existence of Late Neoproterozoic dike swarms does not offer conclusive evidence of the timing of rift initiation, it suggests that local break-up may be much younger than previously hypothesized.

Previous Work: The Bikou Group

Geograpically, the Bikou terrane lies near the northeastern corner of the Tibetan Plateau, where the Qinling Mountains continue into western China under the name of the Kunlun Mountains. The Bikou terrane is 40 to 50 km in width from north to south, and nearly 150 km in length in a generally northeast-southwest direction. The area is remote and rugged, with deeply incised "V" shaped valleys, ranging in elevation from 1.5 km in some of the major river valleys, to an average of 5 to 6 km atop some of the higher peaks. The Bikou Group was originally identified as a Late Neoproterozoic to Devonian succession by Ye and Guan (1944), and included both the volcanic and sedimentary components of the complex. Recently, Zhao and others (1990) separated Paleozoic sedimentary cover from the Bikou Group in the Chinese stratigraphic nomenclature. Tao (1993) further subdivided the Bikou Group by assigning the name of "Hengdan Group" to the dominantly volcaniclastic sedimentary component of the terrane, and retaining the "Bikou Group" name for dominantly volcanic strata within the northeastern portion of the terrane.

The Bikou terrane forms a Precambrian basement uplift surrounded on all sides by highly faulted Paleozoic to Mesozoic sedimentary cover. Bordering the Bikou terrane by

fault contact to the north and west is the Sanhekou Group, a thin belt of highly sheared carbonate and pelitic schist averaging a few km wide in the north but averaging a few 10's of km wide in the west. Immediately to the north of the Sanhekou Group but separated by faults, is the Baishuijiang Group, which averages 3 to 5 km wide, and forms a minimum 100 km long belt trending east/west with possibly greater extent to the west. Tao (1993) included this group as part of the Bikou terrane, although it is now recognized as an accretionary wedge (Xu et al., 1994, 1998; Li et al., 1996; Du et al., 1998a, 1998b) with a maximum age of Early Carboniferous based on microfossils (Feng et al., 1996; Wang et al., 1999). East and southeast of the Bikou terrane is the Miaoxian Group, a Silurian and younger assemblage of highly deformed carbonates and siliciclastic sedimentary rocks (unpublished Chinese Geological Survey maps).

Little is known about the structure and uplift history of the Bikou terrane, but recent reconnaissance in the area indicates that faults bounding the Bikou terrane to the north display dextral shear indicators, and faults bounding the terrane to the south display sinestral shear indicators (Burchfiel et al., 1995). This suggests that the Bikou terrane was extruded westward during Mesozoic shortening (Burchfiel et al., 1995; Wang and Burchfiel, 1998; Wang et al., 2001). However, many faults within the Bikou terrane display a sense of reverse motion (Tao, 1993), indicating either a reverse dip-slip component to these faults, or reactivation as thrust faults. Yan (pers. comm.) indicates that Jurassic alluvial/fluvial conglomerates overlying the Miaoxian Group to the east contain cobbles of meta-volcanic rocks with apparent Bikou Group affinity, indicating exposure during the Jurassic.

The Bikou Group forms the southeastern lithologic belt within the Bikou terrane, and consists largely of marine meta-volcanic rocks, with some minor interbedded meta-sediments (Tao, 1993). Much of the recent study within the Bikou terrane has focused on the Bikou Group, which contains a number of economically important ore bodies, containing gold, silver, nickel, chromium, iron, barium, manganese and others (Zhao et al., 1990; Qin et al., 1994). Stratigraphically, the Bikou Group tends to increase in metamorphic grade, crustal depth and age from west to east (Zhao et al., 1990). Metamorphic grades within the Bikou Group range from lower greenschist facies in the west, to scattered exposures of blueschist facies along the eastern boundary, which together are interpreted to represent A-type subduction of the terrane (Wei, 1995).

The Bikou Group is divided into the southeastern, stratigraphically lower belt, and the northwestern, stratigraphically higher belt. The southeastern belt consists largely of layered lavas and volcanic agglomerate interbedded with minor pelagic sediments, and is intruded by deformed granitoids (Tao, 1993). The lavas range in composition and include basalt, pillow basalt, sodium basalt (spillite), basaltic andesite, andesite, dacite and rhyolite. These rocks commonly show evidence of seawater alteration. The northwestern portion of the Bikou terrane consists largely of a thick sequence of felsic to intermediate tuff and epiclastic tuff, interbedded with mafic to intermediate pillow basalts, pyroclastic flows. Northwestward the amounts of volcaniclastic sand and conglomerate increase (Qin et al., 1992, 1994; Tao, 1993; Xia et al., 1989, 1996a; Yan et al., 2002; Zhao et al., 1990). Intruding the Bikou Group are a number of poorly dated, probable Mesozoic felsic plutons, granitic dikes and sills (unpublished Chinese Geological Survey Maps).

Interpretations of the tectonic setting of the Bikou Terrane vary, but may be summarized as the subduction and arc hypothesis, and the rift hypothesis. Since the primary focus of previous study within the Bikou Terrane has been the Bikou Group, volcanic provenance and geochemistry have been the primary tools used to determine tectonic setting. Geochemical analyses of volcanic rocks in the Bikou Group have been interpreted to represent differing volcanic provenance, despite similar data. The presence of bimodal volcanic rocks, and thick sequences of mafic to ultramafic volcanic rocks have been interpreted as evidence of continental rift provenance (Xia et al., 1996b). Enrichment of incompatible elements forming the bulk of the nickel-chromium deposits is cited as further evidence of rift provenance (Qin et al., 1992, 1994; Xia et al., 1996a). However, nickel-chromium deposits are known to occur in association with subduction arcs as well. Qin and others (1992, 1994) hypothesized that portions of the Bikou Group represent an Archean to Early Proterozoic basement complex, with its most recent history recording Proterozoic rifting.

However, the presence of tholeiitic dikes and pillow lavas are interpreted by some as representing island arc or oceanic island affinity (Pei, 1989; Zhao, et al., 1990; Tao, 1993). Xia and others (1989) demonstrated that alkaline lavas present in the Bikou Group could be produced by differentiation of tholeiitic lava sources within an island arc or continental arc environment. Yan and others (2002, unpublished data) noted the association between submarine volcanism and marine sedimentation, and concluded that the Bikou Group represents a fragment of a subduction-related arc built upon the north margin of the South China (Yangtze) craton.

Previously published age data from the Bikou Group give such a wide range of Archean to Neoproterozoic dates that the geological history of the Bikou terrane has been difficult to interpret. However, considering the alteration of the Bikou Group volcanic rocks, and possible multi-phase metamorphic history, it is not surprising that earlier dating attempts using K-Ar and Rb-Sr techniques failed to produce consistent results. Published ages for the Bikou Group have generally ranged from 1 Ga to 700 Ma (Tao, 1993; Wei, 1995; Zhao et al., 1990) with some older dates of 1.4 Ga (Xia, 1996a), to dates of greater than 2 Ga (Qin et al., 1992, 1994).

The recent application of zircon U-Pb microprobe dating finally resolves some of the debate surrounding the age of the Bikou terrane. The U-Pb zircon microprobe offers the most reliable geochronological technique to date, as the zircon U-Pb system remains closed under low-grade metamorphism common in the Bikou terrane, and is largely unaffected by alteration and chemical weathering. Recent zircon U-Pb microprobe dating of upper and lower members of the Bikou Group by Yan and others (2002, unpublished data) established that magmatism persisted within the Bikou arc from approximately 840 Ma to 760 Ma, suggesting the presence of a long-lived Neoproterozoic arc. These results largely agree with the conventional U-Pb zircon dating performed by Zhao and others (1990), and refute older age estimates as well as Paleozoic age correlations. Results from Hengdan Group detrital zircon dating will be detailed in a later section.

Previous Work: The Hengdan Group

The Hengdan Group comprises the northwestern half of the Bikou terrane, and consists entirely of marine volcaniclastic strata, with minor interbedded epiclastic tuff

and volcanic flows (Tao, 1993). Separated from the Bikou Group by the Fenxiangyuan-Tongqianba (FT) fault, the Hengdan Group is generally affected by only lower greenschist facies metamorphism (Tao, 1993). Structurally, the Hengdan Group is deformed by numerous minor faults and small-scale folds, and contains strong shear fabrics locally. However, the general structure appears to be a moderately to steeply southeast-dipping homocline (Fig. 6). Portions of the Hengdan Group, particularly in the west-central and extreme western portions of the Bikou terrane appear to have escaped strong shear deformation (Yan et al., 2002, unpublished data). Despite the fact that the Hengdan Group is structurally much simpler than the Bikou Group, it has been the focus of relatively few studies, most of which have studied it only from a reconnaissance level (Yan, pers. comm.).

The Hengdan Group consists of a variety of clastic lithologies, including lithic to feldspathic greywacke, pebbly sandstone, grain-supported and matrix-supported conglomerates, phyllitic shales and siltstones, and reworked tuff (Tao, 1993). The lower portion of the Hengdan consists of black to gray slate/phyllite; sandy slate; fine, thin grained-greywacke and minor pebbly sandstone. The upper portion of the Hengdan Group consists of thickly bedded, coarse volcaniclastic sandstone, pebbly sandstone, and pebble to cobble conglomerate. Microfossils have been examined from the pelagic sediments and are interpreted to be local Proterozoic fauna (Tao, 1993). Tholeiitic basalt dikes intruding the Hengdan Group, and lenticular sandstone channels 50 to 200 m wide are reported by Qiang (1999). Overall thickness estimates for the Hengdan Group vary greatly, with some workers citing 9 km (Qiang, 1999), 15 km (Pei, 1992), or greater than

Figure 6. A photo of the Hengdan Group in the White Dragon River valley southeast of the town of Wenxie, view to the southwest with strata dipping to the southeast.

30 km thickness (Tao, 1993). However, it is unclear if the latter estimate refers to width of the outcrop belt or a true stratigraphic thickness.

Similar to the Bikou Group, the Hengdan Group has been interpreted to belong to different basin settings by various authors. Again the hypotheses may be divided into forearc and rift. It is notable however that there is broad agreement that the Hengdan and Bikou Groups are genetically related, with volcanic detritus in the Hengdan Group closely resembling Bikou Group volcanic lithologies. In addition, volcanic ash interbeds in the Hengdan Group closely resemble the thick ash sequences in the upper Bikou Group (Pei, 1992; Tao, 1993; Lu et al., 1996, 1997; Qiang, 1999). However, few authors

familiar with the Hengdan Group agree on the tectonic setting or the age of the Bikou Group.

Supporting the theory that the Bikou Group is the source for volcaniclastic sediment preserved in the Hengdan Group, sandstone petrography and geochemistry has been used to correlate sediments within the Hengdan Group to source areas within the Bikou Group (Pei, 1992). The same study found that sandstone geochemistry matched the alkaline lava and granite sequences prevalent within the Bikou Group. Petrographic analyses performed by Pei (1992), based on the sandstone provenance fields of Dickinson (1985), also suggest that provenance of Hengdan Group sandstones evolved from undissected arc, toward continental arc from the lower to upper Hengdan Group.

Based on these data, Pei (1992) interpreted the tectonic setting of the Hengdan Group as a forearc basin within a continental arc system. However, his analysis revealed that sandstones within the Hengdan Group are composed of up to 35% matrix, which suggests alteration of unstable volcanic grains to clay and may favor quartz in point counting results. Accurately accounting for this alteration would in effect shift the results more solidly into the arc-related field, but suggests that Pei's (1992) results concerning discrimination between the different arc related fields (undissected vs. transitional and dissected) should be viewed with caution. Arc affinity is also corroborated by descriptions of turbidite conglomeratic clasts, composed largely of extrusive volcanic rocks, with minor granite, and chert (Tao, 1993). Tao (1993) described the Hengdan Group as an island arc affiliated forearc trench basin, and envisioned a submarine fan system feeding into a subduction trench along the westerly edge of the Bikou Group, with

a largely longitudinal sediment transport direction. No paleocurrent measurements were recorded to support the theory of longitudinal transport however.

Favoring a continental rift setting, Lu and others (1996, 1997) interpreted the Bikou terrane as Silurian to Devonian in age or younger, by correlating units within the Hengdan Group to local Paleozoic units. Tholeiitic dikes within the lower Hengdan Group (Qiang, 1999) were also taken as evidence of an extensional setting, although no reliable age data exist for the dikes. Qiang (1999) also cited conglomerate clast populations within the lower Hengdan Group, consisting of granite gneiss, quartzite, as well as volcanic rocks, as further evidence for rift provenance. However, it is unclear if these lithologies refer to the Guanjiagou Formation, a unit with an uncertain relationship to the Hengdan Group.

CHAPTER 3

STRATIGRAPHY OF THE HENGDAN GROUP

Methods

During June and July of 2002, a study of the Hengdan Group, Bikou Group, and adjacent geologic units was conducted jointly by a small team from the University of Nevada Las Vegas and the Academy of Geological Sciences in Beijing. The study involved approximately one month of fieldwork within the Hengdan Group and neighboring units, and U-Pb SHRIMP analyses performed at both the Academy of Geological Sciences in Beijing and the Stanford/USGS SHRIMP-RG laboratory in Stanford California.

Sedimentological and stratigraphic observations presented here are derived from six traverses through the Bikou Terrane and adjacent units, and two measured sections compiled within the Hengdan Group (Fig. 7). The first section, located within the central Hengdan Group in Luotong County, consisted of approximately 25 km of section, equating to 15.5 km of true thickness. The second section was measured in Wenxie County approximately 50 km to the southwest, and consisted of approximately 3.2 km of true thickness. In addition to observations and measurements of stratigraphic section,

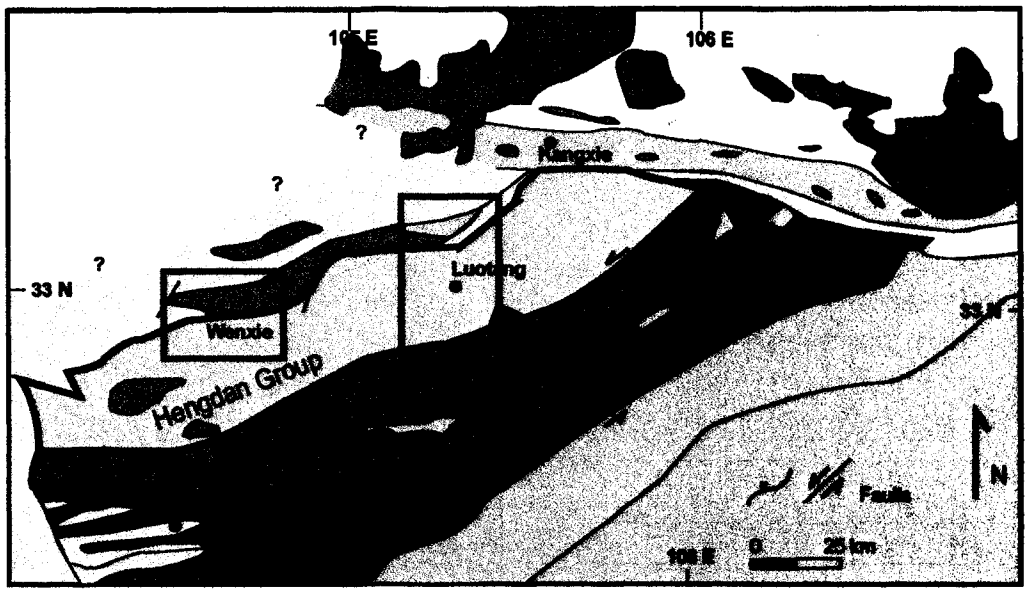

Figure 7. Map of the Bikou terrane with general locations of the Luotang (right) and Wenxie (left) measured sections. See Figure 2 for key to geologic units.

paleocurrent data were collected, and samples were collected for petrography. Both the Luotong and Wenxie locations were selected for stratigraphic measurement due to the fact that metamorphic grade and structural complexity were the lowest observed within the Hengdan Group. However, observations and comparisonsbased on the other reconnaissance traverses are included in the discussion. Section was measured across numerous faults within the Luotang traverse, and their positions are noted within the graphic columnar sections. In general, faults within this section were interpreted to have only minimal to minor offset, due to the fact that different sedimentary facies were not juxtaposed across structural breaks. However, the possibility of repetition or omission of section cannot be completely discounted, so the total section thickness presented here must be considered approximate. Given the great thickness of continuous section measured within the Luotang traverse, the complete measured stratigraphic column is

included within the appendixes (Appendix I). A series of detailed stratigraphic sections illustrating major facies changes are included in the text, and keyed to a reduced-size version of the complete Luotong stratigraphic section (Fig 8). Descriptions of the detailed sections are included in the text, but a legend is included in Appendix I.

Stratigraphic sections were measured using a Bushnell laser-rangefinder through near continuous outcrop exposed along county roads. All apparent thickness measurements were converted to true thickness trigonometrically using the measured strike and dip orientation of bedding, traverse trend and plunge data recorded from the laser-rangefinder. All stratigraphic thicknesses referred to in the figures and text are given in true thickness. Graphic columnar sections were drafted with AppleCORE (Ranger, 1995).

Metamorphic grade within the Hengdan Group is characterized by lower greenschist facies mineral assemblages (Pei, 1992; Tao, 1993; Wei, 1995). Although many fine-scale sedimentary features are no longer visible, moderate to large-scale features generally remain recognizable. Widespread portions of the Hengdan Group have been affected by shear deformation, particularly within the northern and southern portions of the terrane. This deformation is problematic for stratigraphic measurement, and tends to obscure bedding, grain size variations, and has locally caused severe flattening of conglomerate clasts, making accurate clast counting extremely difficult.

Fortunately, the central-west portion of the Hengdan Group has not been as affected by shear deformation and metamorphism, particularly in the vicinity of Luotang County. However, metamorphic grade was found to increase noticeably southeastward, particularly in the vicinity of the FT fault separating the Bikou Group from the Hengdan

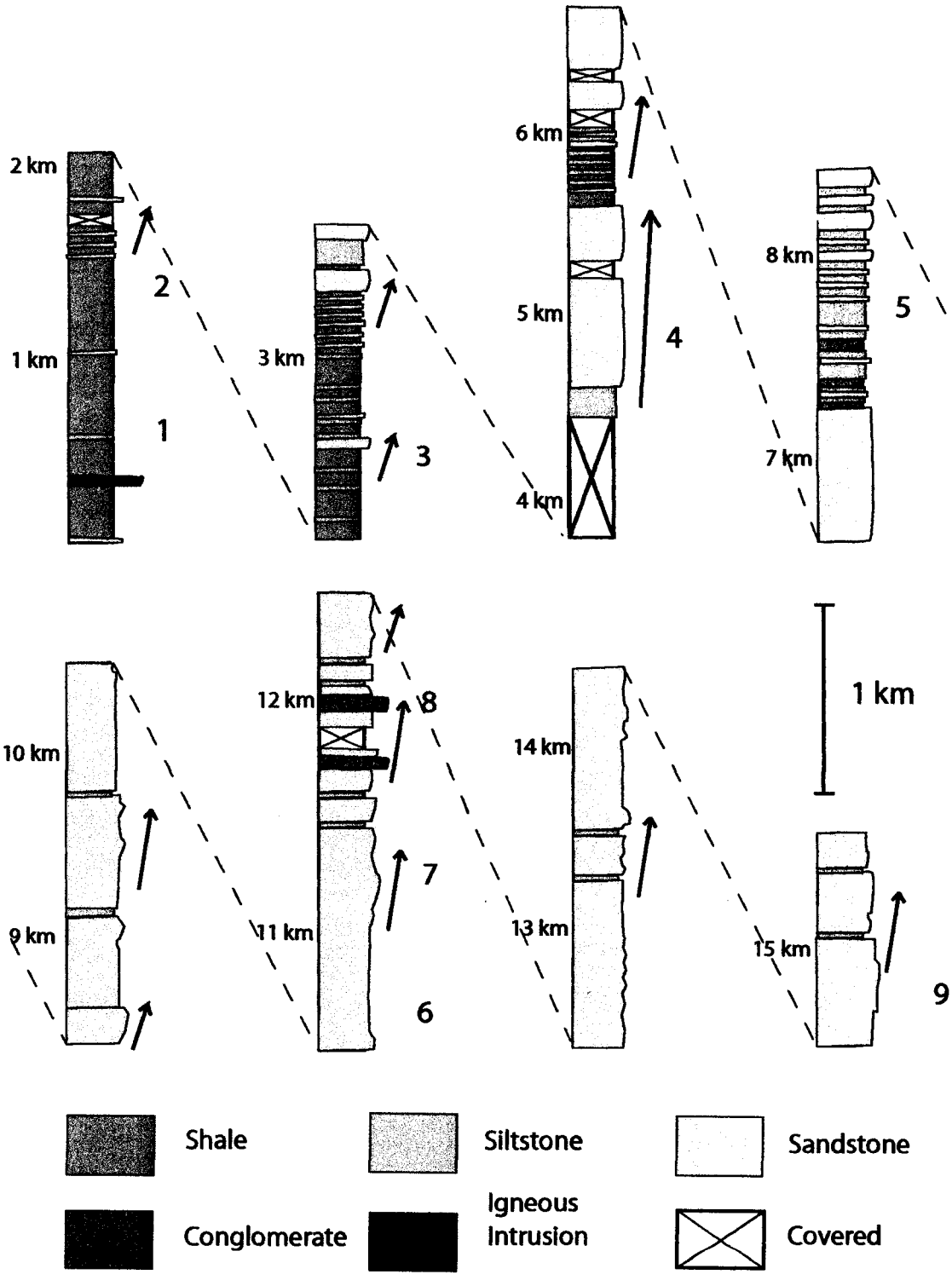

Figure 8: Simplified stratigraphic column for the Lutong traverse. Arrows indicate coarsening upward cycles. Numerals indicate locations of detailed sections.

Group. Nowhere is the basement for the Hengdan Group exposed, and the lowest stratigraphic levels of the Hengdan Group are in fault contact with the carbonate dominated, Devonian Sanhekou Group, or the probable Triassic-aged Guanjiagou Formation (Yan et al., 2003) along the northwestern edge of the Bikou terrane. Refer to Luotang vicinity map (Fig. 9) for traverse location.

Stratigraphy of the Hengdan Group: Luotang Section

Within the vicinity of Luotang, the lowest stratigraphic exposures of the Hengdan Group are in fault contact with the Sanhekou Group. Here the fault separating the Bikou terrane from the Paleozoic units to the northwest is a near-vertical, northwest dipping zone of sheared black marble up to 4 m thick. In this area, the basal Hengdan Group is dominated by thinly laminated to thinly bedded, black to bluish black pelitic phyllites, dipping moderately to steeply northwest. With the exception of a thin bed of pyriferous, fine grained, volcaniclastic sandstone, near the base of the section, sandstone is nearly absent in the lower 1 km of the basin. Within the first 200 m, the dip direction rotates to the SE, and a moderate to steep S dip remains consistent through the remainder of the measured section.

Through much of the lowest interval of the Hengdan Group, thinly bedded black phyllites and silty phyllites form a monotonous, highly repetitious interval as illustrated in detailed section 1 (Fig. 10). Small pyrite cubes are common within the phyllites, and localized zones containing small amounts of graphite. At a point approximately 300 m above the base of the measured section, a 10 m thick felsic sill intrudes the section, and is composed of relatively finely crystalline, muscovite, K-spar leucogranite. Within the thin

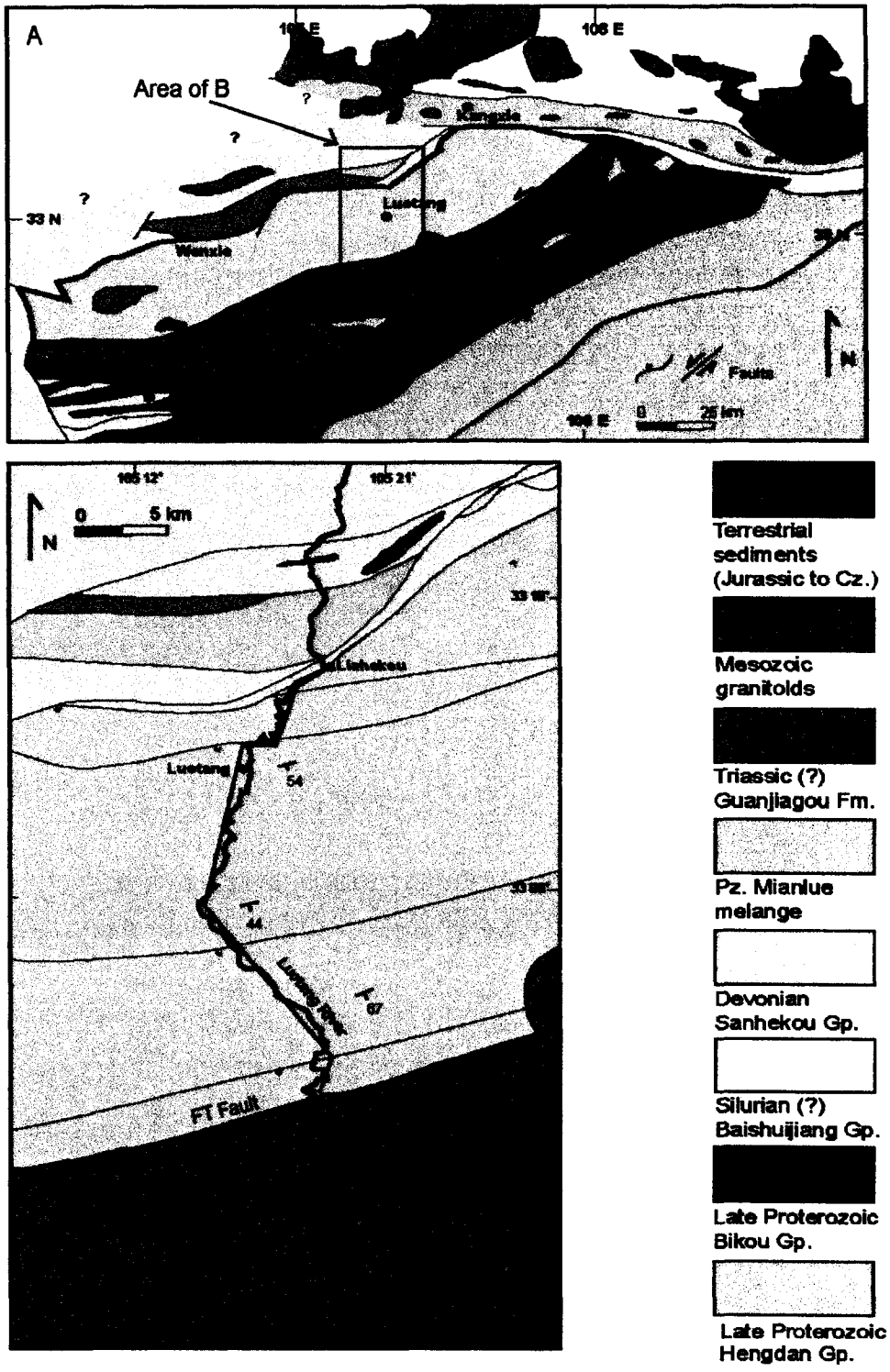

Figure 9. Location map for the vicinity of Luotang. The red line indicates the measured section traverse, which ends north of the town of Masangba and the FT fault separating the Hengdan Group from the Bikou Group.

contact zone, the meta-pelites contain highly abundant small pyrite cubes. This sill forms the only major intrusion within the measured Luotang section.

Up-section from the sill, a few thin, fine grained buff colored phyllite layers were encountered, which may have been originally a very fine-grained tuff. A few of the phyllitic beds within the vicinity of the sill appeared to be slightly convoluted, possibly related to the intrusion, or possibly due to syn-sedimentary deformation. Approximately 500 m above the base of the section, a steeply north dipping fault was encountered in the vicinity of Lianghekou Valley. This fault was considered to be relatively minor, as highly repetitious, finely laminated black phyllites continued across the fault. A few minor faults are exposed south of the main Lianghekou Valley fault, with some localized disrupted bedding. Separation of beds across the faults appeared to measure only a few meters. Near the 900 m interval, color changes sharply from bluish-black to a dark grayish-green, although the beds remain thin with clay to silt sized sediment.

The depositional environment of these dark-colored, highly repetitious meta-pelites is interpreted to be hemipelagic. Thin laminations and consistent clay to silt-sized sediment is indicative of sedimentation within a very low energy setting. The abundance of graphitic or carbon film, associated with possible diagenetic pyrite indicate the preservation of organic matter, which together with the dark coloration suggest an anoxic environment. Hemipelagic deposition is generally characterized by thin beds of mud to silt-sized sediment generally lacking in sedimentary structures. Hemipelagic deposits generally occur on deep marine slopes, basin-plains and are commonly interbedded with turbidite deposits (Stow and Tabrez, 1998). Intervals of alternating fine-grained sand and

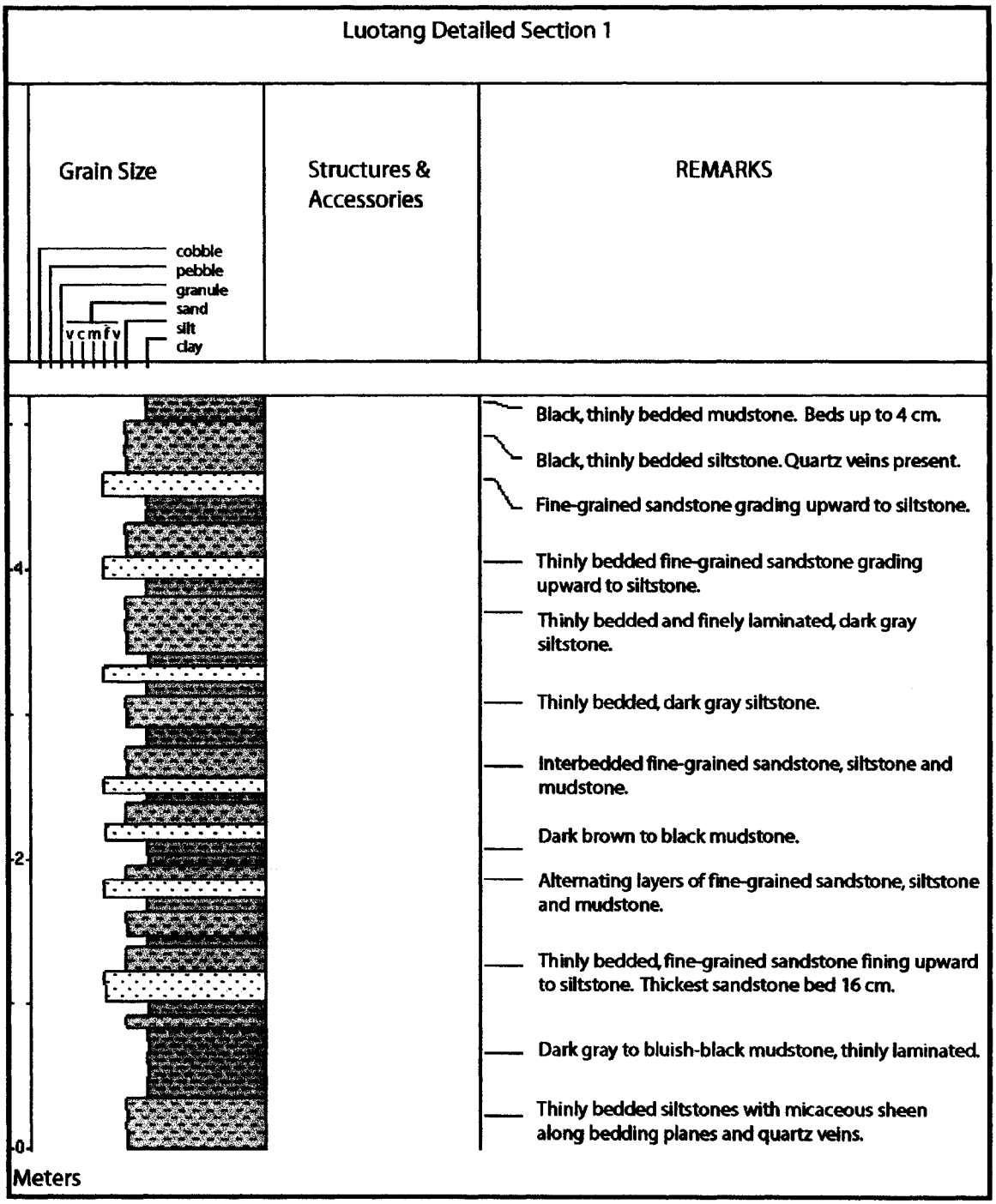

Figure 10. Detailed Section 1, illustrating fine-grained stratigraphy within the lower Hengdan Group.

mud-sized sediment may represent distal turbidite fan sedimentation prograding into the basin-plain environment. The facies is best illustrated by detailed section #2 (Fig 11). Near the 950 m interval, an increase in thin silty to fine grained sandy layers were observed. The fine siltstone beds are thin and planar, and alternate with shale layers. Near 1.1 km, thin planar beds and lenses of fine-grained sandstone up to 8 cm thick become common. The sandstone layers tend to alternate with silty and shaly layers, although the sandstone to shale ratio remains low (approximately 20-30% of the deposit). Non-rhythmic alternating sandstone beds within this section tend to form stringers or wide, thin lenses. Scattered pyrite cubes remain common and graphite becomes increasingly uncommon.

Near the 1.5 km interval, alternating layers of siltstone, shale and fine-grained sandstone becomes increasingly common. Within this portion of the section, the proportion of sandstone to rises to approximately 40%. Farther upsection, the sandstone proportion rises to a peak of approximately 60% between the interval of 1.75 and 1.85 km. Here, the first coarse-grained sandstone beds appear as small lenses interbedded with thin alternating beds of fine to medium grained meta-sandstone, siltstone and shale. The composition of sandstone within this section is both texturally and compositionally immature with abundant diagenetic matrix, and is classified as lithic greywacke (Fig. 12). The poor sorting, angularity and compositional immaturity are indicators of relatively short transport of framework grains.

Above the lenticular, coarse-grained beds, thin, planar alternating beds of fine to medium-grained sandstone and mudrocks continue to approximately the 2.1 km interval, with an approximate 50% sandstone proportion. Immediately above this section of

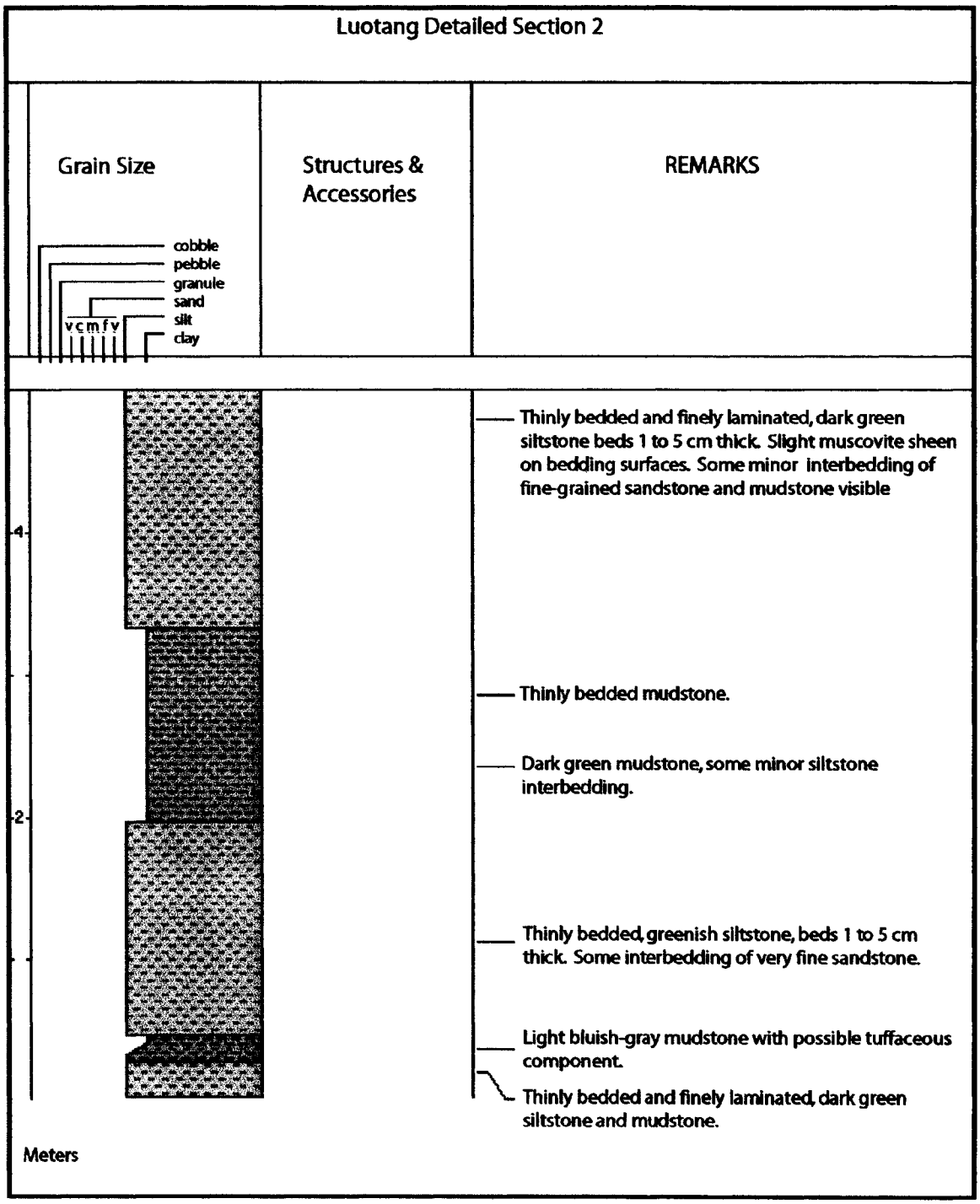

Figure 11. Detailed Section 2, illustrating hemipelagic facies within the lower Hengdan Group, with some interbedding of very dilute turbidity currents possible.

coarser sediment, thinly bedded alternating layers of phyllitic shale, siltstone and fine sandstone dominate for nearly 400 m, with an approximate sand/shale ratio of 20%. Pelitic phyllites in this section again appear-bluish black, with small pyrite cubes. Some relatively thin zones of pelitic phyllites in this interval are also slightly calcareous, a property noted only in this localized zone. The abrupt transition from an increasingly sandstone-dominated system back to a mud-dominated system marks the end of a minor coarsening upward cycle.

The alternating, rhythmic beds of fine to medium grained sandstone, siltstone and shale indicate deposition by dilute, low-density turbidity currents (Bouma, 2000). Given the generally fine grain size and thin beds, deposition is likely to have occurred on the

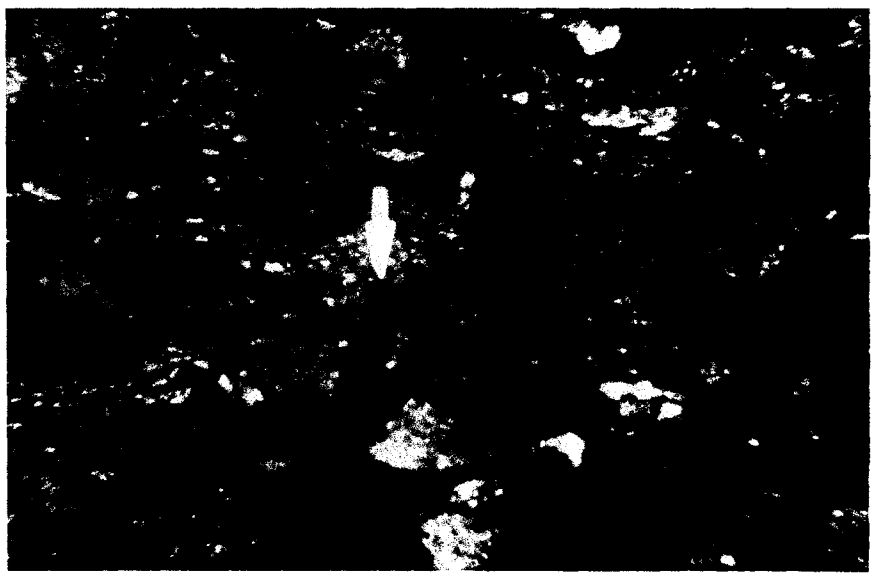

Figure 12. A photomicrograph of sandstone sample 02LT11, displaying poor sorting, angularity, and abundance of feldspar and lithic volcanic grains. The cementing agent is diagenetic clay matrix, indicating that this sample is a lithic greywacke. Arrow is 0.25 mm in length.

distal portions of a submarine fan. Regular thin interbeds of fine to medium-grained sandstone interbedded with shale closely associated with thick hemipelagic shale intervals is commonly indicative of deposition within the fan-fringe or extreme distal submarine fan (Nilsen, 1984). The up-section shift from pelagic deposition to distal turbidite fan deposition is indicative of progradation of submarine fan deposits over basin-plain facies. Shifts from sandstone-dominated sedimentation back to mud-dominated sedimentation indicate possible oscillation of the fan depocenter, and the abandonment and reactivation of sediment lobes at the fringes of the outer fan.

At 2.25 km above the base of the section, another relatively thin interval of medium to coarse-grained sandstone abruptly appears. This interval is noteworthy however, for it is easily distinguished from sandstone-dominated intervals lower in the section by the relatively large-scale channel structures it exhibits (Fig. 13). The channels appear as lens-shaped beds of medium-to coarse-grained sandstone that truncate underlying thinly bedded phyllitic siltstone, shale, and fine-grained sandstone. The largest of the beds measures up to 2 m thick, with a distinctively eroded base. Above the channel structures, thin to moderately thick planar beds of fine-to medium-grained sandstone interbedded with pelites dominate. Sandstone comprises about 50% of this interval, but give way again to a thick silt and mud dominated sequence beginning 2.7 km above the base of the section. This shift marks the end of a second minor coarsening upward cycle, and is illustrated in detailed section #3 (Fig. 14). Moderate to large-scale channels of coarse-grained sandstone are generally indicative of a middle fan facies, however, the fairly localized occurrence observed at this location indicates that the deposit was part of an

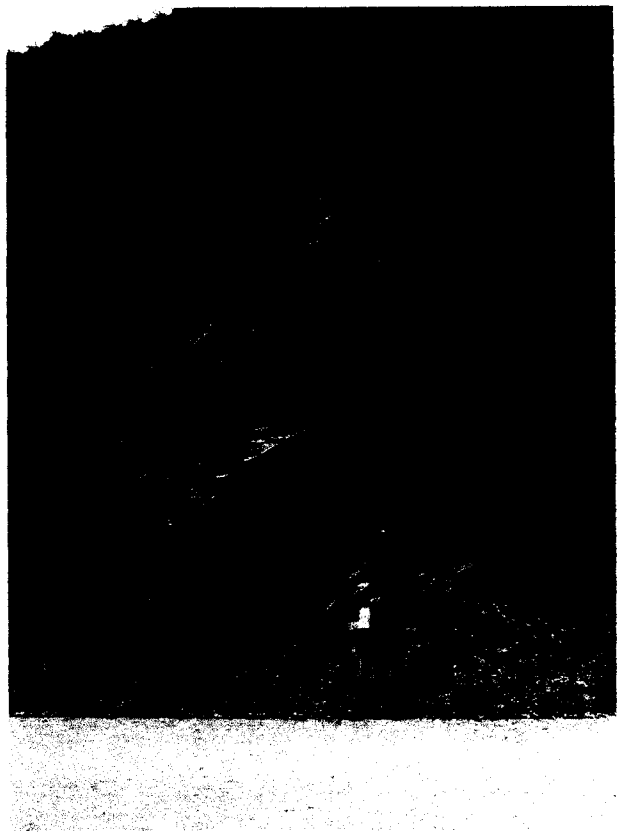

Figure 13. Medium-to coarse-grained sandstone lens truncating underlying sequence of thinly bedded siltstone.

important tributary system that supplied sediment to the outer portions of a submarine fan. The deposit may also represent a minor supra-fan lobe formed by relatively coarse-grained sediment that was able to bypass the middle fan and deposit on the outer fan.

Between the interval of 2.7 km and 3 km, thin alternating beds of dark colored, phyllitic shale and siltstone dominate. Thin beds of fine to medium sandstone and small lenticular sandstone bodies up to 15 cm thick are interspersed throughout the section. The sedimentary facies of this interval alternates between distal submarine fan, and basin plain. Near 3 km however, lenticular bodies of medium-grained sandstone up to 1.5

meters thick begin to appear, followed by a layer of massive, medium-grained sandstone 4 meters thick. Between 3 and 3.4 km, thinly bedded, fine to medium-grained sandstone alternates with beds of phyllitic shale and sandstone. Large lenticular bodies of medium-grained sandstone up to 2 meters thick are interspersed throughout. The interval is capped at 3.4 km by approximately 50 meters of thick, planar-bedded sandstone layers up to several meters thick. The beds appear massive and range from medium-grained to very coarse-grained (granular), and mark the end of a third coarsening upward cycle.

Following the interval of thickly bedded sandstone, thinly bedded, silt to fine-grained sandstone dominated rhythmites of distal submarine fan facies are the dominant lithology. With the exception of a few moderate sized sandstone lenses, and a few scattered beds of planar, medium-grained sandstone, only thin alternating beds were observed until the township of Luotang, near the 3.7 km interval. Here, shops and residences of the community made measurement through this interval impractical, however scattered outcrops of thinly bedded, silty rhythmites were observed. The total interval covered by the township was approximately 0.75 km of section.

South of Luotang, thinly bedded phyllitic siltstone/fine-grained sandstone rhythmites continue. Near the interval of 4.5 km, lenticular beds of medium to coarse-grained sandstone up to 1.5 m thick appear. For the next 100 m, these moderate-sized lenses are stacked between intervals of thinly bedded, silt to fine-sandstone dominated rhythmites. A number of the lenses display tangential crossbed sets that indicate northward paleoflow (Fig 15). Stacked lenses give way to massive, planar, thick-bedded, coarse-grained sandstone and pebbly sandstone. Pebbles appear to consist of gravel-sized, dark colored volcanic clasts, with minor vein quartz. Within many of the thicker beds, which range up

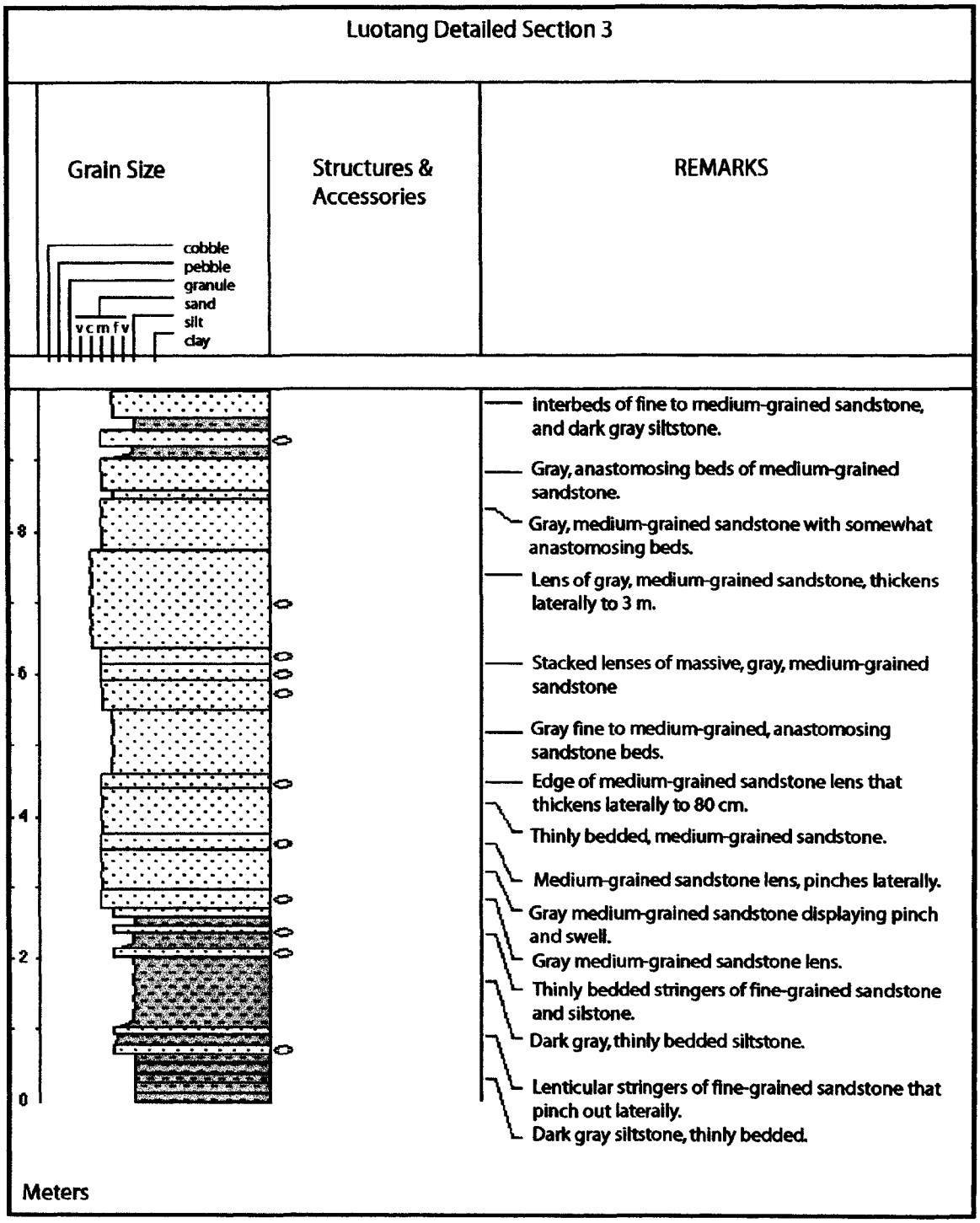

Figure 14. Detailed Section 3, illustrating a coarsening upward cycle from thinly bedded outer-fan siltstone to a sandy distributary channel complex.

to 3 m thick in this section, small black phyllitic rip-clasts are visible. Massive, thick, coarse-grained beds alternate with moderately bedded, medium-grained sandstone commonly displaying planar to tangential crossbeds with northward paleoflow. Small pyrite cubes are common throughout the section.

Crossbedded sandstones occur throughout the middle to upper Hengdan Group, coinciding with the increasing abundance of sand in the depositional system. Crossbed forms range from small-scale tangential and planar sets, to large-scale channel accretionary forms. Wherever recognized, measurements of crossbeds were obtained in order to reconstruct paleo-current directions. Throughout the Hengdan Group, paleocurrent indicators record a northward-radiating paleocurrent direction, indicating transport from the direction of the Bikou Group to the Hengdan basin. Transport directions alternate between north, northeast and northwest, indicating a possible radial dispersion pattern within a submarine fan complex (Fig 16). Thin alternating beds of

Figure 15. Small-scale tangential crossbeds at the base of a sandstone bed.

phyllitic shale, siltstone and fine to medium-grained sandstone reappear near the interval of 5.5 km, marking the end of a fourth coarsening upward cycle. Sandstones within this interval display poor sorting, angularity, and compositional immaturity, similar to lithic graywackes encountered lower in the Luotang section (Fig. 17). Phyllitic shale and siltstone beds average a few cm thick, with sandstone beds averaging 6 cm thick, but ranging up to 12 cm thick. Thin-bedded rhythmites continue to the 5.9 km interval, where a fault, inferred by gouge-like material in a poorly exposed ravine, cuts the section. Above the fault, thin-bedded rhythmites continue to the 6.1 km interval.

The approximately 1 km thick interval from 4.5 to 5.5 km comprises coarse, thick-bedded sandstone characteristic of a prograding mid-fan depositional system. Mid-fan environments are typically characterized by medium to large-sized sandstone channels that fine upward into thinly bedded siltstones and shales, and grade laterally into thin, fine beds of channel levee and overbank facies (Nilsen, 1984). Thinning and fining upward of individual sandstone channels has also been interpreted to represent gradual channel abandonment (Mutti and Normark, 1990). The abrupt shift from a silt-dominated, outer fan system, to a sand-dominated system and back is indicative of the autocyclic switching of an active sediment lobe within a submarine fan. Coarse channel sand is rapidly prograded out over dilute, low-density turbidite deposits until coarse sediment bypasses the active lobe. Following lobe shift, the old lobe is abandoned and overlapped by distal fan and overbank deposits, or hemipelagic drape. Detailed section #4 illustrates coarse-grained stratigraphy within this cycle (Fig. 18).

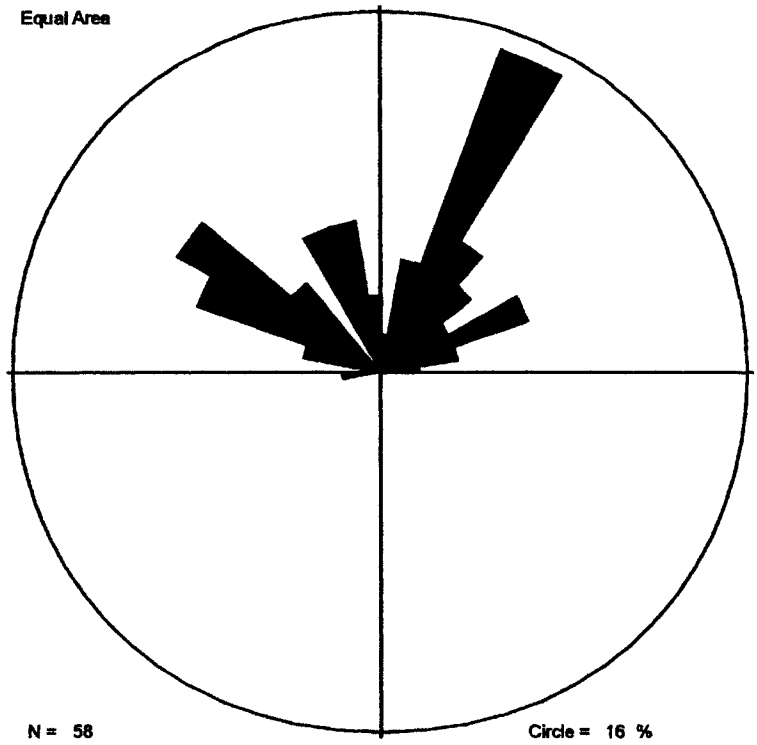

Figure 16. Rose diagram illustrating paleocurrent directions for 58 crossbed sets measured throughout the middle to upper Hengdan Group.

Near the 6.1 km interval, the system switches again to a coarsening upward, medium-grained sand-dominated cycle. Within this section, large channels are largely absent, with the exception of a number of coarse-grained, massive sandstone lenses near the base of the cycle. Thin tabular sandstone beds dominate for the next several hundred meters, with average bed thickness of 10 cm, and maximum bed thickness of about 1 m. The grain size ranges from coarse to fine, although medium to fine grain beds are most common. The sandstone beds appear to fine upwards from coarse or medium to fine sand size, and are often capped by thin siltstone/shale beds. Planar to tangential crossbeds are common within the coarser sandstone beds, with paleoflow direction consistently to the

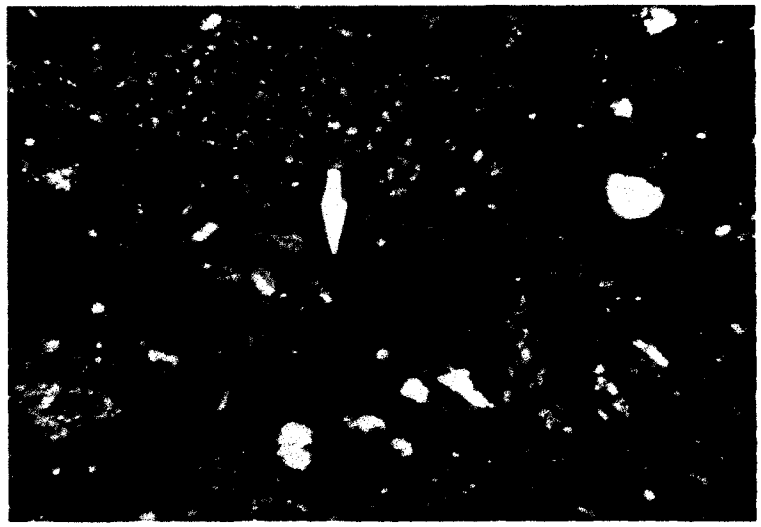

Figure 17. Sandstone photomicrograph of sample 02LT17, a coarse-grained, poorly sorted lithic greywacke. The large grain at lower right is lithic volcanic. The arrow at center is 0.25 mm long.

north. Pyrite cubes up to 1 cm in diameter are also fairly common throughout. The thin alternating beds of sandstone to phyllitic shale within this interval are suggestive of inter-channel, overbank facies deposits. The scattered, thick beds of crossbedded sandstone that appear within the overbank facies sediments are interpreted to have formed as crevasse-splay deposits. Crevasse-splay deposits form when the channel-levee system is breached, causing coarser sheet sands to deposit in the inter-channel areas (Nilsen, 1984). Overbank and crevasse-splay sand sheets within the inter-channel area commonly form very laterally extensive beds (Mutti and Normark, 1990).

The top of the fifth coarsening upward cycle is between the interval of 6.8 and 6.9 km. Here, thick, massive, planar beds of medium to coarse-grained sandstone are common, with a number of coarse-grained lenticular beds displaying tangential

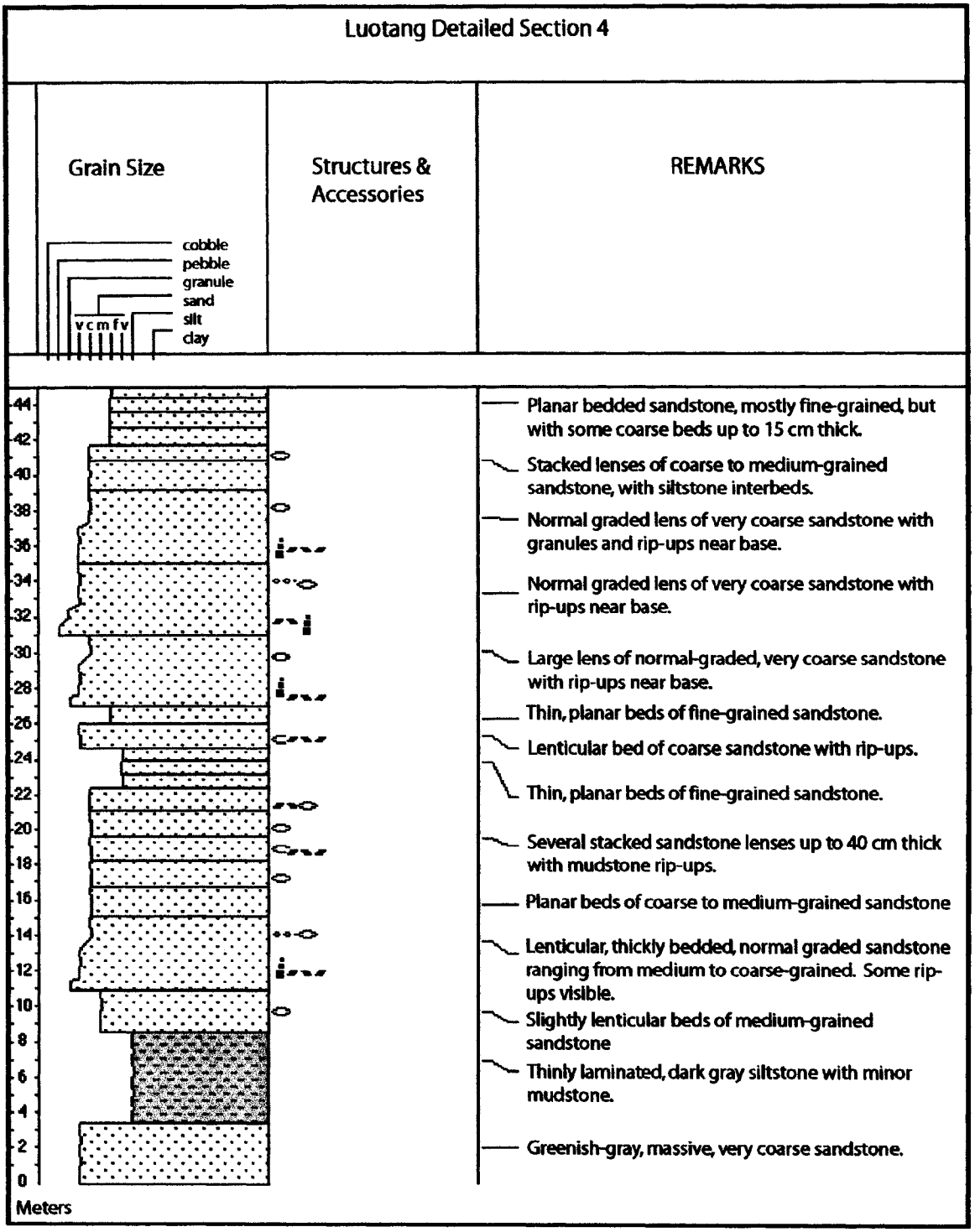

Figure 18. Detailed Section 4, illustrating coarse-grained sandstone channels within a coarsening upward cycle.

crossbeds. The thicker beds are approximately 1 m thick on average, and display minor fining upward cycles with overlying planar beds of fine to medium sandstone that are on average 10 cm thick, and capped by shale/siltstone beds averaging 3 to 4 cm thick. The system remains sandstone dominated up to the 7.2 km interval, but relatively thin planar beds of fine to medium-grained sandstone, 10 to 12 cm thick dominate the remainder of the section.

The 7.2 km interval marks the return of dark bluish-black phyllitic shale and siltstone deposition, although silt-sized sediment is most common. Unlike the lowest measured intervals of the Luotong section, where deposition appeared to have occurred in a hemipelagic setting, the fine grained deposits here display a faint grading of silt to clay sized material, or from fine sand to clay, indicating deposition by dilute turbidity currents or overbank currents on a submarine fan. Individual beds average 4 to 5 cm thick, are tabular in appearance, and contain abundant pyrite cubes. A few medium to coarse-grained beds up to 20 cm thick locally appear throughout this section. Detailed section #5 illustrates stratigraphy within this facies (Fig. 19). A minor fault of probable small offset occurs at the 7.5 km interval. Thin interbeds of fine sandstone, siltstone and shale continue in a highly repetitive succession for over 1 km, to about the 8.3 km interval.

Near 8.3 km, the appearance of a series of large lenticular sandstone beds within the relatively thin, fine-grained beds heralds the shift to coarser sedimentation in what begins to be a familiar pattern. Here medium-grained sandstone beds up to 30 cm thick begin to alternate with the finer, thin-bedded material, followed by a series of stacked sandstone channels up to 1.5 m thick (Fig. 20). Channel fill consists of very coarse to medium sandstone, with dark lithic volcanic grains visible. Sandstones within this interval

continue to display poor sorting, angularity, and immature compositions (Fig. 20). Capping the channel structures are a series of thin, anastamosing beds of medium to fine-grained sandstone, interspersed with much smaller sandstone lenses. The section continues to be medium-grained sandstone dominated for a considerable distance upsection, although beds become thin and mark the end of the sixth coarsening upward cycle. Thinly bedded medium-grained sandstone alternates with 10 to 30 cm thick beds of fining-up coarse-to medium-grained sandstone, capped by 3-8 cm thick beds of fine–grained sandstone and siltstone. Several intervals interspersed throughout the section measure a few tens of meters thick and are dominated by thin beds of flaggy, siltstone and fine-grained sandstone. A few coarse-grained beds, up to 1 m thick, and containing phyllitic rip-up clasts also appear.

Approximately 9.7 km above the base of the measured section, a series of thick tabular beds of coarse to very coarse-grained sandstone appear. Along the banks of the Luotang River are a series of large float blocks of gravel to cobble conglomerate and pebbly sandstone, with cobble composition dominated by dark andesite/basalt and lighter colored tuffs. The blocks appeared to be locally derived and probably were carried down the steep valley flanks by recent landslide activity, although an outcrop could not be located. This section appears to mark the end of the seventh coarsening upward cycle.

Deposition from 9.7 km upward to approximately 10.4 km is marked once again by thin, flaggy beds of fine-grained sandstone to siltstone and shale, averaging only a few cm thick. A few beds of medium-grained sandstone that are 10 to 20 cm thick are interspersed within thin alternating beds of sandstone and shale, along with a few sandstone lenses well under 1 m thick. From 10.4 to 10.5 km minor beds of coarser-

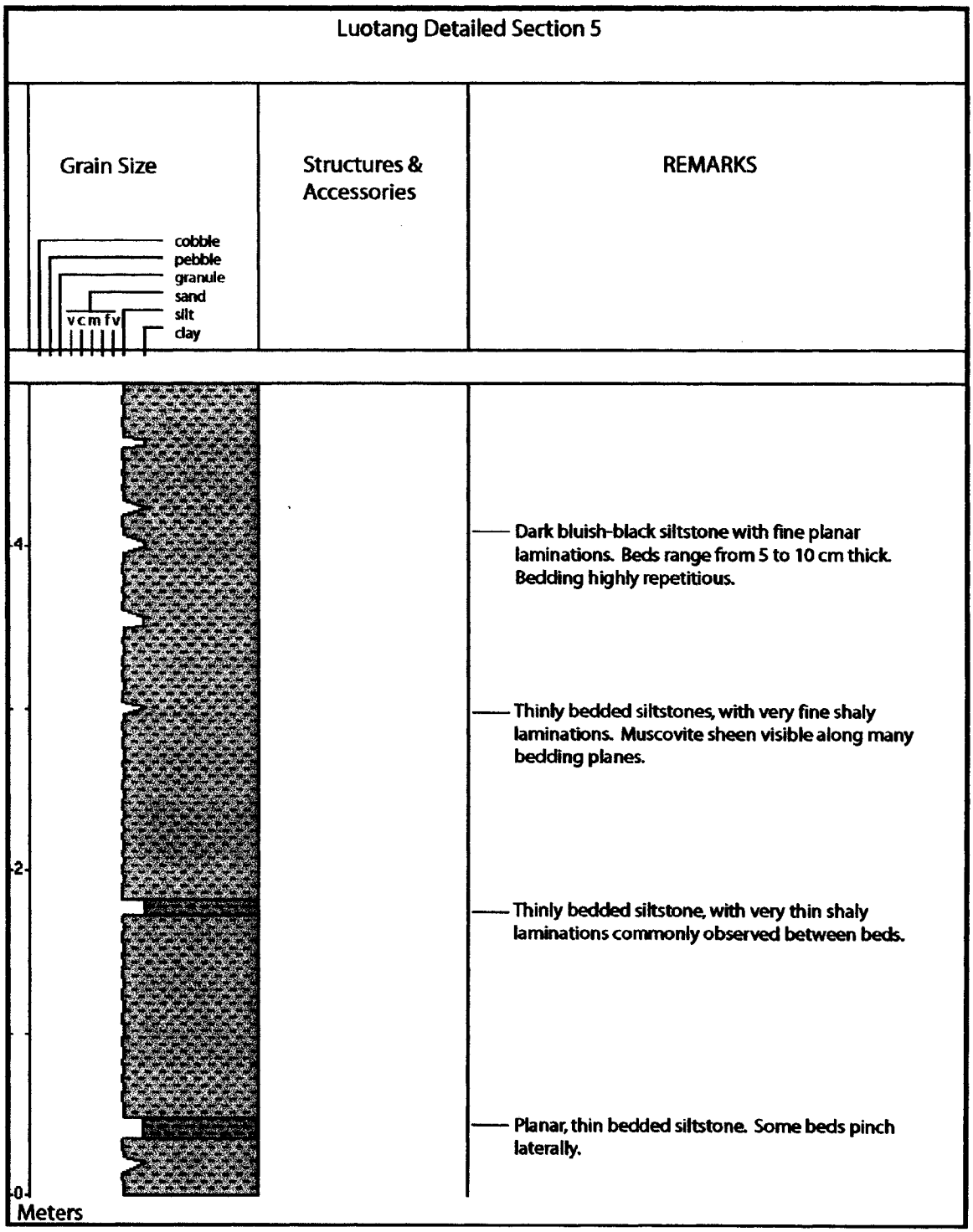

Figure 19. Detailed Section 5, illustrating thinly bedded, fine-grained siltstone and sandy siltstone of probable overbank facies.

Figure 20. Margin of a large sandstone channel within a stacked channel sequence.

grained sandstone appear, but no large channel features or massive beds appear. The beds here range from 10 to 30 cm thick, and alternate from coarse or medium-grained sandstone to fine-grained sandstone, siltstone and shale. A few minor channel structures occur here, but are generally only 20 to 30 cm thick. Above this minor interval of coarser material, thin alternating beds of blackish, fine-grained sandstone and siltstone return, and form a highly repetitious, monotonous section up to the 10.8 km interval. This transition is illustrated in detailed section #6 (Fig 22). The fine-grained strata have

Figure 21. Photomicrograph of sample 02LT19, a coarse-grained lithic graywacke. Dark lithic volcanic grains predominate, although the sample contains a number of relatively large, angular quartz grains. Arrow is 0.25 mm long.

been interpreted to represent overbank facies, with coarser beds possibly marking crevasse-splay deposits, or small-scale channels.

Near 10.8 km, deposition begins to gradually coarsen, and thicker beds begin to appear. Beds of medium to coarse-grained sandstone up to 30 cm thick become more common, and normally graded beds are recognizable, alternating from medium-to fine-grained sandstone to siltstone. Metamorphism also appears to gradually increase with a marked greenish cast to sandstone beds. A fine-grained reworked tuff bed 4 to 5 cm thick is exposed near 10.9 km.

A sudden shift to coarse-grained sandstone deposition occurs near 11 km. Thick, planar, coarse to very coarse-grained sandstone beds become common. Many of these beds contain shaly rip-up clasts and exhibit normal grading. A number of beds contain pebbly sandstone; the pebbles consist of dark volcanic clasts. Sandstones within this

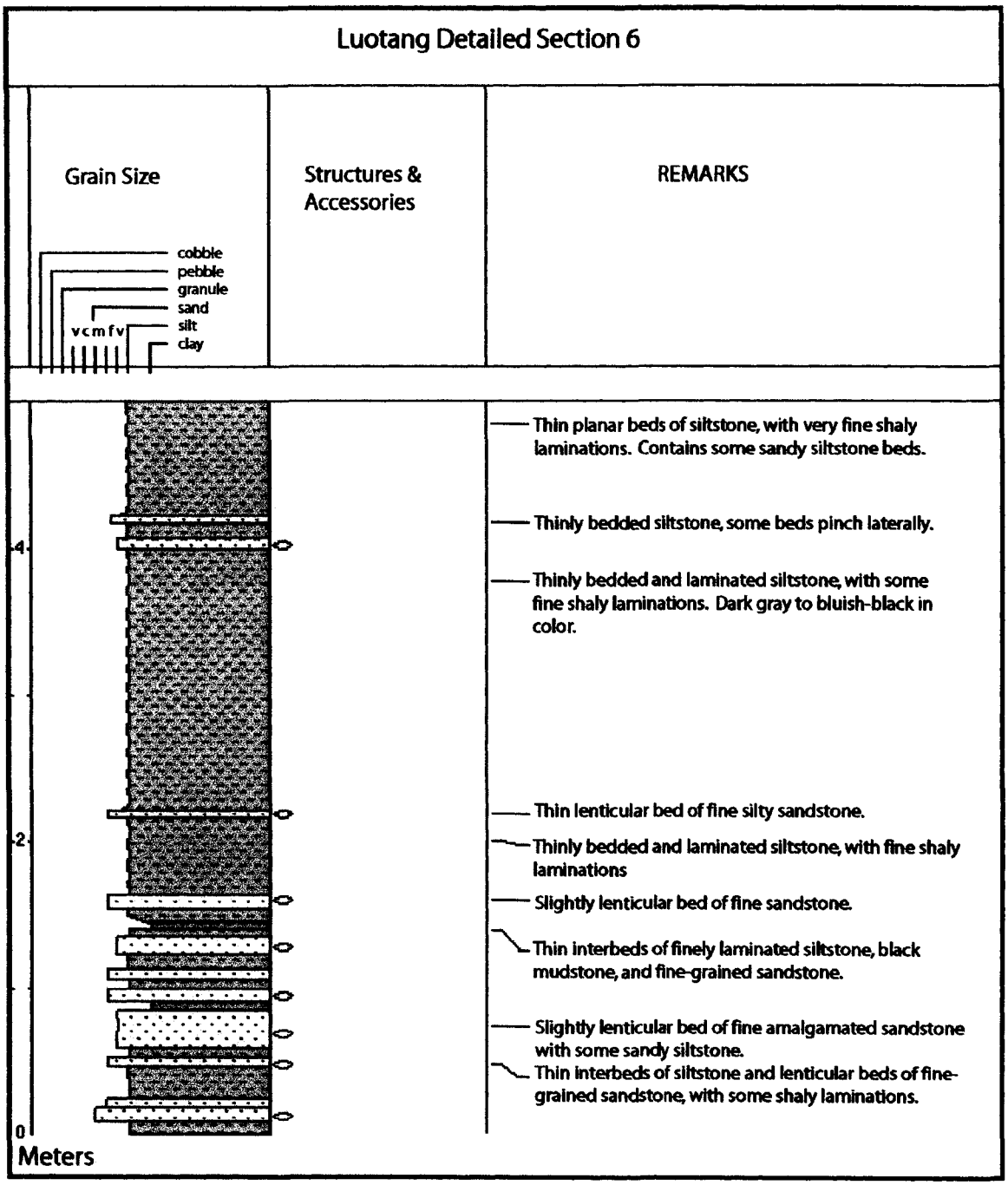

Figure 22. Detailed Section 6, illustrating the interbedding of overbank, cravasse-splay and mid-fan channel facies deposits within the middle Hengdan Group.

Figure 23. Photomicrograph of sample #02LT22, displaying poor sorting and diagenetic matrix, but with an increase in quartz grains relative to felspar or lithic fragments. Arrow is 0.25 mm long.

interval continue to display poor sorting, angularity, and diagenetic matrix, although a slight increase in quartz grains is recognizable (Fig. 23). This part of the section has undergone sufficient deformation to cause minor flattening of the pebbles. The beds range up to 1 meter thick, and contain small pyrite cubes. Up-section, coarse sandstone beds begin to display lenticular form, range up to 1.5 m thick, and are commonly overlain by a series of smaller sandstone lenses and thin planar beds of medium to fine-grained sandstone andsiltstone. Rip-up clasts indicating erosive, high-density turbidity currents continue to be common within the thicker beds. This sequence continues up to 11.5 km, and is represented by detailed section #7 (Fig 24).

The interval from 11.5 to 11.7 km marks a minor return of thinly bedded sediments, capping the eighth coarsening upward cycle, although the system remains sand-dominated for the remainder of the measured section. Within this thinly bedded interval,

medium to fine-grained sandstone with an average bed thickness of 10 cm alternates with minor siltstone beds. Another epiclastic tuff layer approximately 10 cm thick appears near the base of the interval. At 11.7 km, beds of medium to coarse-grained sandstone up to 70 cm thick appear, overlain by increasingly thicker and coarser beds.

Above 11.7 km are numerous coarse to pebbly sandstone beds ranging from 1 to 1.5 m thick. The beds appear normally graded, have erosive bases with rip-up clasts, and are capped by intervals of thinly bedded medium to fine-grained sandstone. Thin tuffaceous intervals, commonly interbedded with finer-grained material capping thick, coarse beds, become increasingly common. Pebbly sandstone to cobble conglomerate intervals appear at the base of thickest beds, with dark colored volcanic clasts most prevalent. Clasts consistently show metamorphic flattening sub-parallel to relict bedding. Between 11.8 and 11.9 km, a number of recent landslide deposits and vegetation-covered slopes obscure much of the underlying geology, although some moderately thick beds of fine to medium-grained sandstone, and small sandstone lenses were still observed.
At 11.9 km, a thin interval of thinly bedded fine-to medium-grained sandstone gives way to massive channel structures. Here, lenticular beds over 2 meters thick are composed primarily of very coarse sandstone. The channel structures are normally graded, and are commonly composed of gravel conglomerate, pebbly sandstone, or granular sandstone near their bases. They truncate thinner beds of alternating medium to fine-grained sandstone, and range from 15 to 40 cm thick.

At 12 km above the base of the section, a number of thick, coarse-grained sandstone channel structures containing large-scale bar-form crossbedding occur (Fig. 24). Such large–scale crossbedding within a submarine fan environment occurs along the outside

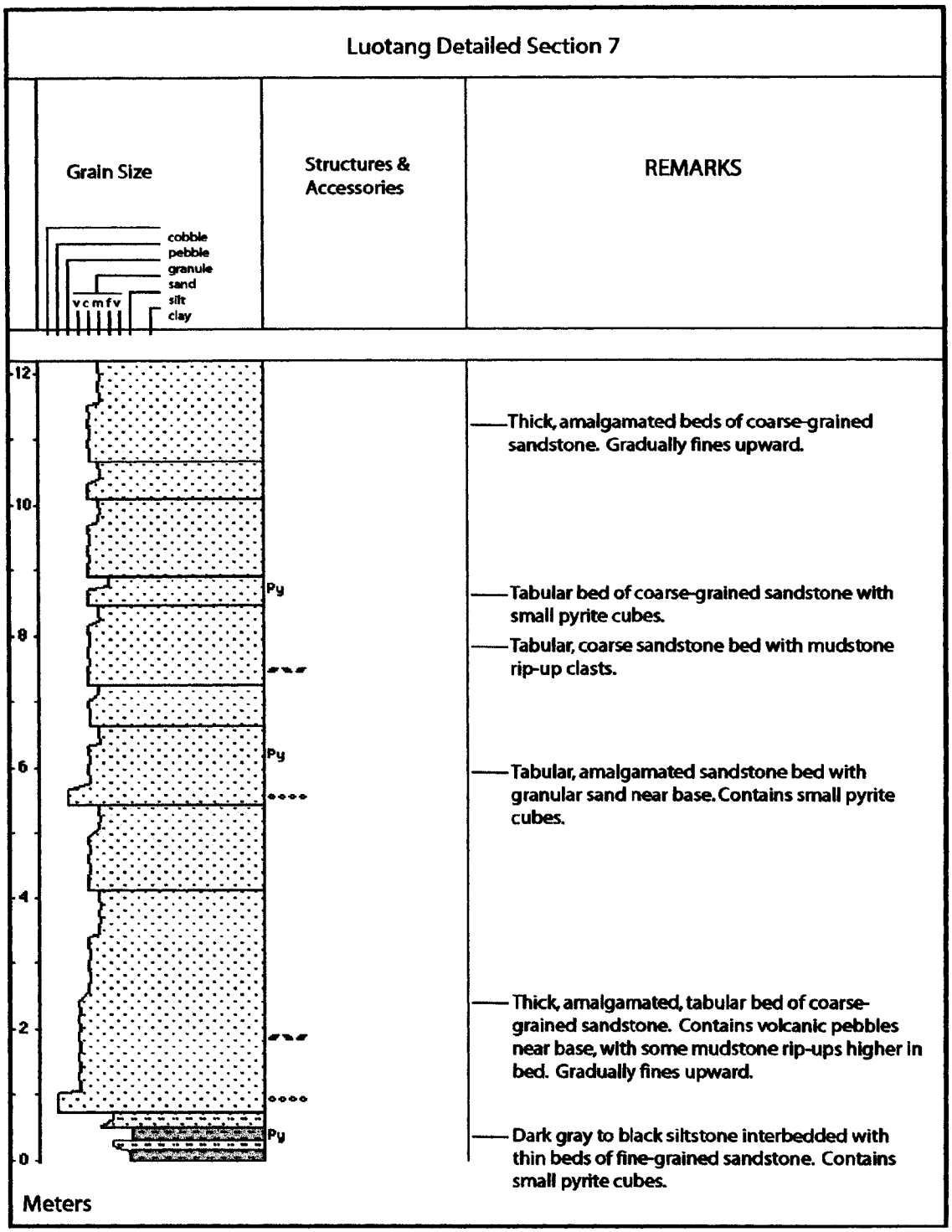

Figure 24. Detailed Section 7, illustrating coarse-grained, amalgamated sandstone beds marking a coarsening-upward shift.

bends of large distributary channels, and form by aggradation when channels migrate laterally (Peakall et al., 2000). Sediment aggradation along the channel wall is caused by overspill of turbidity currents unable to negotiate bends in the distributary channel. Coarser sands are deposited along the channel margin, while finer sediment crests the channel to form overbank deposits.

An amalgamated epiclastic tuff bed up to 1 meter thick with sandy horizons caps the interval, and represents abandonment of the channel. Thinly bedded sandstones of overbank facies dominate the section thereafter for several hundred meters, marking the end of the ninth coarsening upward cycle. The beds consist of medium-to fine-grained sandstone and phyllitic siltstone, with a number of thin ashy beds. Upward through the section beds thicken and coarsen slightly, with a reappearance of thick, coarse-grained sandstone beds near 12.4 km. Here thick, normally-graded beds grade from pebbly sandstone at their bases, to fine-grained sandstone, and are occasionally capped by thin phyllitic siltstone or ashy beds. Epiclastic tuff beds appear with increasing regularity, most often interbedded with finer grained material, but occasionally overlie coarse to pebbly sandstone. Many coarser beds are slightly lenticular in form, and occasionally may be seen truncating underlying sandstone/siltstone beds. The depositional environment of this thickly bedded, coarse-grained sandstone sequence is characteristic of deposition within an inner fan environment, and is illustrated in detailed section #8 (Fig 26). Inner fan deposits typically consist of thickly bedded, coarse- grained amalgamated sandstones that commonly display erosive bases with rip-up clasts, lenticularity, and commonly are interbedded with little or no pelitic sediment (Nilsen, 1984).

Figure 25. A photo of large-scale channel margin crossbedding, a standard clipboard at center bottom for scale.

A shift to thinner, planar sandstone beds occurs at 12.5 km, marking the end of the tenth coarsening upward cycle. Thin planar beds dominate the stratigraphy upsection for more than 1 km. Within this section, beds alternate from coarse to medium-grained sandstone beds 6 to 10 cm thick, to fine-grained sandstone, with minor siltstone and tuff beds 3 to 6 cm thick. Normal grading is common throughout this section, and a number of the coarser, thicker beds have small rip-up clasts. Beds become thicker and increasingly coarse up-section, with a few beds of pebble conglomerate nearly 1 m thick displaying erosive bases and rip-up clasts. An epiclastic tuff bed near the top of this section is approximately 80 cm thick.

Extremely thick channel sandstones return near 13.65 km, with several beds exceeding 3 meters in thickness. Sand within these beds is generally very coarse, ranging

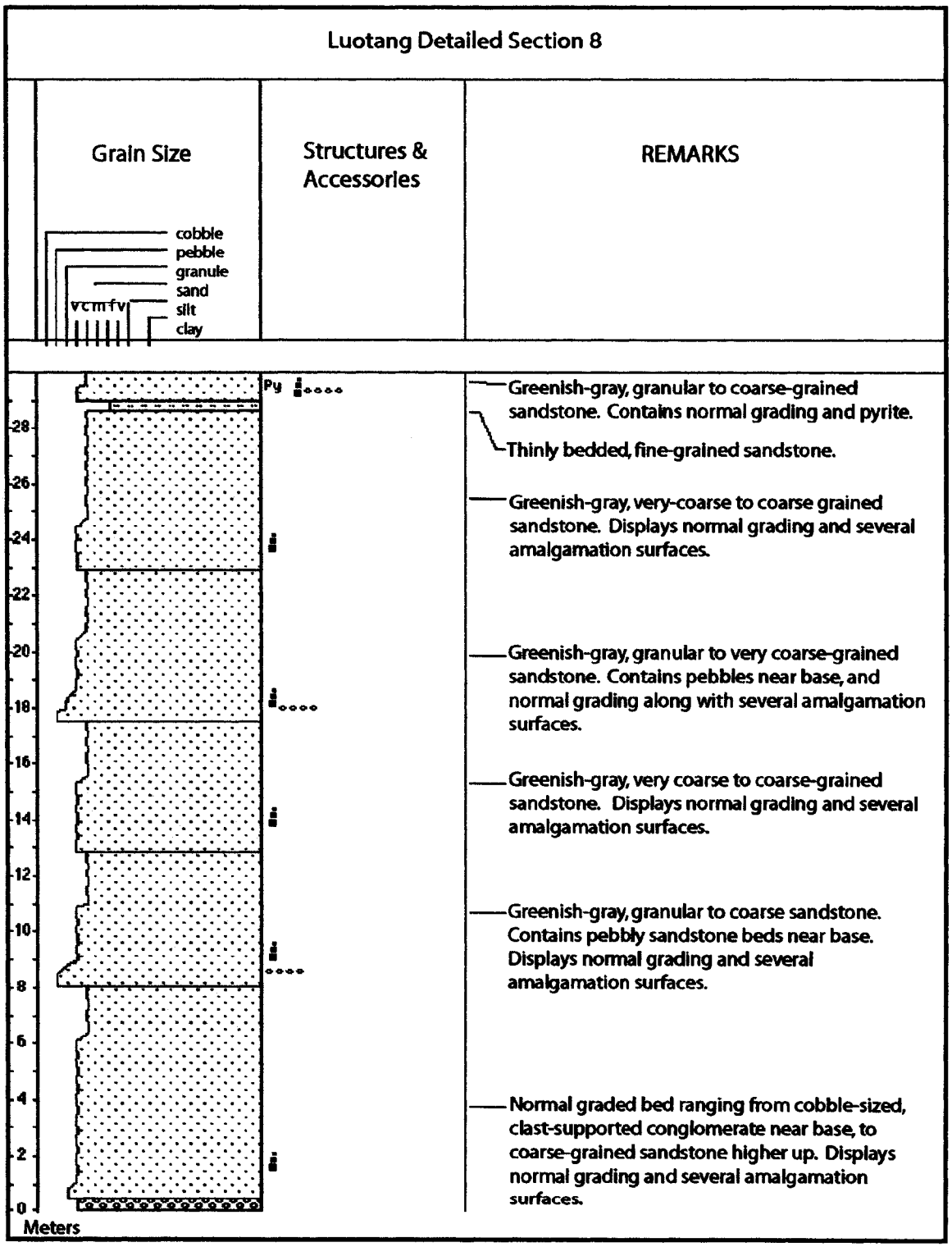

Figure 26. Detailed Section 8, illustrating thick, amalgamated, coarse-grained sandstone beds typical of inner-fan facies.

from pebbly sandstone or granular sandstone, and fining upwards through a series of amalgamated beds. These broad channel sands are in turn capped by thin beds of medium to fine-grained sandstone, and a number of epiclastic ash beds 40 cm to 1 m thick. A series of alternating, normally graded, coarse to fine-grained sandstone beds up to 1 m thick continue up-section for several hundred meters. Tuff beds up to 1 m thick become increasingly common. Tuff sample 02LT37 was collected for geochronology within this interval. Results of the geochronological analyses are presented in Chapter 4. An interval of thinly bedded sandstone from 13.7 to 13.85 km above the base of the section marks the end of the eleventh coarsening upward cycle.

Another interval of extremely thick-bedded sandstone occurs 14.2 km above the base of the section, with individual amalgamated beds exceeding 3 m in thickness. Beds show normal grading near their bases, generally from pebbly sandstone or matrix-supported gravel to cobble conglomerate near their bases, and fine upward to massive coarse-grained sandstone. Pebbles appear consistently flattened by metamorphism, and are predominantly composed of dark-colored volcanic rock. Thick sand intervals are commonly capped by thin alternating sandstones of predominantly medium-grain size, with occasional tuffaceous beds. From 14.3 km to 14.7 km, alternating beds of thick, coarse-grained sandstone, and thinner beds of medium to fine grained sandstone are most common, with a few beds of fining-upward pebbly sandstone. Small pyrite cubes continue to be common throughout the section.

Beginning at 14.7 km, thick bedded, very coarse to pebbly sandstones dominate. Beds range from 80 cm to over a meter thick, display normal grading, and commonly contain pebble to cobble matrix-supported conglomerate near their bases. Metamorphic

grade continues to increase, with conglomeratic clasts showing significant flattening. Grayish-green phyllitic ash and dark volcanic clasts are most common. The rock is a medium-dark green color, and metamorphism begins to obscure grain-size changes. Epiclastic tuff beds begin to appear every few meters, ranging from a few cm thick, to several meters thick. An extremely thick tuffaceous sequence measuring 22 m thick occurs near 15 km. Sample 02LT41 for geochronology was collected near the base of this unit. Relatively thickly bedded, very coarse to pebbly sandstone continues to 15.5 km.

The remaining few hundred meters of measured section consists of thinner beds of alternating coarse to fine-grained sandstone with minor phyllitic siltstone and epiclastic tuff, marking the end of the twelfth coarsening upward cycle. This shift is illustrated in detailed section #9 (Fig. 27). A decision to stop measuring was made near 15.65 km due to the increasing shear deformation and metamorphic grade. The increase in deformation and metamorphic grade appears to be related to the increasing proximity to the FT fault, which separates the Hengdan Group from the upper Bikou Group. The remaining section was walked to the fault contact, which is not locally exposed, and a brief examination of the upper Bikou (Yangba Fm) was made.

The remainder of the Hengdan Group that was not measured consists of alternating thick beds of coarse to pebbly sandstone and conglomerate, with intervals of thinly bedded medium-to fine-grained sandstone. Tuffaceous beds are common, and thin felsic dikes and sills approximately 30 cm thick intrude the section. U-Pb SHRIMP zircon dating of one of these dikes by colleagues at the Chinese Academy of Geological Sciences indicates a Triassic age of approximately 209 $\pm$ 3 Ma (unpublished data). Near

the boundary with the Bikou Group, a muscovite sheen becomes apparent along many of the foliation planes, and pebble clasts are profoundly flattened by deformation (Fig. 28).

The upper Bikou Group at this locality appears very similar to the upper Hengdan Group, and is dominated by coarse-grained turbidite deposits, interbedded with thick sequences of epiclastic ash. A number of thick greenstone beds appear within the sequence, but it is difficult to determine if the mafic or intermediate volcanic rocks were intruded as sills, or formed as lava or pyroclastic flows interbedded with the volcaniclastic turbidites. The depositional environment within this section of the Bikou Group is also similar to the Hengdan Group, and is dominated by marine sediments deposited within a submarine fan environment. The fairly coarse-grained sediments, and increased volcanic input suggest a proximal, inner fan setting. There is no evidence of either shallow marine or terrestrial deposition.

Several days of observations were also made within the central Bikou Group near the town of Bikou. Here the Bikou Group consists of voluminous amounts of tuff and possibly pyroclastic material metamorphosed to schist grade. Bedded intervals of tuff that are several hundred meters thick are common, as are numerous smaller-scale mafic to intermediate lava flows metamorphosed to greenstone. Locally, many of the greenstone units bear thin veinlets of pyrite, chalcopyrite and minor bornite, and an active copper mining operation was observed west of Bikou. However, thin intervals of bedded volcaniclastic sandstone and conglomerate persist, and many of the tuffaceous beds have sandy intervals that suggest re-working in a marine environment or possible fluvial-alluvial environment. Given the metamorphic grade and voluminous fine-grained

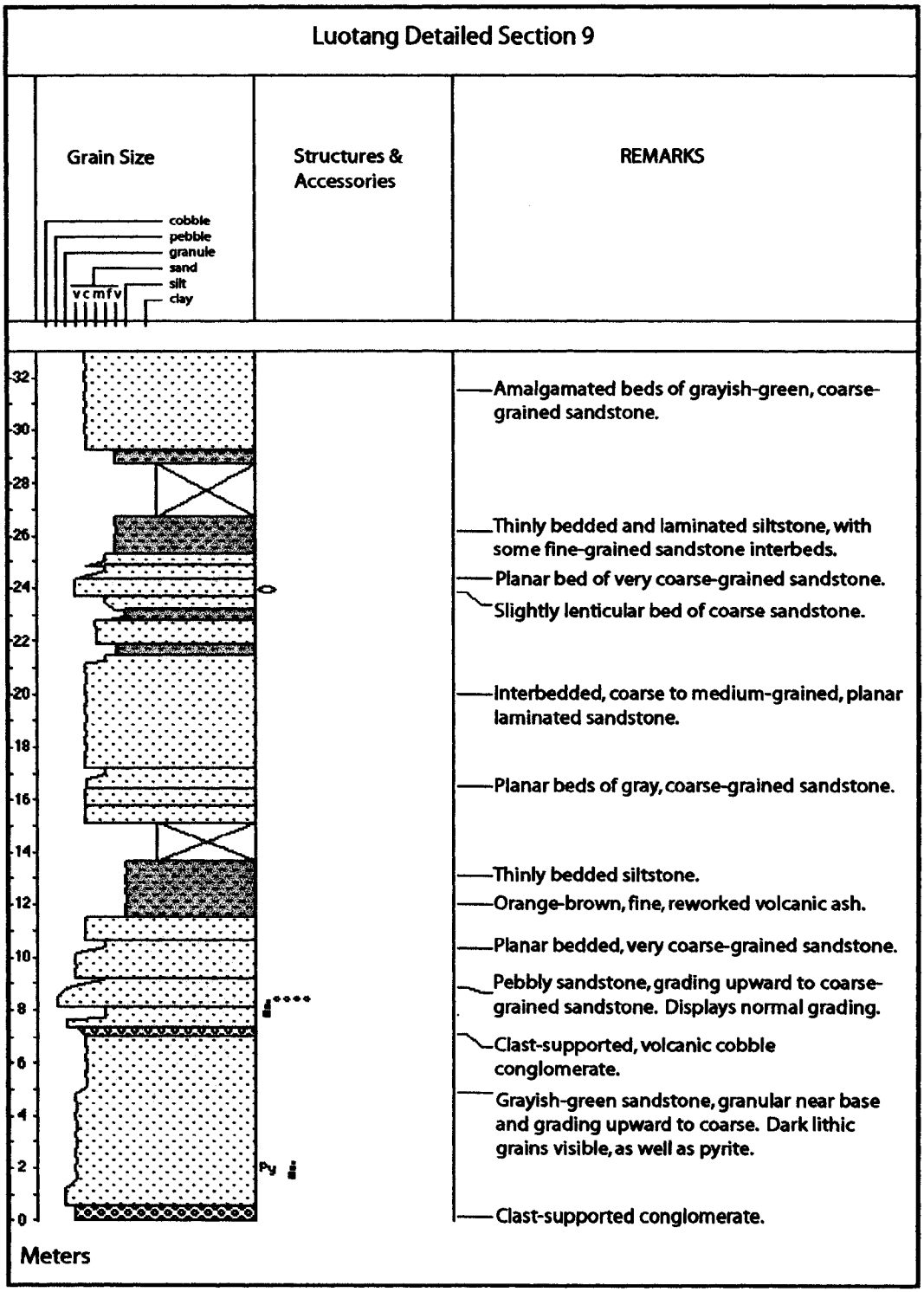

Figure 27. Detailed Section 9, illustrating the end of a coarsening upward cycle.

Figure 27. A photo of a stretched-pebble conglomerate within the upper Hengdan Group adjacent to the FT fault.

tuffaceous material, the distinction between marine, marginal marine or fluvial-alluvial deposition is difficult to determine.

A number of small intrusive bodies were also observed in this portion of the Bikou Group. They range from small stocks, dikes and sills of diorite and granodiorite, to more mafic gabbros and serpentinites. These intrusive bodies appear to have been affected by the same greenschist metamorphism as the tuffaceous to pyroclastic host rock. Bedding and foliation generally continue to dip to the southeast, with numerous faulted intervals recognizable by intense shearing and gouge.

Stratigraphy of the Hengdan Group: Wenxie Section

Similar to the Luotong section, the Hengdan Group within Wenxie County forms a moderate to steeply southeast dipping homocline, and is in fault contact with Paleozoic and younger rocks to the northwest. These strata consist of the carbonate dominated Devonian Sanhekou Group, as well as the Triassic (?) Guanjiagou Formation. The Guanjiagou Formation appears on the Chinese Geological Survey maps (unpublished data) as Sinian (Late Proterozoic) strata. Colleagues from the Chinese Academy of Geological Sciences performed $^{40}Ar/^{39}Ar$ dating of volcanic clasts within debris flow and turbidite deposits of the Guanjiagou Formation following this study, in order to evaluate its relationship with the Hengdan Group. The dating indicates a Triassic or younger age for the Guanjiagou Formation (Yan et al., 2003), correlating possibly to the Triassic Songpan-Ganze remnant ocean basin of Zhou and Graham (1996). However, given the lower greenschist grade of metamorphism (Tao, 1993; Wei, 1995), it is not certain that the ages were not reset. Deposits of the Songpan-Ganze remnant ocean are common to the southwest of the study area. Remnants of local Jurassic and younger sedimentary cover are generally composed of terrestrial sandstones and conglomerates (Yan, pers. comm.). Geologic relationships and the location of both measured and observed sections are detailed on the Wenxie location map (Fig. 29).

Metamorphic grade within the Hengdan Group in the vicinity of Wenxie is of slightly higher grade than in the vicinity of Luotang, but shows a similar gradual increase of grade to the southeast. Stratigraphically, the Wenxie section shows many similarities to the Luotong section, with some relatively minor differences in the style of sedimentation. The Wenxie section was measured within Qujiagou valley, eastward toward the

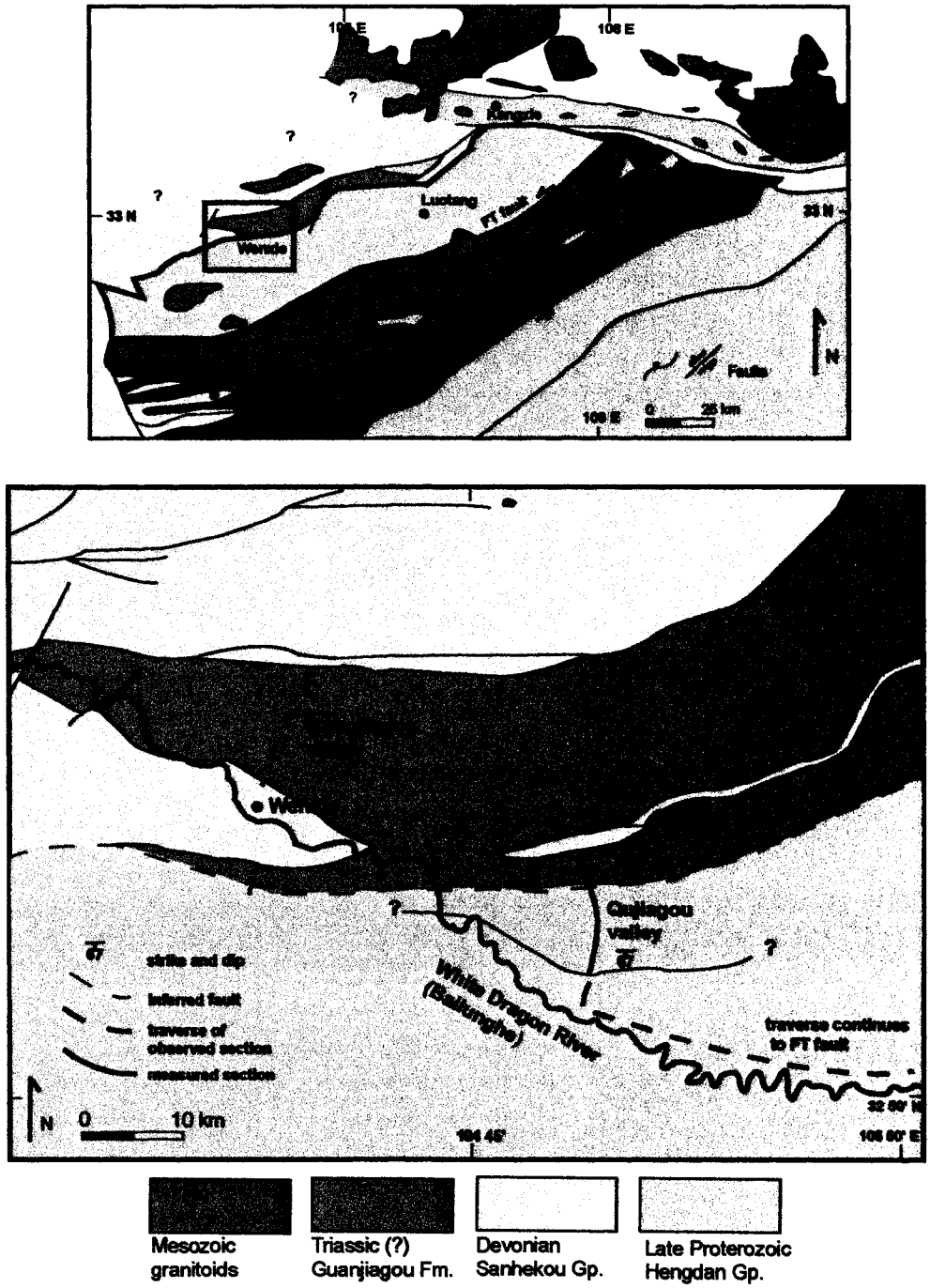

Figure 28. Location map of the Wenxie vicinity. Dashed lines indicate observed section, the measured section is marked by a solid red line.

Bailunghe (White Dragon River). The complete measured section appears within the appendixes (Appendix II). The Qujiagou valley forms a narrow, steep walled canyon in its upper reaches near the contact between the Hengdan Group and the Sanhekou Group, which broadens to the east. The boundary fault is identifiable as a highly sheared and weathered zone of micaceous meta-pelites approximately 100 m wide, with shear fabric dipping very steeply southeast.

The strata appearing as basal Hengdan on the Chinese Geological Survey maps (unpublished data) within Qujiagou valley are largely composed of black, thinly bedded phyllite grade meta-pelites with a number of thickly bedded, matrix-supported debris flows. The lowest 120 m of section consists of matrix-supported pebbly conglomerate beds, ranging from 1 to 1.5 m thick, interbedded with thinner, tabular beds of phyllitic shale, coarse sandstone, and clast supported pebbly conglomerate. A number of the beds appear sheared within close proximity to the bounding fault. The matrix-supported conglomerates are mostly composed of mud-sized sediment, with a mixed pebble-clast population composed of granite, gneiss, quartz, chert, quartzite, and dark colored mafic to felsic volcanic aphenites and porphyrys.

Within the interval of 120 to 480 meters, moderately thick beds of coarse sandstone, pebbly matrix to clast-supported conglomerate ranging from 10 to 30 cm thick are interbedded with thinly bedded, black, carbon-rich phyllitic shales. Some of the coarse sandstone and clast-supported conglomerate beds show signs of normal grading. Above a vegetation-covered interval from 480 to 650 meters containing a few scattered outcrops of thinly bedded black phyllites and fine-grained sandstone, no beds containing anything

coarser that medium-grained sand are encountered for the remainder of the measured section.

There is marked similarity between debris flow deposits and conglomerate clast populations of these units mapped as basal Hengdan in Qujiagou valley, and the Guanjiagou Formation within Guanjiagou valley located a few km to the southwest along strike. It is therefore interpreted that the coarse-grained debris flows of Qujiagou valley are part of the Guanjiagou Formation, and that an inferred fault cuts through the vegetation covered interval separating the debris flows from highly repetitious phyllites within the basal Hengdan Group.

From 650 to 725 meters, thin interbeds of pyrite-rich phyllites and fine sandstone form a highly repetitious interval reminiscent of the basal section in Luotong County. Minor deformation within these beds is possibly soft-sediment folding, but could also be attributed to compaction or tectonism. The interval of 725 m to 1.5 km consists of repetitious alternating thin, planar beds of fine to medium-grained sandstone, siltstone, and black phyllitic shale. Beds average a few cm thick, with some of the medium-grained sandstone beds ranging up to 20 cm thick. Small pyrite cubes up to a few mm in diameter continue to be common throughout the section.

From approximately 1.5 km above the base of the section, sediment grain size decreases, and thin interbeds of alternating black, carbon-rich phyllitic shale and siltstone become the dominant lithology. This interval is extremely repetitious, and is indicative of hemipelagic to very distal turbidite deposition along a fan fringe. The thinly bedded, carbon-rich pelites are also identical to the basal member of the Luotong section. This repetition continues for nearly a km of section, until the color of the sediment grades to

greenish near the 2.4 km interval. However, increasing small-scale deformation, quartz veins and increasingly greenish coloration (possibly a sign of increasing metamorphic grade) and are all that distinguish the remaining upper section from the lower.

Near the 3.2 km interval, a number of highly contorted beds and a zone of intense shearing and deformation nearly 500 m wide indicates the presence of a major fault. Shear fabrics within this zone generally dip steeply to the southeast. To the southeast across this zone, metamorphic grade appears to increase slightly, and as a result section was not measured beyond this structure. Although measurement ceased across the fault, observations of stratigraphic and sedimentological changes continued eastward along the White Dragon River to the boundary of the Bikou Group. Descriptions of thickness given for the remaining section are relative rather than true thickness.

Moving southeastward and upward through the section, the lithology differs little across the fault. For approximately 1 km, thinly bedded, highly repetitious shale/siltstone interbeds continue with some minor folding and contorted bedding. Near the junction with the White Dragon River, thin rhythmic interbeds of fine-grained sandstone, phyllitic siltstone and shale begin to appear, and continue for several hundred meters. Outcrops here show strong shear deformation and numerous quartz veins cut the section. Metamorphism appears to increase toward lower schist grade. Although general grain-size changes delineate bedding, many small-scale sedimentary structures appear overprinted by metamorphism. Pyrite cubes continue to be a common accessory throughout the section.

For the next kilometer, intervals of fine to medium-grained sandstone interbedded with siltstone and shale appear to have formed as small fan lobes within an outer fan

environment. Sand-rich beds are capped by thick intervals of repetitious shale and siltstone, indicating abandonment of sand-rich lobes, followed by burial by hemipelagic sedimentation and dilute turbidity currents. This sequence is a capped by a thick bed of coarse-grained sediment composed of tabular, medium-grained sandstone, thick beds of coarse-grained sandstone, cobbley matrix-supported conglomerates, and thin beds of matrix-supported gravel conglomerate and pebbly sandstone. Matrix-supported conglomerates here have a coarse-grained sand matrix, and cobbles display a pronounced shearing/flattening sub-parallel to the moderate to steeply southeast dip of relict bedding. Identifiable clasts include dark colored volcanic aphenites, vein quartz, and minor granitoids or porphyries.

Following several hundred meters of thickly bedded, coarse-grained sandstone and conglomerate, the sequence thins and fines upward to thin sandstone/shale interbeds, and finally to a thick section of repetitious shale that continues for several hundred meters. This pattern appears to repeat itself shortly thereafter, as an interval of thinly bedded fine to medium-grained sandstone and shale reappears, and gives way to another interval of thickly bedded, coarse-grained sandstone and matrix-supported conglomerates. Conglomerate clasts are profoundly flattened, but are easily visible along foliations. There is an apparent increase in the proportion of dark volcanic aphenites and porphyrys, with a minor contribution of granitic clasts. Thickly-bedded, slightly lenticular, coarse-grained sandstone beds overlie the conglomerates, and are in turn overlain by fining and thinning upward beds of fine-grained sandstone, siltstone and shale. This coarse sediment dominated interval continues for approximately 200 m past the village of Hengdan, where a lengthy alluvium covered interval follows.

The poor sorting and matrix-support of the conglomerate beds described above suggests deposition by debris flows, interbedded with coarse sandstone, graded rhythmites and pelagic shales of turbidite origin. The strata of this interval suggests progradation of coarse-sediment lobes onto hemi-pelagic or distal fan deposits, followed by abandonment due to autocyclic switching of the active deposystem laterally to a new lobe. Although conglomerates and debris flows were not encountered until higher in the section within the Luotong section, the pattern is similar to the submarine fan over basin-plain progradation seen there.

Moving southeastward, thin interbeds of fine to medium-grained sandstone and pelitic phyllite with some coarser tabular beds dominates for several hundred meters. Such deposits are typical of mid-fan environments or the more proximal portions of an outer fan. Of special note within this interval is the appearance of thin ashy beds a few cm thick, seen sporadically interbedded with the alternating beds. This first appearance within the Wenxie section is similar to the stratigraphic position as the first notable ashy beds in the Luotong section, although a direct stratigraphic correlation on this point is difficult to make in light of faulting at the base of both sections and elsewhere.

Immediately above this interval are thick beds of slightly lenticular, matrix-supported cobble conglomerates with matrixes composed of resedimented ash. Overlying these ashy debris flow deposits are a series of thick-bedded, clast supported pebble conglomerates, coarse sandstone, and pebbly sandstone, which commonly exhibit normal grading. Bedding thins and fines upward after approximately 150 m, with thin sandstone, shale, siltstone, and dilute tuffaceous beds most common. This sequence of thick, coarse-grained sediment probably represents the progradation of a submarine fan lobe, with

thinning and fining upward beds indicating channel/lobe abandonment and a return to overbank facies deposition.

The remainder of the Wenxie section, continuing for a few km until the boundary with the Bikou Group, is largely a continuation of the pattern of coarsening and thickening upward lobe progradation, followed by thinning and fining upward lobe abandonment. Together these deposits form a series of stacked progradational lobes and overbank deposits indicative of middle fan deposition. Upsection, debris flow deposits decrease and are replaced by clast-supported pebble conglomerates.

Stratigraphy of the Guanjiagou Formation

Located immediately northwest of the town of Wenxie lies the Guanjiagou Formation, a unit that has a controversial correlation to the Hengdan Group. The Guanjiagou Formation was originally mapped as Devonian, and then reassigned as a Neoproterozoic "tillite" (Yan, pers. comm.; unpublished Chinese Geological Survey maps). Due to the uncertain age of the Guanjiagou Formation, and possible correlation with the Hengdan Group, a closer examination of the Guanjiagou Formation was warranted.

Similar to Qujiagou valley, the Guanjiagou Formation is located within the Guanjiagou Valley, which forms a narrow canyon in its upper reaches and broadens to the south. The Guanjiagou Formation is in fault contact with the Devonian Sanhekou Group (unpublished Chinese Geological Survey maps). The contact comprises a wide, vertically dipping shear zone. Although little section is continuously exposed section in the upper valley, bedding dips generally moderately to steeply to the south/southwest.

The basal beds within the Guanjiagou Formation are composed of black phyllitic shale, with up to 1-meter thick beds of coarse volcaniclastic sandstone, grading upward into medium and fine-grained sandstone, and capped by phyllitic siltstone/shale. The bases of the sandstone units truncate the underlying shale, and some rip-up clasts are apparent. A number of coarse sandy, matrix-supported conglomerates appear in the section (Fig. 30), interbedded with phyllitic shale and coarse graded sandstone. Clasts in the conglomerate are cobble-sized and composed of granitic and dark volcanic rock. Some of the shaly beds within this section exhibit soft-sediment deformation.

Moving up-section a few hundred meters, a number of the coarse, graded sandstone beds exhibit water escape structures such as flame structures and dish-and-pillar structures. Graded sandstone beds continue to exhibit eroded bases, and shale

Figure 30. Volcanic cobbles within a matrix-supported conglomerate.

intervals commonly display soft-sediment folding. Matrix-supported conglomerates continue intermittently, with some clasts reaching boulder size. Granitic and dark volcanic lithologies dominate the clast population, supported in a matrix of mudstone to coarse sandstone. At one location, a shale fold appears beveled off by the erosive base of an overlying coarse sandstone bed, evidence that the folding was syn-sedimentary.

The persistence of sandstone beds exhibiting eroded bases, water escape structures, soft sediment slump structures, and containing boulders (Fig. 31) generally correlates to the high-density turbidity currents of Lowe (1982). These facies divisions generally correspond to deposition within the proximal portion of a submarine fan, possibly near

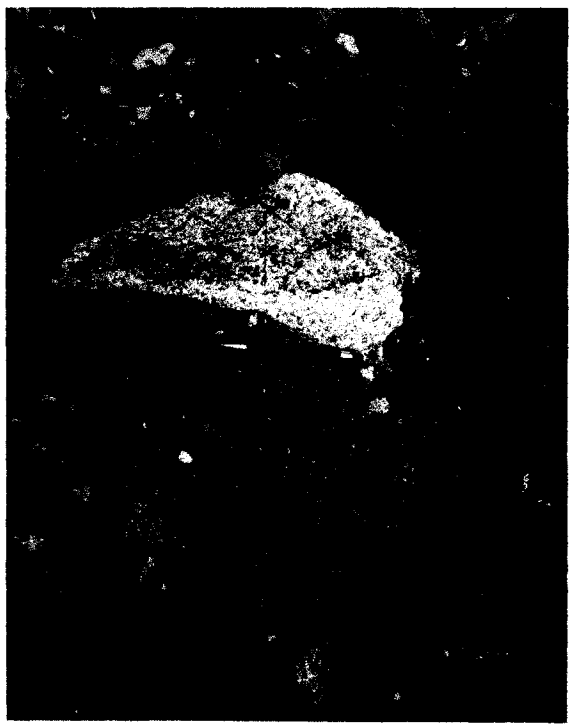

Figure 31. A matrix-supported conglomerate (debris flow) with a water escape structure above a quartzite boulder.

the base of a rise or submarine canyon mouth. However, as large-scale channel features are not recognizable in the limited outcrop along the vegetated valley slopes, this interpretation is difficult to substantiate.

An interval of thick, amalgamated, medium-grained sandstone beds follow for several 10's of meters, followed by more matrix-supported conglomerates. The conglomerate clast population within this section appears to be dominated by intermediate to felsic porphyrys, with minor amounts of granite and dark volcanic aphenites. For several hundred meters upsection, beds of normally graded medium to coarse-grained sandstone, alternating with pelitic intervals and pebbly to cobbley matrix-supported conglomerates continue to dominate. Clast populations repeatedly shift from granite dominated to volcanic dominated, with felsic to intermediate porphyries, dark to gray-green aphenites, and tuffaceous lithologies most common. Some clasts of chert and possibly quartzite also appear. Some beds of granular to pebbly debris flows appear within the section, the granules/pebbles are almost entirely composed of black to reddish brown lithic grains, with a brecciated appearance. Photomicrographs indicate that sandstones within this section are compositionally and texturally immature, but that lithic grains are of mixed volcanic and metamorphic sources (Fig. 32).

The sequence of matrix supported conglomerates with volcanic and plutonic clasts, graded sandstone and pelitic intervals repeats upsection for the remainder of the traverse through Guanjiagou valley, for a total thickness of several km. At several locations, large south-dipping shear zones cut the section, suggesting the possibility of section repetition. The southern boundary of the unit is a south dipping fault contact with a Carboniferous

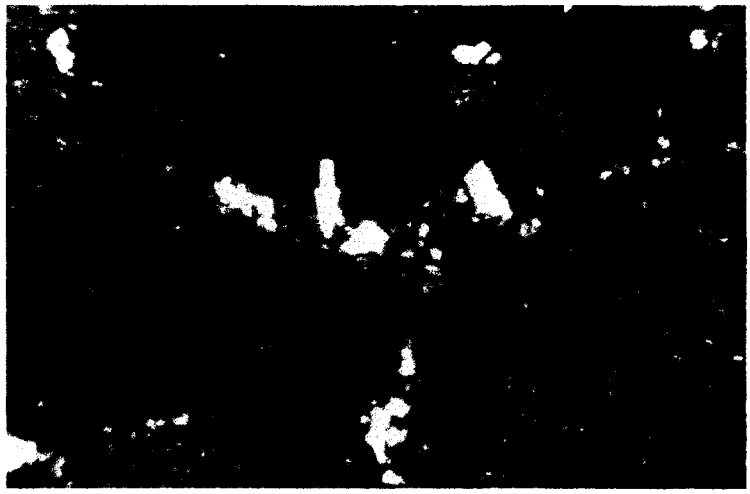

Figure 31. Photomicrograph of sample 02WE43, a granular lithic greywacke composed of mixed volcanic and metamorphic lithic grains. Arrow is 0.25 mm long.

marble unit (unpublished Chinese Geological Survey maps), which in turn is fault-bounded and juxtaposed with the Hengdan Group a few km further south.

Summary and Comparison of the Luotang and the Wenxie Sections of the Hengdan Group

The Luotang and Wenxie sections of the Hengdan Group display strong similarities, with relatively few differences in sedimentary style. Both sections consist of relatively sand-rich marine turbidites with a distinctly immature volcanic arc provenance. Both sections also display a marked prograding and coarsening upward trend, with progressively coarser and thicker beds of sandstone and conglomerate higher in the section, which is in sharp contrast to thick, repetitious intervals of black phyllites of probable basin-plain affinity at the base of the sections. An increasing input of reworked tuff also occurs within the upper portions of both the Luotang and Wenxie sections. By

all indications, the Hengdan basin comprises of relatively deep-marine, volcaniclastic sediments, and nowhere within the basin is there clear evidence of terrestrial or shallow marine sedimentation.

Although correlations between the Guanjiagou Formation and the Hengdan Group remain controversial, a marked difference in sediment provenance exists between these units. The Guanjiagou Formation displays sediments with a mixed volcanic and continental provenance, such as conglomerate clasts composed of quartzite, granitoids and gneiss, whereas the Hengdan Group displays a volcanic arc provenance throughout. A mixed provenance within sandstones is typically indicative of a recycled orogen, or collisional provenance (Dickinson, 1985). Subsequent to the described fieldwork, colleagues at the Chinese Academy of Geological Sciences dated plagioclase within volcanic cobbles collected from Guanjiagou valley using the $^{40}Ar/^{39}Ar$ method. Results indicate that the Guanjiagou Formation may be of Triassic or younger age (Yan et al., 2003), and possibly correlative to the Songpan-Ganze remnant ocean basin of Zhou and Graham (1996). These new data suggest that the Guanjiagou Formation comprises younger sedimentary cover, with no relation to sedimentation within the Late Proterozoic Hengdan Group.

A number of minor differences in sedimentary style occur between the Wenxie and Luotang sections, which are attributable to possible lateral changes in basin morphology. The lack of debris flow deposits within the Luotong section may be a function of shelf width, slope gradient, or sediment supply, although these geometries are nearly impossible to determine due to the fault-dismembered state of the basin today. Similarly, the apparent higher abundance of gravel to cobble-sized sediment within the

Wenxie section may be a function of increased sediment supply due to possible proximity to submarine canyons or deltas feeding sediment from the arc to the basin, although no such conduits have been presently identified. In light of possible facies variations that occur laterally and vertically throughout various basin types, differences in sedimentation between the Luotang and Wenxie sections are minor.

CHAPTER 4

GEOCHRONOLOGY

Introduction

To understand the history and tectonic setting of the Bikou terrane, it is first essential to establish reliable age control. Although numerous attempts have been made to accurately date volcanic units within the Bikou Group, no previous attempt has been made to date the Hengdan Group directly. Dates are also essential to understanding the relationships among the units comprising the Bikou terrane. Until recently, estimated ages for the Hengdan Group were derived from rough correlation with ages obtained from Bikou Group volcanic units. A persistent problem has been the broad range of Middle to Late Proterozoic dates obtained from the Bikou Group based on a variety of dating techniques, including K-Ar, $^{40}Ar/^{39}Ar$, Rb-Sr, and conventional U-Pb. Given the susceptibility of these techniques to alteration, metamorphism or inheritance, reliance on these data has made it difficult to assess the actual volcanic emplacement age of the Bikou Terrane, and thus develop a coherent tectonic history.

Recently, an effort has been undertaken by one of my Chinese collaborators (Yan Quanren of CAGS) to provide reliable age control for the Bikou Group through the use of U-Pb SHRIMP zircon dating of volcanic rocks within the Bikou arc. Mafic to

intermediate lava and rhyolitic tuff samples collected from lower, middle and upper sections of the Bikou Group yielded ages ranging from 846 ± 19 Ma for the lower Bikou Group, 790 ± 15 for the middle Bikou Group, to 776 ± 13 Ma for the upper (Q. Yan, unpublished data). These ages are similar to previously reported conventional U-Pb zircon ages of 764 ± 1.9 Ma, and 768 ± 2.9 for the upper Bikou Group, and an 853.4 ± 3.4 Ma. age for the lower Bikou Group reported by Zhao and others (1990). Given the broad agreement between the conventional U-Pb zircon ages and SHRIMP U-Pb zircon ages, the Bikou arc may be now regarded as a long-lived volcanic center within the Middle Neoproterozoic.

The Hengdan Group is generally considered to be age-correlative to the Bikou Group, as the large volume of volcaniclastic sediment and tuff within the Hengdan Group has an obvious possible source area within the adjacent Bikou arc. This correlation is further strengthened by the fact that within both units metamorphic grade and deformation are similar, no other major Late Proterozoic volcanic units are located within the area, and paleocurrents indicate transport of sediment from the direction of the Bikou arc into the Hengdan basin. However, the Bikou arc and the Hengdan basin are separated by a fault and consequently are not directly correlatable. Therefore, providing age control for the Hengdan basin could either strengthen this correlation or refute it.

One of the important lithologic components found within the Hengdan basin are ashy slates and phyllites that are interbedded commonly with the thinner and finer-grained turbidites of the upper Hengdan Group. Recent studies of Mio-Pliocene forearc deposits of Japan have revealed a large component of resedimented airfall tuff (Stow et al., 1998). These epiclastic deposits are interpreted to have formed as dilute turbidites or

hemipelagic settling, following volcanic activity. Efforts to date zircons within resedimented tuffs using the U-Pb system in Jurassic basins of the Southern Alps (Mundil et al., 1996), and in Devonian basins of Australia (Jagodzinski and Black, 1999) have provided age constraints with high precision. Given the reasonable success of dating epiclastic tuffs using the U-Pb zircon system elsewhere, attempts to date several tuff layers within the Hengdan Group were undertaken both at the Academy of Geological Studies at Beijing, and the Stanford/USGS SHRIMP-RG laboratory in Stanford, California.

Methods

Samples of several reworked tuff layers were collected within the upper portion of the Luotong section, with care taken in the field to select only those tuffs that appeared relatively unmixed with volcaniclastic sand. Thin sections cut from these samples revealed however that almost all of these units were mixed with sand to some degree, indicating tuffaceous sandstone. Two samples were selected for zircon separation, the position of these samples, 02LT37 and 02LT41, are marked on the Luotong stratigraphic column. Both samples are composed of volcaniclastic sand within a matrix of yellowish tan altered tuff (Fig. 33).

The samples were mechanically crushed and sieved to obtain the 60 to 100 micron fraction. The samples were rinsed of clay-sized particles, and then alternately soaked in hydrogen peroxide, and 10% acetic acid solution in order to remove reactive clays and carbonates. Efforts to obtain a heavy mineral fraction first involved using Lithium-metatungstate (L.M.T.), but proved exceedingly time consuming. Heavy mineral

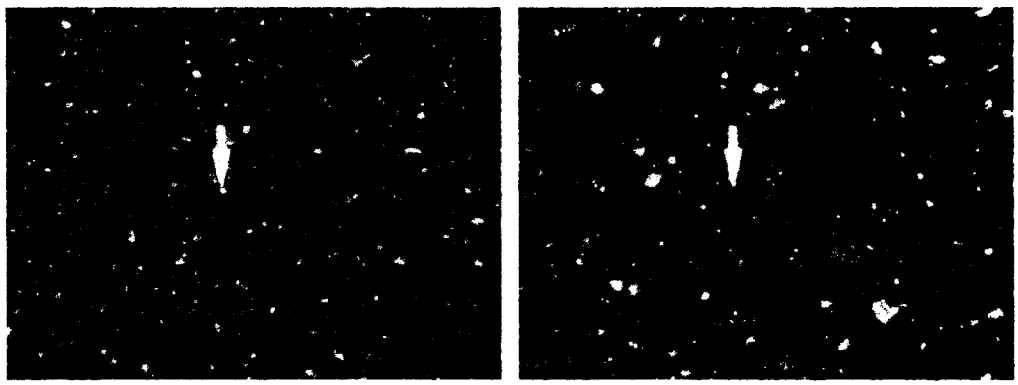

Figure 33. Photomicrographs of samples 02LT37 (left) and 02LT41 (right). Matrix is composed of altered volcanic ash, with fine volcaniclastic sand and silt making up a significant portion of the samples. Arrows are 0.25 mm long.

fractions were obtained through methyl-iodine (M.I.) separation, and contained sphene, zircon, metal oxide and lesser amounts of apatite. Zircons samples were then handpicked and a fraction were evaluated with an SEM. SEM imaging revealed that the zircons are generally 70 microns in length, prismatic and range from euhedral to subhedral, with little evidence of major abrasion due to transport (Fig. 34). The zircons were then shipped to the Stanford/USGS SHRIMP-RG laboratory for mounting and cathodoluminescence (CL) imaging.

The CL imaging revealed that the zircons contained simple oscillatory magmatic growth zonation, with no evidence of systematic inheritance (i.e. inherited cores) (J. Wooden, pers. comm.). The samples were mounted according to standard procedure, accompanied by a 419 Ma laboratory standard. The standard was collected from a quartz diorite of the Braintree Complex of Vermont, and its age was determined by conventional U-Pb analysis (J. Aleinikoff, pers. comm.). In total, 63 unknown grains were analyzed,

Figure 34. SEM image of a detrital zircon from sample 02LT41. Intact crystal facets are indicative of a single-cycle zircon with a short transport distance.

with a standard run every fourth analysis. Efforts were made to avoid analyzing fractured grains, or grains with inclusions, however a few grains still exhibited discordance possibly due to Pb loss along fine fractures. Due to the small size of the grains, and the 35 micron beam width, core to rim ages could not be compared. Therefore, each zircon was dated by a single spot analysis centered near the core of the crystal. Data used to calculate zircon ages is included in the appendices (Appendix III).

Results

The resulting U-Pb ages revealed a largely detrital zircon input, with little or no tuff-sourced zircons. Sample 02LT37 revealed an age range of approximately 799 $\pm$ 9 Ma to 704 $\pm$ 8 Ma, and a single concordant grain with an age of 689 $\pm$ 8 Ma (Fig. 35).

1.

Sample #	204corr 206Pb /238U Age (Ma)	1 Sigma Uncertainty (Ma)
02LT41-1	845.2	4.4
02LT41-2	794.0	6.8
02LT41-3	845.0	8.3
02LT41-4	821.5	8.7
02LT41-5	737.7	5.3
02LT41-6	811.5	10.3
02LT41-7	798.0	10.3
02LT41-8	727.6	8.6
02LT41-9	736.5	8.3
02LT41-10	750.0	10.3
02LT41-11	806.5	10.2
02LT41-12	743.6	8.1
02LT41-13	785.0	9.5
02LT41-14	826.5	11.4
02LT41-15	758.3	11.5
02LT41-16	764.2	10.1
02LT41-17	783.9	10.1
02LT41-18	879.2	10.9
02LT41-19	778.7	11.6
02LT41-20	767.3	10.3
02LT41-21	789.5	10.8
02LT41-22	789.7	9.7
02LT41-23	771.5	8.7
02LT41-24	739.1	10.3
02LT41-25	813.7	11.9
02LT41-26	777.0	9.6
02LT41-27	784.1	10.6
02LT41-28	769.0	10.0
02LT41-29	767.7	13.4
02LT41-30	750.3	10.1
02LT41-31	792.2	9.3
02LT41-32	770.6	14.2

2.

Sample #	204corr 206Pb /238U Age (Ma)	1 Sigma Uncertainty (Ma)
02LT37-1	785.9	8.9
02LT37-2	718.6	8.3
02LT37-3	733.3	9.1
02LT37-4	792.4	11.5
02LT37-5	777.6	8.6
02LT37-6	776.4	9.1
02LT37-7	799.0	10.0
02LT37-8	715.1	8.4
02LT37-9	704.4	7.9
02LT37-10	765.5	9.1
02LT37-11	740.8	9.0
02LT37-12	762.7	11.0
02LT37-13	724.8	10.4
02LT37-14	747.1	8.7
02LT37-15	706.9	9.9
02LT37-16	716.8	10.4
02LT37-17	733.7	10.2
02LT37-18	798.8	8.7
02LT37-19	794.4	9.7
02LT37-20	748.7	9.4
02LT37-21	191.4	11.9
02LT37-22	687.6	7.0
02LT37-23	760.2	8.5
02LT37-24	749.3	8.4
02LT37-25	777.7	11.0
02LT37-26	758.3	10.5
02LT37-27	730.9	8.5
02LT37-28	773.3	9.9
02LT37-29	769.6	8.2
02LT37-30	758.2	9.7

Figure 34. Data table for 204 corrected detrital zircon ages with uncertainty for samples 02LT41 (left) and 02LT37 (right).

The age distribution shows an age peak from approximately 750 to 790 Ma, with relatively few older or younger zircons. Sample 02LT41 is stratigraphically higher and noticeably more sand-rich, and reveals a slightly older age range, from 845 ± 4 Ma to a minimum of 727 ± 9 Ma. A single concordant 879 ± 11 Ma zircon was included in the population, but once again, the main peak in detrital ages centers on the 800 to 750 Ma age range (Fig. 36).

Given these results, an eruptive age for the tuff component cannot be accurately gauged. However, the maximum age for deposits in the upper Hengdan Group must be considered approximately 720 Ma or younger. The detrital age range effectively overlaps the previously reported U-Pb zircon volcanic ages for the Bikou Group of approximately 840 to 750 Ma obtained through SHRIMP U-Pb zircon analyses by my Chinese colleagues (Yan Quanren, unpublished data), as well as conventional U-Pb zircon analysis by Zhao and others (1990). In addition, these detrital ages agree with detrital zircon ages obtained by SHRIMP U-Pb dating of two sandstone and two reworked tuff beds from the middle to upper Hengdan Group, also obtained by my Chinese colleagues at CAGS (Yan, unpublished data) (Fig. 37).

Volumetrically less important are zircons of younger ages, which nonetheless imply sources of younger volcanism in the Bikou arc, ranging from 750 to 705 Ma, and a small number (3) of approximately 680 Ma. Data from CAGS also indicates 3 zircons with a Cambrian age, although relatively high uncertainty (± 50 to 100 Ma) renders these dates suspect. So far, ages of 750 Ma or younger have not been identified within the Bikou arc but may be present, or may represent Bikou arc elements that have subsequently been unroofed or dismembered by faulting. Importantly, no other volcanic source of similar

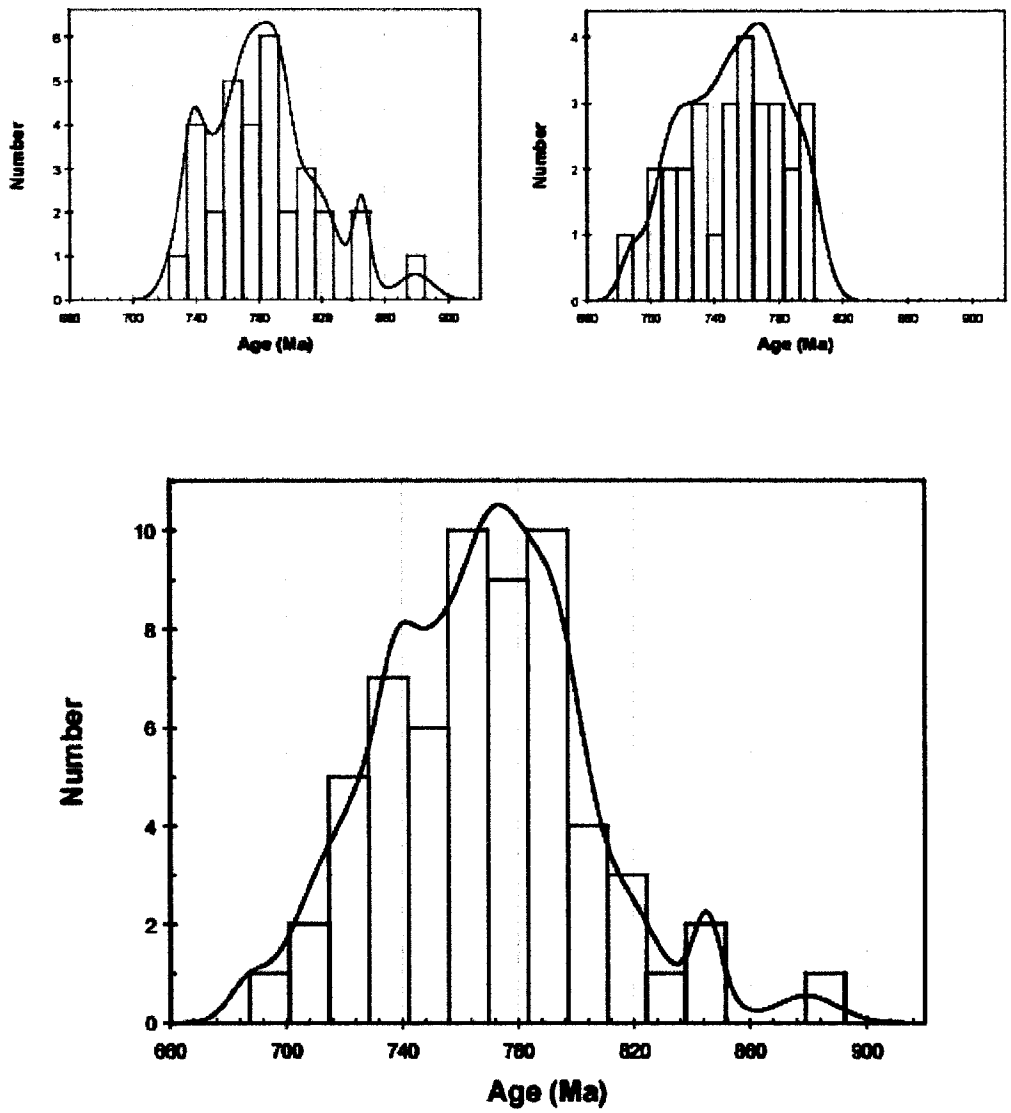

Figure 36. Combined probability plot and histogram of detrital zircon age distributions for sample 02LT37 (upper left) and sample 02LT41 (upper right). The combined age distribution is displayed below, and displays the peak of detrital ages between 730 to 800 Ma

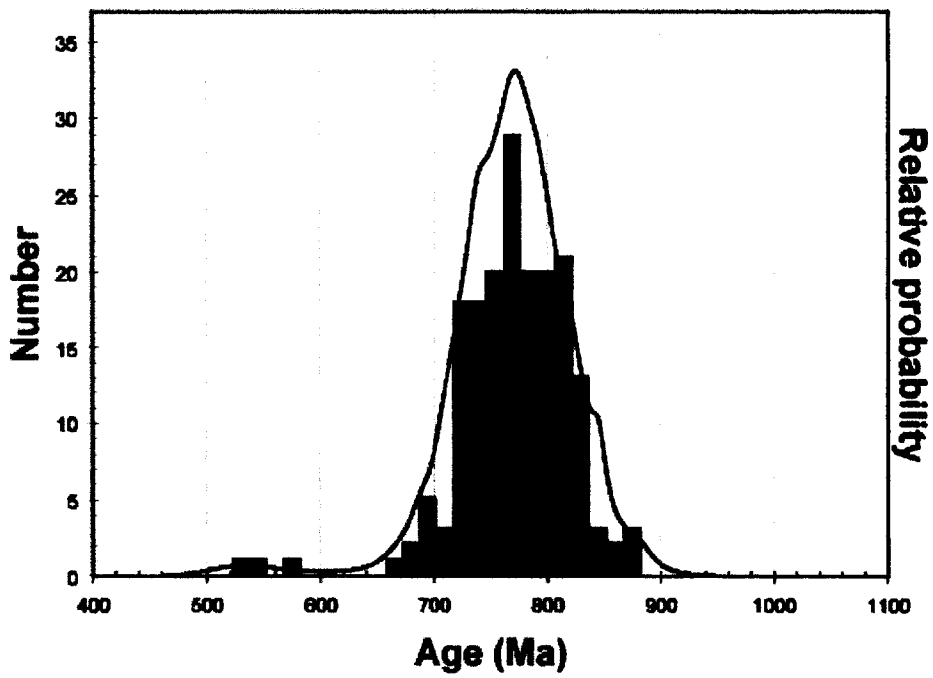

Figure 37. Probability curve compiling 121 detrital ages obtained at CAGS, and the 61 detrital ages obtained at the Stanford/USGS SHRIMP-RG laboratory. The composite curve peaks from approximately 720 to 840 Ma.

age is known locally. The identification of volcanic rocks of this age within the Bikou arc would ultimately improve this correlation.

The fact that the zircon population is overwhelmingly arc-derived rather than dominated by older, continental affinity zircons reflects on the tectonic provenance of the Hengdan basin. Recent detrital zircon studies from the Late Proterozoic/ Early Paleozoic passive margin deposits of western North America (Gehrels et al., 1995), and east Antarctica (Goodge et al., 2002), indicate pulses of detrital zircons coinciding with rift-related volcanism, but an overall age spectrum dominated by older Proterozoic to

Archean multi-cycle zircons. In contrast, detrital age spectrums from the Mesozoic forearc of California are dominated by arc-related zircons, with minor amounts of older continental-derived zircons (DeGraaf-Surpless et al., 2002). The presence of one Middle Proterozoic (1.095 Ga $\pm$ 67 Ma) and six Early Proterozoic (2.011 Ga. $\pm$ 65 Ma to 2.47 Ga. $\pm$ 50 Ma) detrital zircons identified by my colleagues at CAGS (Yan, unpublished data, 2002) suggests a very minor continental-derived sediment contribution to the basin, which we have interpreted as sourced from the Yangtze Plate.

CHAPTER 5

DISCUSSION: THE TECTONIC SETTING OF THE BIKOU TERRANE

Given the conflicting interpretations that the Bikou terrane represents either a continental arc, or a continental rift-to-drift assemblage, it is useful to compare the stratigraphy of the Bikou terrane to well-studied forearc, proto-oceanic rift troughs and rift-to-drift passive margin sequences world-wide. It is through such comparison that recognizable patterns of depositional systems, sediment provenance, basin morphology, and duration and style of volcanism must be used to create a plausible model of tectonic setting.

Turbidite systems have been well studied in modern settings and as ancient deposits, and occur in a wide variety of tectonic settings. Turbidites have been recognized in foreland basins, forearc basins, passive margins, and rift-to-drift sequences, so the existence of voluminous turbidites within the Hengdan basin alone does not support either a proto-oceanic rift or forearc setting. Within these broad plate tectonic settings, turbidites have been recognized in association with submarine fans, delta fronts and lacustrine settings. The lack of terrestrial deposits within the Hengdan basin however, excludes lacustrine and deltaic settings. Submarine fans come in a wide variety of forms,

most of which are largely dependant on sediment supply, basin morphology, sediment transport distance and tectonics.

The turbidite system that dominated sedimentation within the Hengdan basin may be characterized as a volcaniclastic sand-rich system. Sand-rich turbidite systems are dominated by sediment that is medium-grained sand-sized or coarser, display nonefficient transport (i.e., poor sorting and immature sands), actively prograde, and display a marked decrease in grain size toward the distal portions of the fan (Bouma, 2000). Sand-rich turbidite systems generally form adjacent to narrow, mountainous coastal areas with narrow shelf width, and short sediment transport. Sand-rich systems therefore generally indicate deposition within basins and plate margins adjacent to active orogenic belts.

The most obvious source area for the Hengdan Group is the adjacent Bikou arc, given paleocurrent directions, similarities between volcaniclastic detritus in the Hengdan Group with volcanic rocks in the Bikou Group, and the new U-Pb detrital zircon ages of volcaniclastic/mixed epiclastic rocks that overlap volcanic ages within the arc (unpublished data). The question remains however, whether the Bikou arc comprised an active magmatic arc, or a rift-related volcanic assemblage. For the purposes of evaluating these two conflicting hypotheses, numerous lines of evidence obtained from both the Hengdan basin and the Bikou arc prove to be strong indications of tectonic provenance when compared to well-studied continental rift-to-drift sedimentary assemblages (also referred to as nascent ocean basins, or proto-oceanic rifts) and forearc basins.

Comparison of the Bikou Terrane to Nascent Ocean Basins

A number of rift-to-drift successions provide useful comparisons to evaluate theories that the Bikou terrane formed in a continental rift setting. Rift-to-drift successions along the western margin of Laurentia provide an analog for proposed Late Proterozoic rifting along the Yangtze Block, particularly in light of theories that the South China Block was located adjacent to Laurentia prior to the break-up of Rodinia (Li et al., 1995, 1999). Rift-to-drift succession along the Mesozoic northern Atlantic margin also provide a well-studied analog to super-continent break-up, and the Red Sea rift of the Middle East/North Africa provides a modern analog for development of a nascent ocean, or proto-oceanic basin (Leeder, 1995). If the Bikou terrane represents a continental rift or rift-to-drift succession, similarities between the stratigraphy of the Bikou Group and other rift successions should exist.

Within the Red Sea system, diffuse magmatism related to rifting began at approximately 50 Ma, with more vigorous volcanic activity beginning at approximately 30 Ma (Pallister, 1987). Extension and large-scale block faulting was underway by 25 Ma, with volcanism increasingly centered along the Red Sea central axis (Bohannon et al., 1989). Prior to 20 Ma, the style of magmatism was typified by alkaline bimodal eruptions, flows, and dike intrusions, and then switched primarily to the intrusion of massive gabbroic dikes and stocks (Pallister, 1987). Volcanic flows are commonly interbedded with terrestrial or marginal marine sediments within the Red Sea system (Crossley et al., 1992). Active continental rifting had largely transitioned to oceanic spreading in the Pliocene at approximately 3 to 4 Ma (Cochran, 1983). These data suggest that large-scale volcanism related to Red Sea rifting took place over a relatively

short duration, perhaps over 25 m.y., while Bikou magmatism spans over a 100 m.y. interval.

The break-up of Pangea is recorded along the northern Atlantic margin of the eastern U.S. and Morocco by Late Triassic to Early Jurassic basaltic to andestic flows, and rhyolitic flows and tuff units (Lorenz, 1987, 1988). These volcanic units are typically interbedded with terrestrial sediments however, and form successions of volcanic flows and sediment no more than 2 to 3 km thick. Offshore wells along the southeastern United States have penetrated a sequence of alkali basalt and rhyolite cobbles of Late Triassic age, but little is known about the thickness or full extent of this volcanic phase (de Boer et al., 1988). Although portions of the Bikou Group have been compared to rift-related flood basalt assemblages (Xia et al., 1996b), the interbedding of deep marine sediments with the volcanic strata of the Bikou Group (Tao, 1993) makes this comparison unlikely.

The Late Proterozoic rifting of western Laurentia is associated with the Windermere Group, a succession of terrestrial sediments interbedded with volcanic flows and ash beds recently dated by zircon U-Pb SHRIMP as ca. 680 Ma (Lund et al., 2003). A number of small-scale mafic flows, dikes, and pillow basalts of Vendian to Early Cambrian age are also reported by Levy and Christie-Blick (1989). Similar to the Red Sea and Atlantic rifts, these volcanic units are interbedded with terrestrial to shallow marine successions within western North America. It is important to note that no volcanic successions or flood basalts of thickness, age, or duration of the Bikou Group volcanic assemblage have been identified along the western Laurentian margin.

Along the northern margin of the Atlantic Ocean, offshore seismic and magnetic anomaly data has indicated the widespread existence of a thick series of seaward-dipping

volcanic reflectors buried beneath younger passive margin deposits. Based on geophysical properties, these assemblages have been widely interpreted to represent "volcanic wedges" composed of stratified mafic volcanic and volcaniclastic material forming a Jurassic transition from attenuated continental to oceanic crust (Mutter et al., 1982, Austin et al., 1990, Holbrook and Keleman, 1993, Sheridan et al., 1993). Indications are that this volcanic wedge formed along at least 1,000 km of the western Atlantic margin and portions of the eastern margin, is 10 to 25 km thick and approximately 150 km wide (Holbrook and Keleman, 1993, Sheridan et al., 1993). Based on magnetic anomaly data, Bohannon (1986) concluded that large portions of the Red Sea shelf is underlain by a mafic volcanic transitional crust approximately 25 km wide and averaging 10 km thick, possibly similar to the Atlantic volcanic wedge.

Although no detailed physical descriptions of the stratigraphy of the Atlantic (or Red Sea) volcanic wedge exist, of all the tectonostratigraphic elements of the Atlantic rift system, the Bikou Group bears the most resemblance to a volcanic wedge. However, the problem remains that although the Bikou arc is the product of long-lived volcanism, indications are that the volcanic Atlantic wedge was emplaced during a relatively short interval in the Middle Jurassic (Austin et al., 1990, Sheridan et al., 1993). Secondly, although the Atlantic volcanic wedge is covered by a thick siliciclastic sediment sequence, this sequence appears to be derived from a continental source. Seismic reflection indicates that extensive carbonates and evaporites underlie the siliciclastic prism (Klitgord et al., 1988), indicating shallow marine conditions during transition from rift to drift. If the Bikou arc formed as a volcanic wedge during Rodinia breakup, it is logical to assume that the Hengdan Group should have formed as a drift phase

siliciclastic pile of continental-derived sediment rather than volcaniclastic sediment derived largely from the Bikou arc.

Strong similarities in early rift sedimentation may be seen in the Red Sea rift, Atlantic margin, and western Laurentian margin. Active extension within the Red Sea rift during the Late Oligocene and Early Miocene lead to the development of numerous discrete rift basins and half grabens, and early syn-rift sedimentation largely comprised very coarse conglomeratic fluvial/alluvial fan deltas adjacent to margin uplifts. These deposits consist of poorly sorted sand and conglomerates arranged in large Gilbert-type deltas that fine toward the central Red Sea basin (Gawthorpe and Colella, 1990). Within the central rift basins, early syn-rift sedimentation was characterized by deposition of fine-grained lacustrine shales, marls, cherts and carbonates or playa muds and evaporites (Bohannon et al., 1989; Crossley et al., 1992; Hughes and Beydoun, 1992). Syn-rift sedimentation within the proto-Atlantic rift followed a similar pattern throughout the system.

Comparison of Late Triassic to Early Jurassic syn-rift strata of the eastern United States, and western Europe indicate that deposition was dominated by alluvial fan breccias, conglomerates, debris flows and sieve-deposits, braided to meandering fluvial sandstone, mudstone and coal, lacustrine shales, playa mudstones and evaporites, and eolian sands (Lorenz, 1987, Zeigler, 1988). In the Late Triassic of Morocco, similar coarse alluvial-fluvial deposits are common, as are lacustrine deposits, and extensive playa-deposited mudstone/evaporite red-beds (Lorenz, 1988). Sedimentation within Late Proterozoic proto-Pacific rift basins of the western United States is also dominated by fanglomerates, fluvial deposits, mudstone/dolomite units and minor anhydrite of possible playa to marginal marine facies (Levy and Christie-Blick, 1989).

Marine incursion transitioning to drift-phase sedimentation is also recorded by similar stratigraphy within the western Laurentian, northern Atlantic margin, and Red Sea rifts. Within the Red Sea region, marine incursions led to largely fine-grained chemical precipitates that overlap earlier coarse-grained terrestrial deposits (Crossley et al., 1992; Bohannon et al., 1989). Restricted marine conditions within the central to southern Red Sea during this same time interval led to the deposition of up to 3 km of evaporite deposits along the main rift trough axis (Cochran, 1983). More recent deposition within the Red Sea basin is characterized by shallow marine carbonate deposition of siliciclastic and lime muds, coquinas, and isolated sabhkas (Hughes and Beydoun, 1992; El-Sammak and Shabaan, 1996). Importantly, turbidite deposition throughout the history of the Red Sea basin has been negligible, and today only small-scale, thin sandy to muddy turbidite deposits have been identified in the central Red Sea basin (Crossley et al., 1992).

Marine incursions into the northern proto-Atlantic rift system led to the deposition of thick marine-influenced evaporite deposits, followed by establishment of extensive carbonate deposition (Zeigler, 1988). In Morocco, similar deposits record marine incursion and transition from terrestrial to dominantly marine carbonate deposition (Warme, 1988). Geophysical studies have identified widespread evaporite and carbonate deposition along the northern Atlantic margin, overlapping earlier graben-bound syn-rift terrestrial basins (Klitgord et al., 1988, Manspeizer and Cousminer, 1988, Poag and Valentine, 1988). Later drift-phase deposition along the eastern margin of the United States is recorded in boreholes and geophysical logs by fine-grained carbonaceous shales, marls, glauconitic shales and sequences of fining-upward shale, siltstone and sand (Poag and Valentine, 1988). Along the margin of Morocco, the early drift-phase carbonate

platform was drowned and replaced by siliciclastic sedimentation in the form of thick continent-derived deltaic systems that deposited mud, silt, sand, and marl (Heyman, 1989).

Within the southwestern United States, the paleo-Pacific rift-to-drift transition is marked by shales, siltstones and quartz arenites that transition from braidplain or marginal marine settings to intertidal shales and carbonates near the Cambrian boundary (Prave, 1991). This observation is in agreement with thermal subsidence curves for lower Paleozoic passive margin deposits in the southwestern U.S. and the southern Canadian Rockies, indicating rapid cooling and thermal subsidence of the passive margin from Vendian (latest Precambrian) through Cambrian times (Bond and Kominz, 1984; Bond et al, 1985; Levy and Christie-Blick, 1991). This pattern of terrestrial sedimentation overlapped by shallow marine deposits is a common feature within rift-to-drift transitions. However, the Hengdan basin records no early phase of terrestrial sedimentation, no marginal or shallow marine deposits marking marine incursion of propagating proto-oceanic rift, no chemical precipitates, and displays coarsening upward rather than fining-upward sedimentation.

Lastly, the issue of sediment provenance is of major importance when evaluating continental rift and arc settings for the Bikou terrane. Within the Red Sea rift system, early rift sandstones are characterized as quartzofeldspathic with only minor volcanic-lithic components, and more recent sands are more mature having been derived largely from the exposed Arabian and Nubian Shields (Crossley et al., 1992). Within the northern Atlantic rift basins, similar quartzofeldspathic to quartz arenitic sandstone compositions are recorded (Lorenz, 1987, 1988). Sandstone compositions along the

western Laurentian margin are largely quartzofeldspathic to quartz-arenitic, with only minor volcaniclastic sandstone and conglomerate within syn-rift deposits (Bond et al., 1985; Levy and Christie-Blick, 1989; Prave, 1991). Lithic components within sandstones of the paleo-Pacific margin are largely derived from granite, chert and quartzite, with little or no lithic volcanic material.

Similarly, detrital zircon U-Pb analyses from western North American Early Paleozoic passive margin sediments reveals that Grenville-aged to Archean continental crust was the prime siliciclastic sediment source (Gehrels et al., 1995). A Nd isotope study of Pahrump Group through Early Cambrian siliciclastic units confirms that fine-grained detritus was largely derived from local Early to Middle Proterozoic granitic basement (Farmer and Ball, 1997). The trend toward higher quartz and feldspar ratios at the expense of lithic detrital grains in sandstones of rift or passive margin affinity was noted by Dickinson (1980, 1985) when developing his tectonic provenance classification scheme for sandstones, now widely recognized as the standard for sandstone provenance analysis. The dominance of mature, craton-derived sediment is a common feature in continental rift and passive margin basins, however, the detrital zircon age spectrum of the Hengdan Group indicates little or no craton input.

From the overview of stratigraphy and volcanism associated with the Neogene Red Sea rift, the Mesozoic breakup of Pangea, and the Late Precambrian proto-Pacific rift system of western North America, it is clear that few similarities exist between the Bikou terrane and well-studied rift sequences. The Bikou terrane displays none of the classic characteristics of a continental rift basin, and contains many features that have no analog within rift to drift passive margin sequences. Nowhere in the Bikou terrane are

terriginous syn-rift sediments, although in most rift systems, syn-rift basins tend to be preserved (Sengor, 1995). Rather, the Bikou arc is associated at every stage with marine sediments (Tao, 1993), which contradicts a pre-continental rift volcanism interpretation. Similarly, early marine incursions into these proto-oceanic rift troughs led to evaporite and carbonate sedimentation, and drift-phase sedimentation is characterized by carbonate and shale deposition that may be followed by deposition fine-grained continental-derived siliciclastic sediment. In none of these rift basin examples is there evidence for large-scale volcaniclastic turbidite deposits, or pronounced coarsening-upward trends.

Comparison of the Bikou Terrane to Forearc Basins

Unlike comparisons with rift basins and drift-phase sedimentation, comparisons of sedimentation and arc magmatism within the Bikou terrane to both modern and ancient arc systems show many similarities. These similarities comprise the style of sedimentation and arc composition, and extend to duration of arc magmatism, evolution of the arc/basin system, and the provenance relationships between arc and basin based on sand composition and detrital zircon age distribution. Although the Bikou terrane has been strongly affected by tectonism subsequent to Late Proterozoic time, these combined stratigraphic, provenance, and geochronological data clearly favor an arc/forearc setting for the Bikou terrane.

Although many conflicting theories address the tectonic setting of the Hengdan basin, most previous workers agree upon a number of important features. The first key feature of the Hengdan basin is that it is composed almost entirely of marine sediments, ranging from hemipelagic to submarine fan settings, with no clear indication of shallow marine or

terrestrial sedimentation. Secondly, sediment within the basin comprises mainly coarse volcaniclastic detritus in the form of lithic graywackes, volcaniclastic conglomerates, and mixed-clast conglomerates. Thirdly, although actual thickness estimates vary due to faulting and lack of biostratigraphic/chronostratigraphic control, most previous workers concur that the tremendous stratigraphic thickness of the Hengdan basin ranges from 9 to 15 km or more (Pei, 1989, 1992; Tao, 1993; Qin et al. 1994; Lu et al., 1996, 1997; Druschke et al., 2002; Yan et al., 2002).

A great deal of data have been compiled on both modern and ancient arc/forearc systems, especially within the circum-Pacific region. To illustrate similarities in forearc structure and sedimentation, a number of studies have compared information gathered from numerous modern and ancient forearc systems. Forearc basins typically form on volcanic arc or continental crust, and develop when sediment ponds between the arc massif and an uplifted accretionary prism (Dickinson and Seely, 1979). Deposits within forearc basins are typically comprised of immature, volcaniclastic-rich sediments and commonly form as restricted deep marine basins that may or may not transgress to shallow marine or terrestrial sedimentation over time (Dickinson and Seely, 1979). Submarine fans and hemipelagic slope to basin plain settings are most common within forearc basins, along with shallow marine shelves at the basin margins, and fringing fan-deltas (Dickinson and Seely, 1979; Dickinson, 1995).

Studies of modern forearc basins in several locations also indicate basin fill attains a thickness comparable to the Hengdan basin. The modern Cook basin of Alaska, the Luzon basin of the Philippines, and the Tobago Trough of the Lesser Antilles each contain between 10 and 15 km of sediments spanning tens of millions of years of

sedimentation (Dickinson, 1995). The Mesozoic Great Valley forearc of California attained a thickness of 15.2 km, and is composed largely of deep marine volcaniclastic turbidites deposited during the span of arc activity from the Late Jurassic to the Late Cretaceous, with sedimentation continuing into the Tertiary (Moxon, 1988). This tremendous stratigraphic thickness stands in sharp contrast to the average 4 to 6 km of Atlantic syn-rift basin fill (Lorenz, 1987), or the maximum 13 km thickness of the Mesozoic to recent eastern United States post-rift, passive margin sedimentary prism (Klitgord et al., 1988).

Sandstone provenance analysis schemes compiled by Dickinson (1985), have become the general standard for determining tectonic provenance of sandstones based upon their detrital framework grain compositions. By comparing a large number of sandstone and sand samples from numerous modern and ancient magmatic arc deposits worldwide, Dickinson determined that sands deposited within a magmatic arc provenance (including forearc, trench, and trench-slope basins) tended to be enriched in lithic volcanic and feldspar grains, and relatively quartz-poor. Sandstones within forearc basins therefore tend to range from volcanic-lithic rich litharenites to feldspathic arenites. In contrast, Dickinson (1985) determined that sandstone compositions within rift basin and passive margin sequences tend to be quartz-rich, which is in agreement with the previous rift examples of the Red Sea (Crossley et al., 1992), the proto-Atlantic (Lorenz, 1987), and the proto-Pacific rift of western North America (Bond et al., 1984; Levy and Christie-Blick, 1989).

Provenance analysis of sandstones within the Mesozoic Great Valley forearc of California indicates that the majority of basin-filling sandstones are both texturally and

compositionally immature. Lithic volcanic clast percentage within sandstone tends to be high, but trends toward greater maturity during the later phases of forearc deposition due to increased erosion of the arc and unroofing of plutonic arc components (Ingersoll, 1983). The same trend of increasing sand maturity over time was detected within the Hengdan Group through petrographic analysis. Pei (1989) indicated that sandstone compositions within the lower Hengdan Group plot within the immature arc field of Dickinson's (1980, 1985) QFL diagram, while sandstones within the upper Hengdan Group plot within the dissected arc field (Fig. 38).

Pei (1989) indicated that many of these graywackes were composed of 30% or more diagenetic matrix. This indicates that the original compositions may have been even more immature, given that lithic volcanic and feldspar grains alter to form pseudomatrix during diagenesis and metamorphism (Dickinson, 1970). Petrographic slides from the Hengdan Group examined during this study revealed that much of the sandstone was highly altered, which creates large uncertainties in point-counting. However, the poor sorting, abundant lithic volcanic grains and diagenetic matrix generally supports Pei's (1989) conclusion of arc provenance. The high percentage of matrix (30% or more) reported by Pei (1989) indicates that original sandstone framework composition was even more feldspar and lithic volcanic grain rich, which would have shifted the provenance deeper (downward) into the arc provenance field.

The dominance of submarine fan facies sedimentation, and the prograding and coarsening upward sequences seen in both the Hengdan Group and the Great Valley Group are strong evidence of similar tectonic settings. Stratigraphically, the lower Great Valley Group comprises basin-plain, outer submarine fan deposits, and locally inner fan

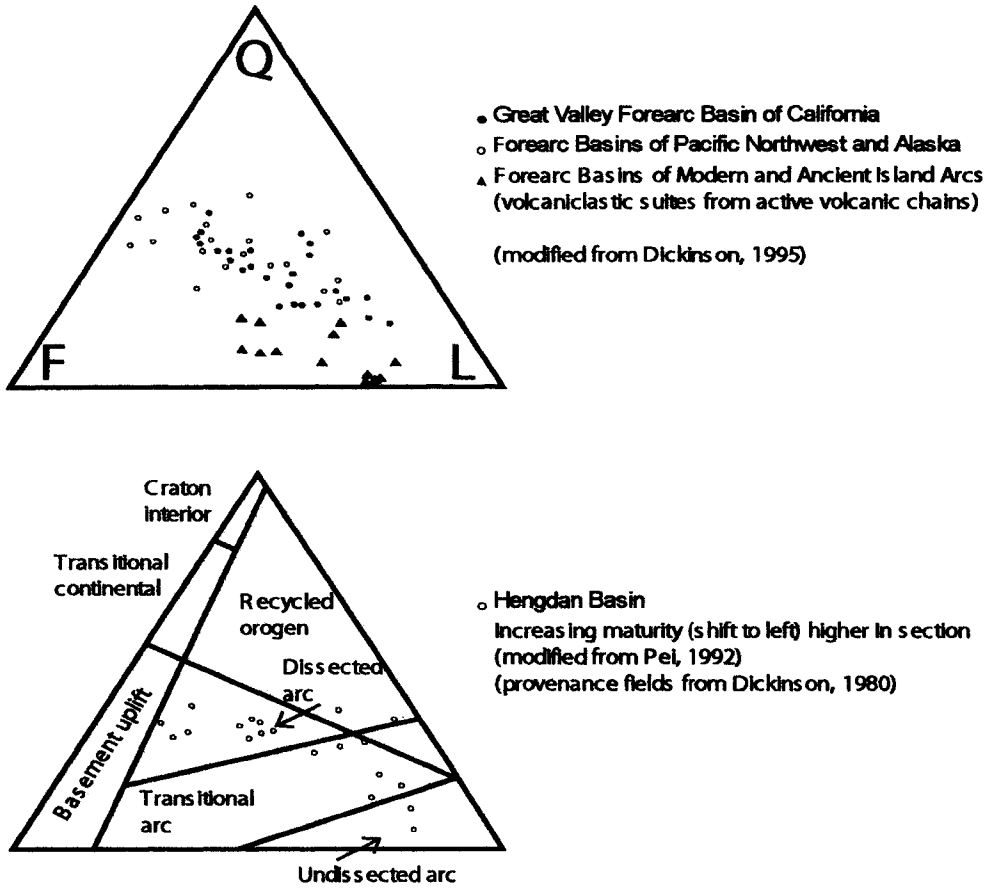

Figure 37. Comparison of sandstone composition between the Hengdan Group and a number of well studied forearc basins. The Hengdan Group plots largely within the arc field, and shows strong similarities to other well-known continental forearcs.

conglomeratic lenses. The middle to upper Great Valley Group continues to coarsen, with increasing sand to shale ratios, and eventually transitions from outer to middle fan facies (Ingersoll, 1978, Moxon, 1988; Dickinson, 1995). This same transition is seen in the Hengdan Group, within a very similar stratigraphic interval.

The tendency for forearc basin fill to be largely derived from the adjacent arc is illustrated in the Great Valley Group not only in the immaturity of the sediments, but also

in the detrital zircon population. A recent study of detrital zircon age distributions within the Great Valley Group indicates that the vast majority of zircons are derived from the Mesozoic Sierra Nevada arc, with zircon population peaks largely coincident with known episodes of active magmatism (DeGraaf-Surpless et al., 2002). Although older Mesozoic, Paleozoic and even Precambrian zircons are present within the forearc strata, they are a very small percentage of the population. The fact that detrital zircons within the Hengdan basin largely overlap the ages of volcanic assemblages within the Bikou arc is further evidence supporting a forearc setting for the Hengdan basin. The arc provenance displayed by Hengdan sandstones and detrital zircons is again in sharp contrast with the continental-provenance of many rift to passive margin sedimentary sequences, particularly the Grenville-aged to Archean craton detrital zircon provenance of the western North American passive margin (Gehrels et al., 1995).

The presence of significant amounts of tuff within the upper Hengdan Group, and mixed tuff, volcaniclastic sandstone, conglomerate, and volcanic flows within the upper Bikou Group is difficult to reconcile with continental rift models. The increase in tuff units within the upper portions of the Hengdan stratigraphy and the Bikou arc is difficult to explain in the context of a shift from rift to drift, when volcanism typically transitions from episodic eruption to continuous oceanic spreading as indicated in the Red Sea (Bohannon et al., 1989, Pallister, 1987), and the nascent Atlantic Ocean (Manspeizer and Cousminer, 1988). However, tuff and even pyroclastic to hyaloclastic volcanic material are common components within many forearc regions, including modern Japan, Alaska, and the ancient Great Valley Group (Dickinson, 1995).

In the Miocene-Pliocene Miura forearc basin of Japan, tuffaceous, scoreaceous and pyroclastic volcanic material is interbedded with neritic shelf sediments and shows signs of wave reworking. Tuffaceous and pyroclastic material are also common components in debris flow units and turbidity currents. In some cases, tuff is interpreted to have accumulated by hemipelagic settling or redeposition as dilute turbidity currents following eruption, in other cases tuffaceous debris flows and turbidites may have been remobilized after initial deposition (Stow et al., 1998). In the case of the Hengdan Group, thick tuffaceous intervals seen in the Luotang section may have formed as mixed sand and volcanic ash turbidity currents, whereas within the Wenxie section they appear to have largely formed as debris flows.

Within the Cretaceous forearc of Baja Mexico, deposits are predominantly fine to coarsely crystalline tuffs, tuff breccias, (epidotized) basaltic to andesitic hyaloclastites, and non-explosive basalt/andesite flows interbedded with volcaniclastic sandstone and shale that were deposited in a deep marine setting (White and Busby-Spera, 1987). The presence of these thick, subaqueous deposited tuffs, flows, and minor volcaniclastic sediment is interpreted to have formed on the submarine flanks of an active volcano. This assemblage strongly resembles portions of the upper Bikou Group, where beds up to several km thick consist primarily of marine deposited tuff, with strongly epidotized and/or chloritized basalt/andesite, and minor amounts of volcaniclastic sandstone and conglomerate. In contrast, it is difficult to explain this assemblage within a continental rift to drift setting.

The primitive geochemistry of mafic and ultramafic volcanic units, and bimodality within the volcanic stratigraphy of the lower Bikou Group has been the strongest

evidence for rift provenance. Thick tholeiitic basalt flows, occasionally interbedded with rhyolite, and the presence of layered mafic intrusions has been cited as evidence of pre-rift volcanism, and likened to flood basalt sequences found in regions of extension (Xia et al., 1996a, 1996b). However, mafic intrusions with primitive MORB characteristics are commonly associated with young arc sequences, forming as supra-subduction, back-arc, or intra-arc ophiolites in an extensional arc setting (Dickinson, 1995; Hamilton, 1995). Thick sequences of gabbros and peridotites are exposed in association with accreted or dissected subduction arcs in the Alps, Pakistan, and Alaska, and are interpreted to have formed as lower arc crust (Hamilton, 1995). Therefore, primitive mantle characteristics, mafic underplating, and volcanic bimodality may be explained in a rift or volcanic arc setting. Conversely, enrichment of LREE's in the same volcanic sequence, and the association of immature arc-related marine sediments is difficult to account for in a continental rift setting.

The Bikou terrane is best described as an arc/forearc assemblage based on the following lines of evidence: (1) the textural and compositional immaturity of clastic deposits within the Bikou terrane, diagnostic of magmatic arc to dissected arc provenance, and at odds with rift provenance; (2) the 9 to 15 km thickness of primarily volcaniclastic deposits within the Hengdan basin, similar to many forearc basins found worldwide in the ancient and modern world, but double the thickness of most syn-rift basins; (3) the lengthy duration of volcanism within the Bikou arc spanning at least 70 Ma., and possibly as much as 140 Ma, which suggests a long-lived continental arc; (4) detrital zircon ages that overlap the arc age, but show very few older zircons of continental affinity; and (5) the distinctive coarsening upward stratigraphy of the

Hengdan basin, similar to known forearc stratigraphy but unlike fining-upward passive margin stratigraphy. These lines of evidence alone are in stark contrast to rift sequences, and make the correlation between the Bikou terrane and a continental breakup sequence highly unlikely.

A number of features common within continental arc sequences are missing in the Bikou terrane, most notably an accretionary wedge of Late Proterozoic age. Forearc basins generally tend to fill over time and transition from deep marine to shallow marine or terrestrial sedimentation, although it is possible for a forearc basin to remain unfilled throughout its history (Dickinson and Seely, 1979). It is possible that some of the volcaniclastic sediment within the upper Bikou Group was deposited in a shallow marine setting, however, sedimentary structures to confirm this are generally lacking. Given the fact that major terrane bounding and terrane crossing faults surrounding the Bikou terrane may have been caused by left lateral "escape" following the North and South China Plate collision (Burchfiel et al., 1995; Wang et al., 2003), the Bikou terrane may be regarded as a displaced and fragmented terrane. Additional elements of the Bikou arc system may have been similarly displaced, or remain buried under thick Phanerozoic cover.

CHAPTER 6

TECTONIC IMPLICATIONS OF LATE PROTEROZOIC SUBDUCTION ALONG THE NORTH YANGTZE BLOCK MARGIN

The establishment of accurate age control and the determination of tectonic setting for the Bikou terrane has profound implications for the Late Proterozoic tectonic history of the Yangtze Plate. In recent years much debate has surrounded the timing of continental separation responsible for the establishment of the Late Proterozoic through Early Paleozoic passive margin of South China, and whether or not South China was part of the super-continent Rodinia. Until recently, the lack of reliable paleomagnetic data coupled with poor age control of South China Precambrian sedimentary sequences, volcanic intrusions and metamorphic events has led to the omission of the South China Block from many Rodinia reconstructions. Popular reconstructions such as SWEAT (Moores, 1991) and AUSWUS (Karlstrom et al., 1999) make no mention of South China. However, many researchers have concluded that South China likely was a part of the Late Proterozoic supercontinent based on recent paleomagnetic data and stratigraphic links (Li et al., 1995, 1999; Piper and Zhang, 1997; Zhang and Piper, 1997; Evans et al., 2000). Understanding the tectonic provenance and age of deposits found near the margin of the

South China Plate provides a means to evaluate recent Late Proterozoic plate reconstructions incorporating South China.

Rodinia is generally regarded as having been assembled during the ca. 1.1 to 0.9 Ga Grenville orogeny, and incorporated Laurentia, Australia, India, and portions of Africa, South America, and Eurasia. More controversial is the timing of Rodinia breakup, which led to major plate reorganization and the establishment of numerous passive margin sequences worldwide. Currently this debate has focused on whether breakup occurred earlier, ca. 850-700 Ma, or later, ca. 650 Ma to Early Cambrian. Debate has also focused on whether rifting took place simultaneously across Rodinia, or was diachronous, given conflicting stratigraphic and geochronological evidence.

The South China Plate is composed of the Yangtze craton to the west, and the Cathaysia craton to the east, with current debate on whether their suturing occurred during the Grenville, ca. 1 Ga (Li et al. 2002), or later at approximately 800 Ma (Zhao and Cawood 1999; Gu et al., 2002; Zhou et al., 2002b). Li (1999) obtained similar SHRIMP and conventional U-Pb zircon ages from peraluminous granites along the suture between the Yangtze and Cathaysia Plates, ranging from 824 $\pm$ 4, to 819 $\pm$ 9 Ma, which were interpreted as final suturing. Recent conventional U-Pb and ion-microprobe U-Pb dating has constrained the age of volcanic assemblages along the northern and western Yangtze Plate as approximately 840 Ma, to 720 Ma, although there is strong debate as to whether volcanism during the Late Proterozoic was formed in a subduction setting, or a intra-cratonic extensional setting.

However, a number of recent studies indicate that volcanism along the Yangtze Plate margin during the interval of ca. 850 to 720 Ma is the result of subduction rather than

rifting. Zhou and others (2002a) dated volcanic assemblages along the northern margin of the Yangtze Plate in the vicinity of the Bikou terrane using SHRIMP U-Pb of zircon indicate that magmatism was active from at least ca. 820 to 780 Ma. Furthermore, geochemistry of mafic volcanism within these localities indicates enrichment in LREE and Pb, suggesting continental arc magmatism (Zhou et al., 2002a). A similar study by Zhou and others (2002b) along the western margin of the Yangtze Plate indicates magmatism was active from approximately 868 $\pm$ 10 Ma to 717 $\pm$ 10 Ma, and is interpreted to have formed in an island arc or continental arc setting.

Stratigraphic evidence from numerous sources suggests that Rodinia breakup did not occur until the latest Precambrian. A 750 Ma breakup time has been inferred by many researchers based upon dike swarms in Australia, and from Sturtian glacial deposits intermixed with syn-rift deposits in many parts of the world. Recent U-Pb microprobe zircon dating of volcanic rocks interbedded with Sturtian glacial rocks in Idaho has revealed an age of 685 $\pm$ 7 Ma, which is much younger than the generally accepted 750 to 700 Ma age for Sturtian glacial deposits (Lund et al., 2003). Although dike swarms and syn-rift deposits in numerous locations worldwide have been taken as evidence of continental separation events, in some cases these deposits may indicate extension without continental separation.

An excellent example of this situation is revealed along the western Laurentian margin, where evidence exists for ca. 1 Ga, ca. 700 Ma, and ca. 600 to Early Cambrian rift-related volcanism and sedimentation. However, despite these multiple episodes, the only undeniable evidence for continental separation is the formation of long-lived, thick, passive margin marine sedimentation. Thermal subsidence curves for the early Paleozoic

passive margin sequences of both the southwestern U.S. and the southern Canadian Rockies indicate separation occurred during the latest Precambrian to Early Cambrian (Bond et al., 1984, 1985; Bond and Kominz, 1984; Levy and Christie-Blick 1991). Prave (1999) also remarked on a major unconformity separating syn-rift deposits of the lower Pahrump Group, and syn-rift deposits of the upper Pahrump Group overlapped by passive margin deposits as evidence for an earlier failed rift event along the western Laurentian margin.

Evidence for latest Precambrian to Early Cambrian rifting comes also from the Siberian passive margin, where volcanism and syn-extensional faulting occurred in the Early Cambrian, near the base of the passive margin succession (Pelechaty, 1996; Sears and Price, 2003). By correlating Grenville-aged belts across Siberia and western Laurentia, and using paleontological evidence, Sears and Price (2003) conclude that Siberia rifted from western North America rather than South China, Australia or Antarctica. Recent U-Pb SHRIMP detrital zircon dating from the Beardmore Group in Antarctica indicates a predominance of first-cycle Latest Precambrian to Early Cambrian zircons in early passive margin deposits (645-525 Ma), reflecting rift-related magmatism (Goodge et al., 2002). In addition, mafic intrusions that had earlier been taken as evidence for ca. 750 Ma rifting were re-dated, and found to be 668 $\pm$ 1 Ma. These new data shed doubt on earlier hypotheses that Australia and Antarctica separated at ca. 750 Ma. Paleomagnetic constraints and dike swarm ages from Norway indicate opening of the Iapetus between Baltica and Laurentia at approximately 600 Ma (Torsvik et al., 1995).

The recent "younging" of rift-related events based on more modern geochronological techniques as evidenced by Lund and others (2003), and Goodge and others (2002), indicates that rift related events dated by Rb-Sr, K-Ar, and Sm-Nd methods should be re-examined. Growing evidence of Latest Precambrian to Early Cambrian continental separation increasingly sheds doubt on theories for older Rodinia breakup ages, as well as current estimates for South China rifting. The possibility that volcanism and sedimentation hypothesized to be rift-related, is in fact subduction related also sheds doubt on the "missing-link" theory, and tends to support Late Proterozoic supercontinent reconstructions that place South China in a marginal, rather than intra-cratonic position, as postulated by Hoffman (1991) or the Rodinia alternative "Paleopangea" of Piper (2000).

The question remains however, if the ca. 850-700 Ma volcanism along the margin of the Yangtze Plate is subduction related, when did rifting to form the passive margin of South China take place? Currently, the initiation of the South China passive margin is poorly constrained, but if the subduction theory is correct, it could be assumed to have formed subsequent to the shut-off of subduction related magmatism ca. 705 Ma. A series of small mafic dike swarms intruding the Bikou Group have yielded $^{40}Ar/^{39}Ar$ ages ranging from 660 $\pm$ 2 Ma, to 650 $\pm$ 4 Ma (Yan, unpublished data.). These ages roughly overlap the poorly constrained Sm-Nd ages of 764 $\pm$ 164 Ma. for the Wudang Group, another volcanic complex located on the north margin of the Yangtze craton (Zhou et al., 1999; Zhang and Zhou, 1999). Although these data are sparse, they suggest a possible younger rifting age for South China.

Another unanswered question is, did collision with Rodinia or another micro-plate end subduction? Little evidence exists of a collision following subduction that produced the Bikou terrane, in the form of widespread metamorphism. However, as the highly complex Phanerozoic metamorphic history for the Qinling Mountains has largely overprinted older structures and fabrics, Late Proterozoic metamorphism and structures would be difficult to distinguish. Zhou and others (2002b) theorized that South China may have been an isolated micro-continent, and that shut off of magmatism may have caused the Yangtze margin to subside and become passive. This explanation seems unlikely however, as all contemporaneous passive margins apparently evolved from continental rifting. Obviously a great deal of future work must be performed to discover whether collision followed subduction, if rifting led to passive margin sedimentation and precisely when, and if in fact subduction rather than rift-related tectonics characterize Yangtze margin deposits during the 850 to 700 Ma interval of the Late Proterozoic.

CHAPTER 7

SUMMARY AND CONCLUSIONS

The modern Qinling Mountains of central China are the product of a complex history involving Paleozoic to Mesozoic continental collision between the North and South China Plates, and rejuvenation of structures and uplift due to Pacific subduction and far-field collisions in Southeast Asia and the Tibetan Plateau. Revealed within Precambrian basement uplifts along the margin of South China are a series of volcano-sedimentary terranes, conflictingly interpreted to represent either continental subduction, or continental rifting during the Late Proterozoic.

Recent studies of the Late Proterozoic Bikou terrane have created a similar controversy, as researchers have principally used geochemistry to interpret continental rift provenance and continental arc from a thick complex of mafic to felsic rocks known as the Bikou Group. Recent SHRIMP U-Pb dating of zircon from the Bikou arc has identified volcanic stratigraphy ranging from approximately 840 to 770 Ma in age (Yan, unpublished data, 2002). Largely overlooked from the discussion of tectonic provenance has been the minor interbedded marine volcanic rocks within the Bikou arc, and an adjacent thick volcaniclastic marine basin known as the Hengdan Group.

The Hengdan Group comprises a 10 to 15 km thick succession of volcaniclastic sand-rich turbidites. Facies associations range from hemipelagic basin-plain and fan-fringe deposits near the base of the succession, and prograde through outer fan, mid-fan and finally to inner fan in a coarsening upward progression. Epiclastic tuff is common within the upper portion of the sequence. Paleocurrents within the Hengdan Group imply south to north transport (i.e., from the direction of the Bikou arc). SHRIMP U-Pb dates on detrital zircon from the upper Hengdan Group indicate an age range of 830 to 700 Ma, largely overlapping previous ages obtained from the Bikou arc.

Comparisons of the Hengdan Group with many well-known forearc and rift-to-drift phase sedimentary sequences imply that the Hengdan basin is best described as a forearc basin. This interpretation is based on the extreme thickness of immature, volcaniclastic sediments, lack of terrestrial or marginal marine sedimentation, the coarsening upward trend, and a detrital zircon population with only a very minor component of older continental derived zircons. These features are similar to features observed within the Mesozoic Great Valley forearc basin of California and other forearc sequences, and are distinctly incongruent with rift sedimentation. Comparisons with the Red Sea rift, the Mesozoic Atlantic rift, and the Paleo-Pacific rift of western North America indicate that rift sequences commonly preserve early terrestrial and marginal marine sequences, show deepening and fining upward, and contain mature siliciclastic sediment largely derived from continental sources.

Currently, controversy exists regarding the tectonic provenance of many Late Proterozoic volcano-sedimentary terranes located along the northern and western margin of the South China (Yangtze) Plate. Volcanism during the interval of 850 to 750 Ma has

been taken as evidence of a volcanic plume preceding the breakup of Rodinia (Li et al., 1999). Alternatively, this same volcanism has been taken as evidence for a large-scale continental arc (Zhou et al., 2002a, 2002b). The recognition of the Bikou terrane as a continental arc/forearc favors the latter theory.

If the northern and western margins of the Yangtze Plate prove to have hosted a long-lived Late Proterozoic continental arc/forearc system, it will have implications for Rodinia reconstructions that include the South China Block. The presence of subduction invalidates the "missing link" theory of Li and others (1995), which places the South China Plate in an intra-cratonic setting during the Late Proterozoic. Long-lived subduction may prove that South China was not a part of Rodinia, as suggested by Zhou and others (2002b), or may prove that South China formed part of the margin of Rodinia. Alternately, South China may have accreted relatively late in the history of the Late Proterozoic supercontinent. If this proves to be the case, the identification of Late Proterozoic arcs may provide yet another tool for supercontinent correlation and reconstruction.

REFERENCES CITED

Ames, L., Tilton, G.R., Gaozhi, and Zhou, 1993, Timing of collision of the Sino-Korean and Yangtse cratons: U-Pb zircon dating of coesite-bearing eclogites: Geology, v. 21, p. 339-342.

Ames, L., Zhou, G., and Xiong, B., 1996, Geochronology and isotopic character of ultrahigh-pressure metamorphism with implications for collision of the Sino-Korean and Yangzte cratons, central China: Tectonics, v. 15, p. 472-489.

Arne, D., Brenton, W., Wilson, C., Chen, S. F., Foster, D., Luo, Z. L., Liu, S. G., and Dirks, P., 1997, Differential exhumation in response to episodic thrusting along the eastern margin of the Tibetan Plateau: Tectonophysics, v. 280, p. 239-256.

Austin, J. A., Jr., Stoffa, P. L., Phillips, J. D., Oh, J., Sawyer, D. S., Purdy, G. M., Reiter, E., and Makris, J., 1990, Crustal structure of the southeast Georgia embayment-Carolina trough: Preliminary results of a composite seismic image of a continental suture(?) and a volcanic passive margin: Geology, v. 18, p. 1023-1027.

Bohannon, R. G., 1986, Tectonic configuration of the western Arabian continental margin, southern Red Sea: Tectonics, v. 5, p. 477-499.

Bohannon, R. G., Naeser, C. W., Schmidt, D. L., and Zimmerman, R. A., 1989, The timing of uplift, volcanism, and rifting peripheral to the Red Sea: A case for passive rifting?: Journal of Geophysical Research, v. 94, p. 1683-1701.

Bond, G. C., Christie-Blick, N., Kominz, M. A., and Devlin, W. J., 1985, An early Cambrian rift to post-rift transition in the Cordillera of western North America: Nature, v. 315, p. 742-745.

Bond, G. C., and Kominz, M. A., 1984, Construction of tectonic subsidence curves for the early Paleozoic miogeocline of the southern Canadian Rockies: Implications for subsidence mechanisms, age of breakup and crustal thinning: Geological Society of America Bulletin, v. 95, p. 155-173.

Bond, G. C., Nickeson, P. A., and Kominz, M. A., 1984, Breakup of a supercontinent between 625 Ma and 555 Ma: new evidence and implications for continental histories: Earth and Planetary Science Letters, v. 70, p. 325-345.

Bouma, A. H., 2000, Fine-grained, mud-rich turbidite systems: Model and comparison with coarse-grained, sand-rich systems: *in* Bouma, A. H., Stone, C. G., eds., Fine-grained turbidite systems, AAPG Memoir 72/SEPM Special Publication 68, p. 9-19.

Bruguier, O., Lancelot, J. R., and Malavielle, 1997, U-Pb dating on single detrital zircon grains from the Triassic Songpan-Ganze flysch (central China): Provenance and tectonic correlations: Earth and Planetary Science Letters, v. 152, p. 217-231.

Burchfiel, B. C., Chen, Z., and Liu, Y., 1995, Tectonics of the Longmen Shan and adjacent regions, central China: International Geology Review, v. 37, p. 661-735.

Cochran, J. R., 1983, A model for development of the Red Sea: AAPG Bulletin, v. 67, p. 41-69.

Crossley, R., Watkins, C., Raven, M., Cripps, D., Carnell, A., and Williams, D., 1992, The sedimentary evolution of the Red Sea and the Gulf of Aden: Journal of Petroleum Geology, v. 15, p. 157-172.

Dalziel I. W. D., 1992, On the organization of American plates in the Neoproterozoic and the breakout of Laurentia: GSA Today, v. 2, p. 240-241.

de Boer J. Z., McHone, J. G., Puffer, J. H., Ragland, P. C., and Whittington, D., 1988, Mesozoic and Cenozoic magmatism: The Geology of North America, The Atlantic Continental Margin, Sheridan, R. E., Grow, J. A., eds., vol. 1-2, p. 217-241.

DeGraaf-Surpless, K., Graham, S. A., Wooden, J. L., and McWilliams, M. O., 2002, Detrital zircon provenance analysis of the Great Valley Group, California: arc-forearc system: Geological Society of America Bulletin, v. 114, p. 1564-1580.

Dickinson, W. R., 1970, Interpreting detrital modes of greywacke and arkose: Journal of Sedimentary Petrology, v. 40, p. 695-707.

Dickinson, W. R., 1985, Interpreting provenance relations from detrital modes of sandstones, *in* Zuffa, G. G. (ed), Provenance of arenites, p. 333-361.

Dickinson, W. R., 1995, Forearc basins: *in* Busby, C. J., and Ingersoll, R. V., eds., Tectonics of Sedimentary Basins, Blackwell Science, p. 221-261.

Dickinson, W. R., and Seely, D. R., 1979, Structure and stratigraphy of forearc regions: AAPG Bulletin, v. 63, p. 2-31.

Dickinson, W. R., and Valloni, R., 1980, Plate settings and provenance of sands in modern ocean basins: Geology, v. 8, p. 82-86

Druschke, P., Hanson, A. D., Yan, Q., and Wang, Z., 2002, Recognition of a Late Paleozoic arc/forearc developed on the north margin of the South China Plate, Southwestern Qinling Mountains, China: Geological Society of America Abstracts with Programs, v 34, p. 376-377.

Du, Y., Sheng, Y., Feng, Q., Gu, S., Cheng, J., Yang, Y., and Li, R, 1998a, Disintegration of the "Sanhekou Group" in the Mianxian-Lueyang area, south Qinling and its geological significance: Journal of Stratigraphy (in Chinese with English abstract), v. 22, p. 170-175.

Du, Y., Sheng. Y, Feng, Q., Wang, Z., and Gu, S., 1998b, New recognition of non-Smith stratigraphy and paleo-oceanography of Mianxian-Lueyang paleosuture in southern Qinling, China: Journal of Graduate School, China University of Geosciences (in Chinese with English abstract), v. 12, p. 25-31.

El-Sammak, A. A., and Shaaban, M. N., 1996, Carbonate geochemistry and mineralogy of short cores, Gulf of Suez, Egypt: Carbonates and Evaporites, v. 11, p. 155-161.

Evans, D. A., Li, Z. X., Kirschvink, J. L., and Wingate, M. T., 2000, A high-quality mid-Neoproterozoic paleomagnetic pole from South China, with implications for ice ages and the breakup configuration of Rodinia: Precambrian Research, v. 100, p. 313-334.

Farmer, G. L., and Ball, T. T., 1997, Sources of Middle Proterozoic to Early Cambrian siliciclastic sedimentary rocks in the Great Basin: A Nd isotope study: Geological Society of America Bulletin, v. 109, p. 1193-1205.

Feng, Q. L., Du, Y. S., Yin, H. F., Shen, J. H., and Xu, J. F., 1996, Carboniferous radiolarian fauna firstly discovered in Mian-Lue ophiolitic mélange belt of South Qinling Mountains: Science in China (Series D), v. 39, p. 87-92.

Gao, S., Zhang, B., and Li, Z., 1990, Geochemical evidence for Proterozoic continental arc and continental-margin rift magmatism along the northern margin of the Yangtze Craton, South China: Precambrian Research, v. 47, p. 205-221.

Gao, S., Zhang, B., Gu, X., Xie, Q., Gao, C., and Guo, X., 1995, Silurian-Devonian provenance changes of South Qinling basins: implications for accretion of the Yangtze (South China) to the North China cratons: Tectonophysics, v. 250, p. 183-197.

Gao, S., Zhang, B., Wang, D., Ouyang, J., and Xie, Q., 1996, Geochemical evidence for the Proterozoic orogenic belt and its adjacent margins of the North China and Yangtze cratons: Precambrian Research, v. 80, p. 23-48.

Gawthorpe, R. L., and Colella, A., 1990, Tectonic controls on coarse-grained delta depositional systems in rift basins: International Association of Sedimentologists Special Publication, v. 10, p. 113-128.

Gehrels, G. E., Dickinson, W. R., Ross, G. M., Stewart, J. H., and Howell, D. G., 1995, Detrital zircon reference for Cambrian to Triassic miogeoclinal strata of western North America: Geology, v. 23, p. 831-834.

Goodge, J. W., Myrow, P., Williams, I. S., and Bowring, S. A., 2002, Age and provenance of the Beardmore Group, Antarctica: Constraints on Rodinia Supercontinent Breakup: Journal of Geology, v. 110, p. 393-406.

Grimmer, J. C., Jonckheere, R., Enkelmann, E., Ratschbacher, L., Hacker, B. R., Blythe, E., Wagner, G. A., Wu, Q., Liu, S., and Dong, S., 2002, Cretaceous-Cenozoic history of the southern Tan-Lu fault zone: apatite fission-track and structural constraints from the Dabie Shan (eastern China): Tectonophysics, v. 359, p. 225-253.

Gu, X. X., Liu, J. M., Zheng, M., H., and Tang, J. X., 2002, Provenance and tectonic setting of the Proterozoic turbidites in Hunan, South China: Geochemical evidence: Journal of Geology, v. 72, p. 393-407.

Hacker, B. R., Ratschbacher, L., Webb, L., and Dong, S., 1995, What brought them up?: Exhumation of the Dabie Shan ultrahigh-pressure rocks: Geology, v. 23, p. 743-746.

Hacker, B. R., Ratschbacher, L., Webb, L., McWilliams, M. O., Ireland, T., Calvert, A., Dong, S., Wenk, H. R., and Chateigner, D., 2000, Exhumation of ultrahigh-pressure continental crust in east central China: Late Triassic-Early Jurassic tectonic unroofing: Journal of Geophysical Research, v. 105, p. 13, 339-13,364.

Hamilton, W. B., 1995, Subduction systems and magmatism: *in* Smellie, J. L., ed., Volcanism associated with extension at consuming plate margins: Geological Society Special Publication, v. 81, p. 3-28.

Hanson, A. D, Yan, Q., Druschke, P., and Wang, Z., 2002, The southwestern Qinling Shan of Central China: a Late Paleozoic subduction/accretionary system and continental arc/forearc constructed upon the north-facing Devonian passive margin of the South China Block: Geological Society of America Abstracts with Programs, v. 34, p. 509.

Heyman, M. A. W., 1989, Tectonic and depositional history of the Moroccan continental margin: *in* Tankard, A. J., Balkwill, H. R., eds., Extensional tectonics and stratigraphy of the North Atlantic margins: AAPG Memoir 46, p. 323-340.

Hoffman, P. F., 1991, Did the breakout of Laurentia turn Gondwanaland inside-out?: Science, v. 252, p. 1409-1412.

HolbrookV. S., and Kelemen, P. B., 1993, Large igneous province on the US Atlantic margin and implications for magmatism during continental breakup: Nature, v. 364, p. 433-364.

Hsu, K. J., Wang, Q., Li., J., Zhou, D., and Sun., S., 1987, Tectonic evolution of the Qinling Mountains, China: Eclogae geologica Helvetica, v. 80, p. 735-752.

Hughes, G. W., and Beydoun, Z., 1992, The Red Sea-Gulf of Aden: Biostratigraphy, lithostratigraphy and paleoenvironments: Journal of Petroleum Geology, v. 15, p. 135-156.

Ingersoll, R. V., 1978, Paleogeography and paleotectonics of the Late Mesozoic forearc basin of northern and central California: *in* Howell D. G., and McDougall, K., eds., Mesozoic paleogeography of the western United States, Pacific Coast Paleogeography Symposium No. 2, p. 471-482.

Ingersoll, R. V., 1983, Petrofacies and provenance of Late Mesozoic forearc basin, northern and central California: AAPG Bulletin, v. 67, p. 1125-1142.

Jagodzinski, E. A., and Black, L. P., 1999, U-Pb dating of silicic lavas, sills, and syneruptive resedimented volcaniclastic deposits of the Lower Devonian Crudine Group, Hill End Trough, New South Wales: Australian Journal of Earth Sciences, v. 46, p. 749-764.

Karlstrom, K. E., Williams, M. L., McLelland, J., Geissman, J. W., and Ahall, K., 1999, Refining Rodinia: Geologic evidence for the Australia-western U. S. connection in the Proterozoic: GSA Today, v. 9, p. 1-8.

Klitgord, K. D., Hutchinson, D. R., and Schouten, H., 1988, U.S. Atlantic continental margin; structural and tectonic framework: *in* Sheridan, R. E., Grow, J. A., eds., The Geology of North America, The Atlantic Continental Margin, vol. I-2, p. 19-55.

Kroner, A., Compston, W., Zhang, G., Guo, A., and Todt, W., 1988, Age and tectonic setting of Late Archean greenstone-gneiss terrain in Henan Province, China, as revealed by single-grain zircon dating: Geology, v. 16, p. 211-215.

Lai, S., Zhang, G., Yang, Y., and Cheng, J., 1997, Petrology and geochemistry features of the metamorphic volcanic rocks in Mianxian-Lueyang Suture Zone, South Qinling: Acta Petrologica Sinica (in Chinese with English abstract), v. 13, p. 563-573.

Leeder, M. R. 1995: Continental rifts and proto-oceanic rift troughs: *in* Busby, C. J., and Ingersoll, R. V., eds., Tectonics of Sedimentary Basins, Blackwell Science, p. 119-148.

Lerch, M.F., Xue, F., Kroner, A., Zhang, G.W., and Todt, W., 1995, A Middle Silurian-Early Devonian magmatic arc in the Qinling Mountains of Central China: Journal of Geology, v. 103, p. 437-449.

Levy, M., and Christie-Blick, N., 1989, Stratigraphy and tectonic framework of upper Proterozoic and Cambrian rocks in the western United States: in Levy, M., Christie-Blick, N., eds., Late Proterozoic and Cambrian Tectonics, Sedimentation, and Record of Metazoan Radiation in the Western United States, American Geophysical Union Field Trip Guidebook T331, v. 1, p. 7-21.

Levy, M., and Christie-Blick, N., 1991, Tectonic subsidence of the early Paleozoic passive continental margin in eastern California and southern Nevada: Geological Society of America Bulletin, v. 103, p. 1590-1606.

Li, Z. X., Li, X. H, and Powell, C. M., 1995, South China in Rodinia: Part of the missing link between Australia-East Antarctica and Laurentia?: Geology, v. 23, p. 407-410.

Li, S., Sun, W., Zhang, G., Chen, J., and Yang, Y., 1996, Chronology and geochemistry of metavolcanic rocks from Heigouxia Valley in the Mian-Lue tectonic zone, South Qinling—Evidence for a Paleozoic oceanic basin and its close time: Science in China (Series D), v. 39, p. 300-310.

Li, X. H., 1999, U-Pb zircon ages of granites from the southern margin of the Yangtze Block: timing of Neoproterozoic Jinning Orogeny in SE China and implications for Rodinia assembly: Precambrian Research, v. 97, p. 43-57.

Li, Z. X., Li, X. H., Kinny, P. D., and Wang, J., 1999, The breakup of Rodinia: did it start with a mantle plume beneath South China?: Earth and Planetary Science Letters, v. 173, p. 171-181.

Li, Z. X., Li, X. H., Zhou, H., and Kinny, P. D., 2002, Grenvillian continental collision in South China: New SHRIMP U-Pb zircon results and implications for the configuration of Rodinia: Geology, v. 30, p. 163-166.

Liu, D., Nutman, A., Compston, W., Wu, J., and Shen Q., 1992, Remnants of >3800 Ma crust in the Chinese part of the Sino-Korean craton: Geology, v. 20, p. 339-342.

Lowe, D. R., 1982, Sediment gravity flows; II, depositional models with special reference to the deposits of high-density turbidity currents: Journal of Sedimentary Petrology, v. 52, p. 279-297.

Lorenz, J. C., 1987, Triassic-Jurassic rift-basin sedimentology: History and methods: Van Nostrand Reinhold, 315 p.

Lorenz, J. C., 1988, Synthesis of Late Paleozoic and Triassic redbed sedimentation in Morocco: *in* Jacobshagen, V., ed. The Atlas system of Morocco, Lecture Notes in Earth Science, v. 15, p. 139-168.

Lu, Y., Huang, J., Du, D., and Jia, J., 1996, Age and stratigraphic correlation of Bikou Group: Journal of Qinling Geology (in Chinese), v. 44, p. 1-9.

Lu, Y., Huang, J., Du, D., and Jia, J., 1997, Age and stratigraphic correlation of the Bikou Group: Regional Geology of China (in Chinese), v. 16, p. 305-314.

Lund, K., Aleinikoff, J. N., Evans, K. V., and Fanning, C. M., 2003, SHRIMP U-Pb geochronology of Neoproterozoic Windermere Supergroup, central Idaho: Implications for rifting of western Laurentia and synchroneity of Sturtian glacial deposits: Geological Society of America Bulletin, v. 115, p. 349-372.

Manspeizer, W., and Cousminer, H. L., 1988, Late Triassic-Early Jurassic synrift basins of the U.S. Atlantic margin: *in* Sheridan, R. E., and Grow, J. A., eds., The Geology of North America, The Atlantic Continental Margin, vol. 1-2, p. 197-216.

Meng, Q., and Zhang, G., 1999, Timing of collision of the North and South China blocks: controversy and reconciliation: Geology, v. 27, p. 123-126.

Meng, Q., and Zhang, G., 2000, Geologic framework and tectonic evolution of the Qinling orogen, central China: Tectonophysics, v. 323, p. 183-196.

Moores, E. M., 1991, Southwest U.S.-East Antarctic (SWEAT) connection: A hypothesis: Geology, v. 19, p. 425-428.

Moxon, I. W., 1988, Sequence stratigraphy of the Great Valley basin in the context of convergent margin tectonics: *in* Graham, S. A., ed., Studies of the Geology of the San Joaquin Basin: Pacific Section S.E.P.M, v. 60, p. 3-28.

Mundil, R., Brack, P., Meier, M., Rieber, R., and Oberli, F., 1996, High resolution U-Pb dating of Middle Triassic volcaniclastics: time-scale calibration and verification of tuning parameters for carbonate sedimentation: Earth and Planetary Science Letters, v. 141, p. 137-151.

Mutter, J. C., Talwani, M., and Stoffa, P. L., 1982, Origin of seaward-dipping reflectors in oceanic crust off the Norwegian margin by "subaerial sea-floor spreading": Geology, v. 10, p. 353-357.

Mutti, E., and Normark, W. R., 1990, Comparing examples of modern and ancient turbidite systems: Problems and concepts in deep marine sedimentation: *in* Brown, G.C., Gorsline, D.S., and Schweller, W.J., eds., Depositional models and case histories in hydrocarbon exploration and development: Pacific Section S.E.P.M., v. 66, p. 153-198.

Nie, S., Yin, A., Rowley, D. B., and Jin, Y., 1994, Exhumation of the Dabie Shan ultra-high pressure rocks and accumulation of the Songpan-Ganzi flysch sequence, central China: Geology, v. 22, p. 999-1002.

Nilsen, T. H., 1984, Turbidite facies associations: SEPM Short Course: Modern and Ancient Deep Sea-Fan Sedimentation, Nilsen, T. H., Nelson, C. H., eds., vol.14, p. 197-300.

Oberhansli, R., Martinotti, G., Schmid, R., and Liu, X., 2002, Preservation of primary volcanic textures in the ultrahigh-pressure terrain of Dabie Shan: Geology, v. 30, p. 699-702.

Pallister, J. S., 1987, Magmatic history of Red Sea rifting: Perspective from the Saudi Arabian coastal plain: Geological Society of American Bulletin: v. 98, p. 400-417.

Peakall, J., McCaffrey, W. D., Kneller, B. C., Stelting, C. E., McHargue, T. R., and Schweller, W. J., 2000, A process model for the evolution of submarine fan channels: implications for sedimentary architecture, *in* Bouma, A. H., Stone, C. G., eds., Fine-grained turbidite systems: AAPG Memoir 72/SEPM Special Publication 68, p. 73-88.

Pei, X., 1989, The features and tectonic significance of rock assemblage(s) in the Bikou Group, Southern Qinling: Journal of Xi'an College of Geology (in Chinese with English abstract), p. 47-55.

Pei, X, 1992, The features and the tectonic settings of the flysch formation in the Bikou area, the southern Qinling Journal of Xi'an College of Geology (in Chinese with English abstract) v. 14, p. 42-49.

Pelechaty, S. M., 1996, Stratigraphic evidence for the Siberia Laurentia connection and Early Cambrian rifting: Geology, v. 24, p. 719-722.

Piper, J. D. A., 2000, The Neoproterozoic supercontinent: Rodinia or Paleopangea?: Earth and Planetary Science Letters, v. 176, p. 131-146.

Piper, J. D. A., and Zhang, Q. R., 1997, Palaeomagnetism of Neoproterozoic glacial rocks of the Huabei Shield: the North China Block in Gondwana: Tectonophysics, v. 283, p. 145-171.

Poag, C. W., and Valentine, P. C., 1988, Mesozoic and Cenozoic stratigraphy of the United States Atlantic continental shelf and slope: *in* Sheridan, R. E., and Grow, J. A., eds., The Geology of North America, The Atlantic Continental Margin, vol. I-2, p. 67-85.

Prave, A. R., 1991, Depositional and sequence stratigraphic framework of the Lower Cambrian Zabriskie Quartzite: Implications for regional correlations and the Early Cambrian paleogeography of the Death Valley region, California and Nevada: Geological Society of America Bulletin, v. 104, p. 505-515.

Qiang, Y., 1999, Stratigraphic correlation of the Bikou Terrane: Earth Science (in Chinese), v. 24, p. 251-255.

Qin, K., He, S., and Song, S. 1992, Isotopic geochronology and its significance in the Bikou Terrane, China: Northwest Geoscience, (in Chinese) v. 13, p. 98-110.

Qin, K., Jin, H., and Zhao, D., 1994, Tectonic evolution and mineralization in the Bikou ancient island arc belt: Henan Geology (in Chinese), v. 12, p. 304-317.

Qiu, Y. M., Gao, S., McNaughton, N. J., Groves, D. I., and Ling, W., 2000, First evidence of >3.2 Ga. continental crust in the Yangtze craton of south China and its implications for Archean crustal evolution and Phanerozoic tectonics: Geology, v. 28, p. 11-14.

Ranger, M., 1995, AppelCORE, University of Alberta at Calgary

Ratschbacher, L., Hacker, B. R., Webb, L. E., McWilliams, M., Ireland, T., Dong, S., Calvert, A., Chateigner, D., and Wenk, H. R., 2000, Exhumation of the ultrahigh-pressure continental crust in east central China: Cretaceous and Cenozoic unroofing and the Tan-Lu fault: Journal of Geophysical Research, v. 105, p. 13,303-13,338.

Rowley, D. B., Xue, F., Tucker, R. D., Peng, Z. X., Backer, J., and Davis, A., 1997, Ages of ultrahigh pressure metamorphism and protolith orthogneisses from eastern Dabie Shan: U/Pb zircon geochronology: Earth and Planetary Science Letters, v. 151, p. 191-203.

Sears, J. W., Price, R. A., 2003, Tightening the Siberian connection to western Laurentia: Geological Society of America Bulletin, v. 115, p. 943-953.

Sengor, A. M. C., 1985, East Asian tectonic collage: Nature, v. 318, p. 16-17.

Sengor, A. M. C., 1995, Sedimentation and tectonics of fossil rifts: *in* Busby, C. J., and Ingersoll, R. V., eds., Tectonics of Sedimentary Basins, Blackwell Science, p. 53-117.

Sheridan, R. E., Musser, D. L., Glover, L, III, Talwani, M., Ewing, J. I., Holbrook, W. S., Purdy, G. M., Hawman, R., and Smithson, S., 1993, Deep seismic reflection data of EDGE U.S. mid-Atlantic continental-margin experiment: Implications for Appalachian sutures and Mesozoic rifting and magmatic underplating: Geology, v. 21, p. 563-567.

Stow, D. A. V., and Tabrez, A. R., 1998, Hemipelagites: processes, facies, model: *in* Stoker M. S., Evans, D., Cramp, A., eds., Geological Processes on Continental Margins: Sedimentation, Mass-Wasting and Stability, p. 317-337.

Stow, D. A. V., Taira, A., Ogawa, Y., Soh, W., Taniguchi, H., and Pickering, K. T., 1998, Volcaniclastic sediments, process interaction and depositional setting of the Mio-Pliocene Miura Group, SE Japan: Sedimentary Geology, v. 115, p. 351-381.

Sun, W., Li, S., Chen, Y., and Li, Y., 2002, Timing of synorogenic granitoids in the South Qinling, Central China: Constraints on the evolution of the Qinling-Dabie orogenic belt: Journal of Geology, v. 110, p. 427-468.

Sun, Y., Chen, Z., Liu, Y., and Wang, T., 2000, Junction and evolution of the Qinling, Qilian and Kunlun orogenic belts: Acta Geologica Sinica, v. 74, p. 223-228.

Tao, H., 1993, Rock assemblages of the North Margin of the Yangtze Plate: Historical evolution of tectonics along north rim of the Yangtze Plate: Northwest University Publishing House (in Chinese), p. 8-60.

Torsvik, T. H., Lohmann, K. C., and Sturt, B. A., 1995, Vendian glaciations and their relation to the dispersal of Rodinia: Paleomagnetic constraints: Geology, v. 23, p. 727-730.

Wang E., and Burchfiel, C., 1998, Mesozoic shortening and elongation along the Qinling orogenic belt between the North and South China cratons: Geological Society of America Abstracts with Programs, v. 30, p. 108.

Wang E., Meng, Q., Chen, Z., and Chen, L., 2001, Early Mesozoic left lateral movements along the Longmenshan fault belt, Sichuan, China and its implications: Earth Science Frontiers (in Chinese with English abstract), v. 8, p. 375-384.

Wang, E., Meng, Q., Burchfiel, B. C., and Zhang, G., 2003: Mesozoic large-scale lateral extrusion, rotation, and uplift of the Tongbai-Dabie Shan Belt in east China: Geology, v. 31, p. 307-310.

Wang, Z., Chen, H., Li, J., Hao, J., Zhao, Y., Han, F., and Hao, J., 1999, Discovery of radiolarian fossils in the Xixiang Group, the southern Qinling, central China, and its implications: Science in China (Series D), v. 42, p. 337-343.

Warme, J. E., 1988, Jurassic carbonate facies of the central and eastern High Atlas rift, Morocco: *in* Jacobshagen, V., ed. The Atlas system of Morocco, Lecture Notes in Earth Science, v. 15, p. 169-199.

Watson, M. P., Hayward, A. B., Parkinson, D. N., and Zhang, Z. M., 1987, Plate tectonic history, basin development and petroleum source rock deposition onshore China: Marine and Petroleum Geology, v. 4, p. 203-225.

Webb, L. E., Hacker, B. R., Ratschbacher, L., McWilliams M. O., and Dong, S. 1999, Thermochronologic constraints on deformation and cooling history of high- and ultrahigh-pressure rocks in the Qinling-Dabie orogen, eastern China: Tectonics, v. 18, p. 621-638.

Wei, C., 1995, Metamorphism of the Bikou Group in the Shanxi-Gansu-Sichuan border region: Acta Geologica Sinica, v. 8, p. 53-67.

White, J. D. L., and Busby-Spera, C.J., 1987, Deep marine arc apron deposits and syndepositional magmatism in the Alistos group at Punta Cono, Baja California, Mexico: Sedimentology, v. 34, p. 911-927.

Xia, L., Xia, Z., and Xu, X., 1996a, Properties of middle-late Proterozoic rocks in South Qinling and the Precambrian continental break-up: Science in China (Series D), v. 39, p. 256-265.

Xia, L., Xia, Z., and Xu, X., 1996b, The confirmation of continental flood basalt of the Proterozoic Xixiang Group in the South Qinling Mountains, and its geological implications: Geological Review (in Chinese with English abstract), v. 42, p. 513-522.

Xia, Z., Xia, L., Ren, Y., Zhang, C., Yang, J., and Han, S., 1989, The study and petrology of marine volcanic rocks of Bikou Group from southern Qinling Mountains: Bulletin of Xian Institute of Geology and Mineral Resources, v. 25, p. 97-107.

Xiao, S., 1990, A preliminary study of volcanism of the Bikou Group in Shaanxi Province: p. 198-211.

Xu, S., Okay, A.I., Ji, S., Sengor, A. M .C., Su, W., Liu, Y., and Jiang, L., 1992, Diamond from the Dabie Shan metamorphic rocks and its implications for tectonic setting: Science, v. 256, p. 80-82.

Xu, J., Zhang, B., and Han, Y., 1994, Recognition of ophiolite belt and granulite in northern area of Mian-Lue, Southern Qinling, China, and their implication: Journal of China University of Geoscience, (in Chinese) v. 5, p. 25-27.

Xu, J., Yu, X., Li, X., Han, Y., Shen, J., and Zhang, B, 1998, Discovery of the highly depleted N-MORB-type volcanic rocks: new evidence for the Mianlue paleo-ocean: Chinese Science Bulletin, v. 43, p. 510-514.

Xu, J., Wang, Q., and Yu, X., 2000, Geochemistry of high-Mg andesites and adakitic andesite from the Sanchanzi block of the Main-Lue ophiolitic mélange in the Qinling Mountains, central China: Evidence of partial melting of the subducted Paleo-Tethyan crust: Geochemical Journal, v. 34, p. 359-377.

Xue, F., Lerch, M. F., Kroner, A., and Reischmann, T., 1996, Tectonic evolution of the East Qinling Mountains, China, in the Paleozoic: a review and a new tectonic model: Tectonophysics, v. 253, p. 271-284.

Yan, Q., Wang, Z., Hanson, A., D., Druschke, P., Wang, T., and Yan, Z., 2002, Hengdan turbidite terrane: Filling in a Late Paleozoic forearc basin developed on the passive margin on the Yangtze Plate: Geological Bulletin of China (in Chinese with English abstract), v. 21, p. 495-500.

Yan, Q., Wang, Z., Hanson, A. D., Druschke, P., and Wang, T., 2003, The Guanjiagou Section of the South Qinling and its tectonic implications: Science in China (in press).

Yang, Z., and Besse, J., 2001, New Mesozoic apparent polar wander path for south China: Tectonic consequences: Journal of Geophysical Research, v. 106, p. 8493-8520.

Ye, L. J., and Guan, S. C., 1944, Geology in mid-south Gansu: Special Issue of Geology (in Chinese) A19.

Yin, H., and Huang, D., 1996, Early Paleozoic evolution of the Zhen'an-Xichuan Block and the small Qinling multi-island ocean basin: Acta Geologica Sinica (English Edition), v. 9, p. 1-15.

Zhai, X., Day, H., Hacker, B., and You, Z., 1998, Paleozoic metamorphism in the Qinling orogen, Tongbai Mountains, central China: Geology, v. 26, p. 371-374.

Zhang, Z., Liou, J., and Coleman, R., 1984, An outline of the plate tectonics of China: Geological Society of America Bulletin, v. 95, p. 295-311.

Zhang, Z., Liou, J., and Coleman, R., 1989, The Mesozoic and Cenozoic tectonism in eastern China: *in* Ben-Avraham, Z., ed., the Evolution of the Pacific Ocean Margins, Oxford Monographs on Geology and Geophysics, v. 8, p. 124-139.

Zhang, Y. Q., Vergely, P., and Mercier, J., 1995, Active faulting in and along the Qinling Range (China) inferred from SPOT imagery analysis and extrusion tectonics of south China: Tectonophysics, v. 243, p. 69-95.

Zhang, G., Meng, Q., Yu, Z., Sun, Y., Zhou, D., and Guo, A., 1996, Orogenesis and dynamics of the Qinling orogen: Science in China (Series D), v. 39, p. 225-234.

Zhang, H. F., Gao, S., Zhang, B. R., Luo, T. C., and Lin, W. L., 1997, Pb isotopes of granitoids suggest Devonian accretion of Yangtze (South China) craton to North China craton: Geology, v. 25, p. 1015-1018.

Zhang, Q. R., and Piper, J. D. A., 1997: Paleomagnetic study of Neoproterozoic glacial rocks of the Yangzi Block: palaeolatitude and configuration of South China in the late Proterozoic supercontinent: Precambrian Research, v. 85, p. 173-199.

Zhang, C., and Zhou, D., 1999, Rifting of Wudang Block during Chenjiang Period of Neoproterozoic in South Qinling of China: geochemical evidence from Wudang basic dyke swarm: Gondwana Research, v. 4, p. 529-532.

Zhao, G., and Cawood, P. A., 1999, Tectonothermal evolution of the Mayuan assemblage in the Cathaysia block: Implications for Neoproterozoic collision related assembly of the South China craton: American Journal of Science, v. 299, p. 309-339.

Zhao, X., and Coe, R. S., 1987, Paleomagnetic constraints on the collision and rotation of North and South China: Nature, v. 327, p. 141-144.

Zhao, X., Ma, S., Zou, X., and Xiu, Z., 1990, The study of the age, sequence, volcanism and mineralization of Bikou Group in Qinling-Dabieshan: Bulletin of Xian Institute of Geology and Mineral Resources (in Chinese with English abstract), v. 29, p. 1-128.

Zhou, D., and Graham, S., 1996, Songpan-Ganzi Triassic flysch complex as a remnant ocean basin : Geological Society of America Bulletin, v. 107 p. 281-299.

Zhou, D., Zhang, C., Liu, L., Wang, J., and Zhou, X., 1999, A discussion on the rifting of ancient Yangtze continent in the Neoproterozoic: Gondwana Research, v. 2, p. 544-446.

Zhou, M., Kennedy, A. K., Sun, M., Malpas, J., and Lesher, C. M., 2002a, Neoproterozoic arc-related mafic intrusions along the northern margin of South China: Implications for the accretion of Rodinia: The Journal of Geology, v. 110, p. 611-618.

Zhou, M., Yan, D., Kennedy, A., Li, Y., and Ding, J., 2002b, SHRIMP U-Pb zircon geochronological and geochemical evidence for Neoproterozoic arc-magmatism along the western margin of the Yangtze Block, South China: Earth and Planetary Science Letters, v. 196, p. 51-67.

Ziegler, P. A., 1988, Evolution of the Arctic-North Atlantic and the western Tethys: AAPG memoir 43, p. 37-96.

APPENDIX I

LEGEND FOR DETAILED AND CONTINUOUS SECTIONS

LUOTANG CONTINUOUS SECTION PART 1-16

Appendix I contains the legend used for all sections within this manuscript, as well as the compilation of the complete 15.6 km thick Luotang Continuous Section. The purpose of the continuous sections is to depict variation in gross grain size of siliciclastic sediment within the basin, provide thickness estimates for the basin, show stratigraphic trends, and to show the locations of key sedimentologic or tectonic structures and samples.

Appendix I. Legend for use with detailed and continuous sections.

The legend contains colors and symbols used to illustrate lithology and sedimentological structures within detailed and continuous sections throughout this manuscript.

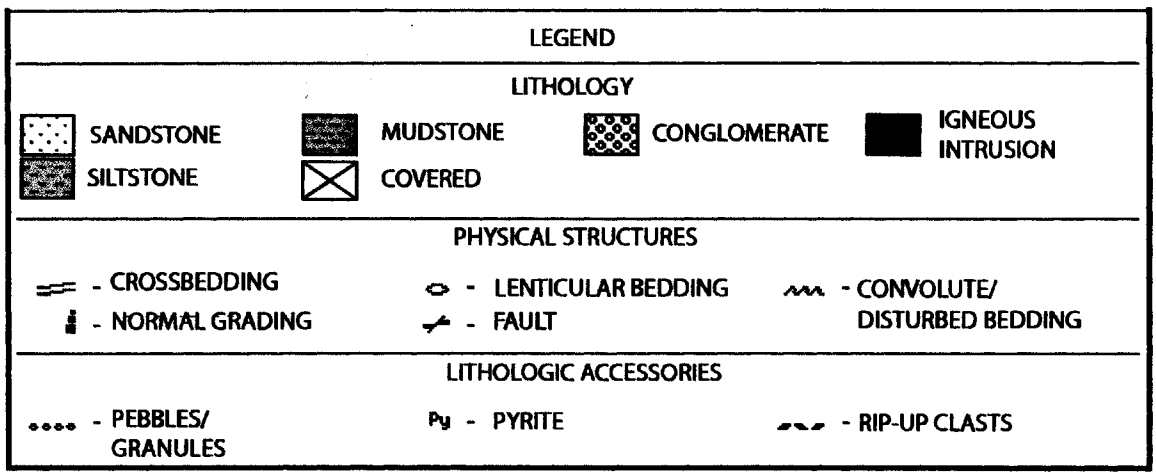

Appendix I

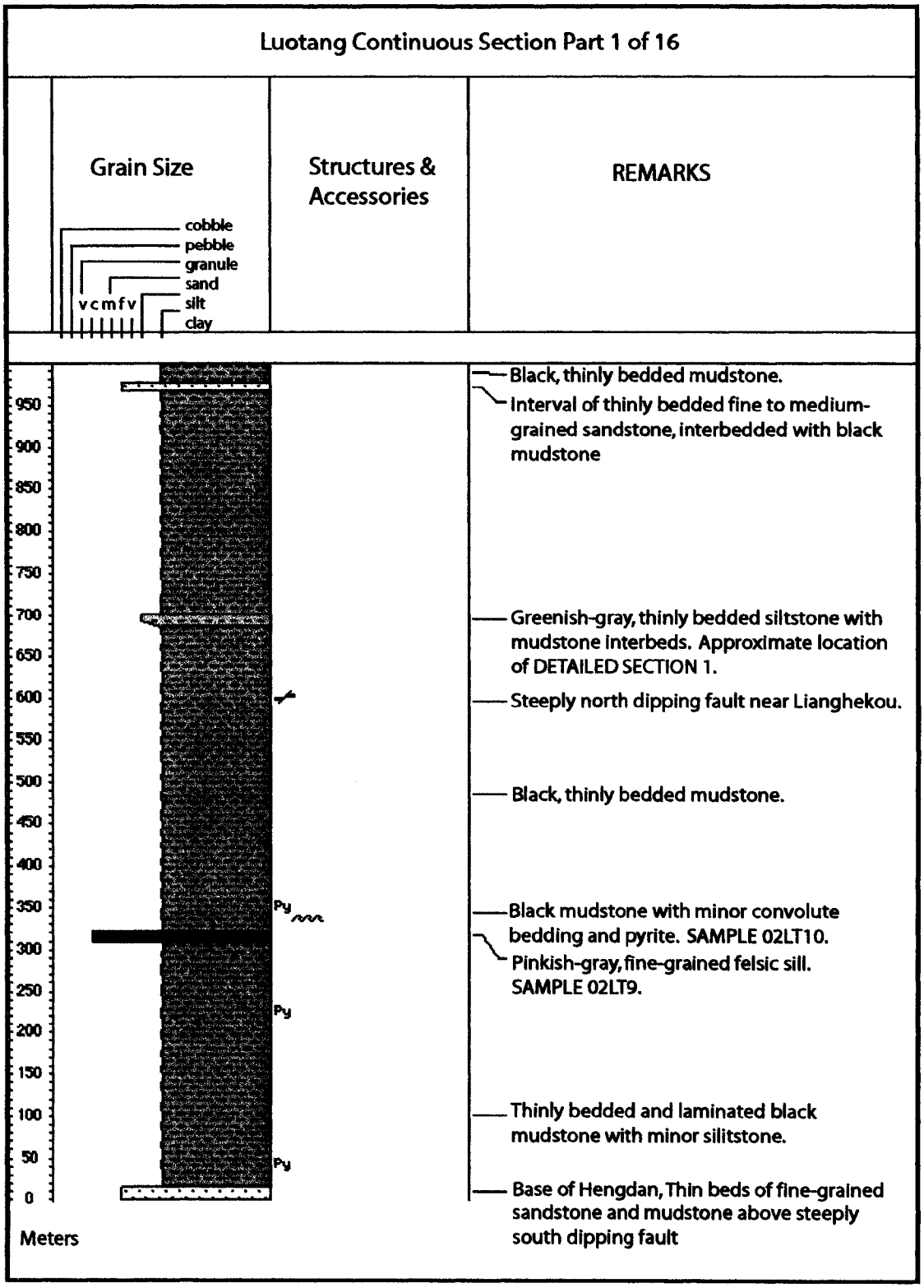

Appendix I

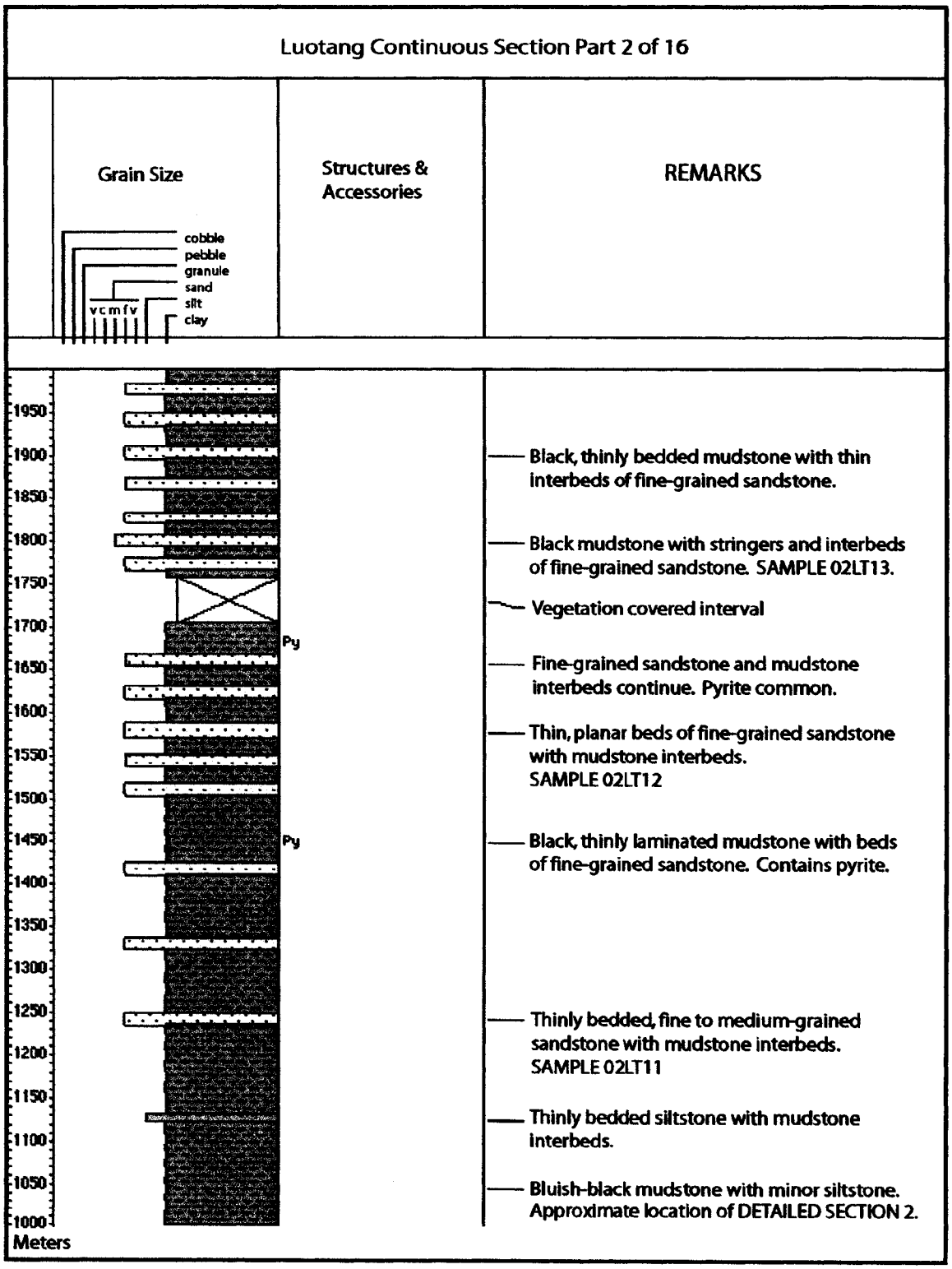

Appendix I

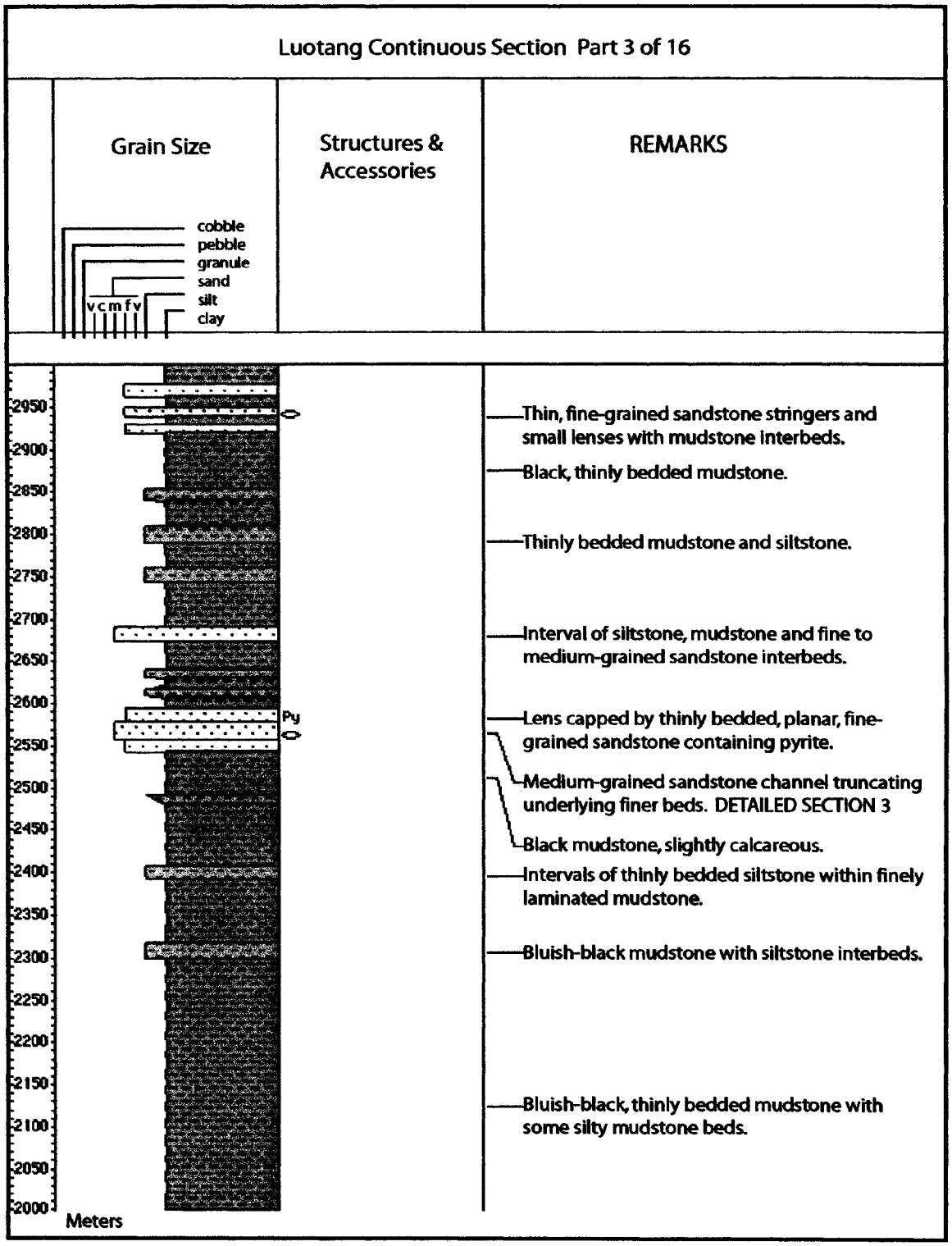

Appendix I

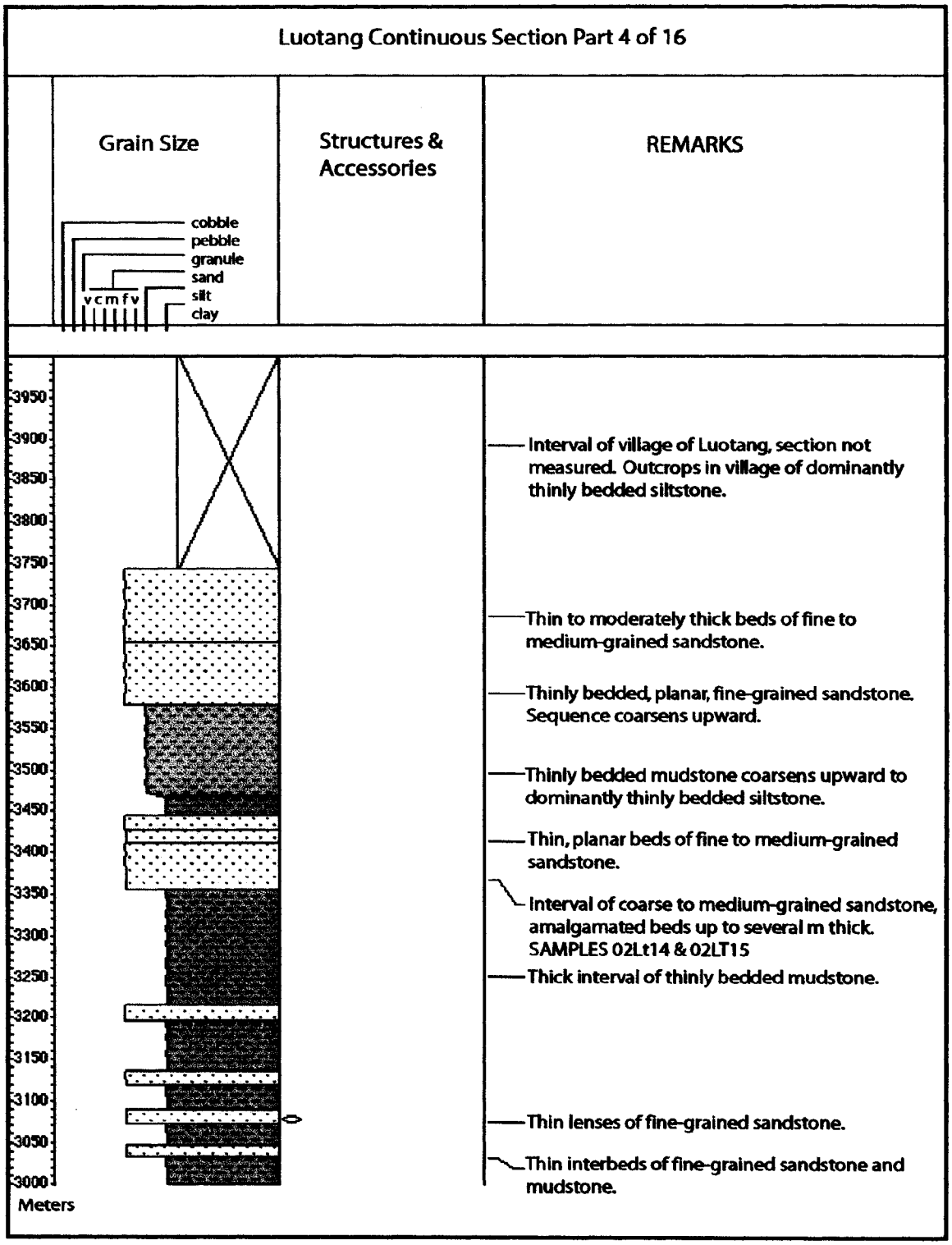

Appendix I

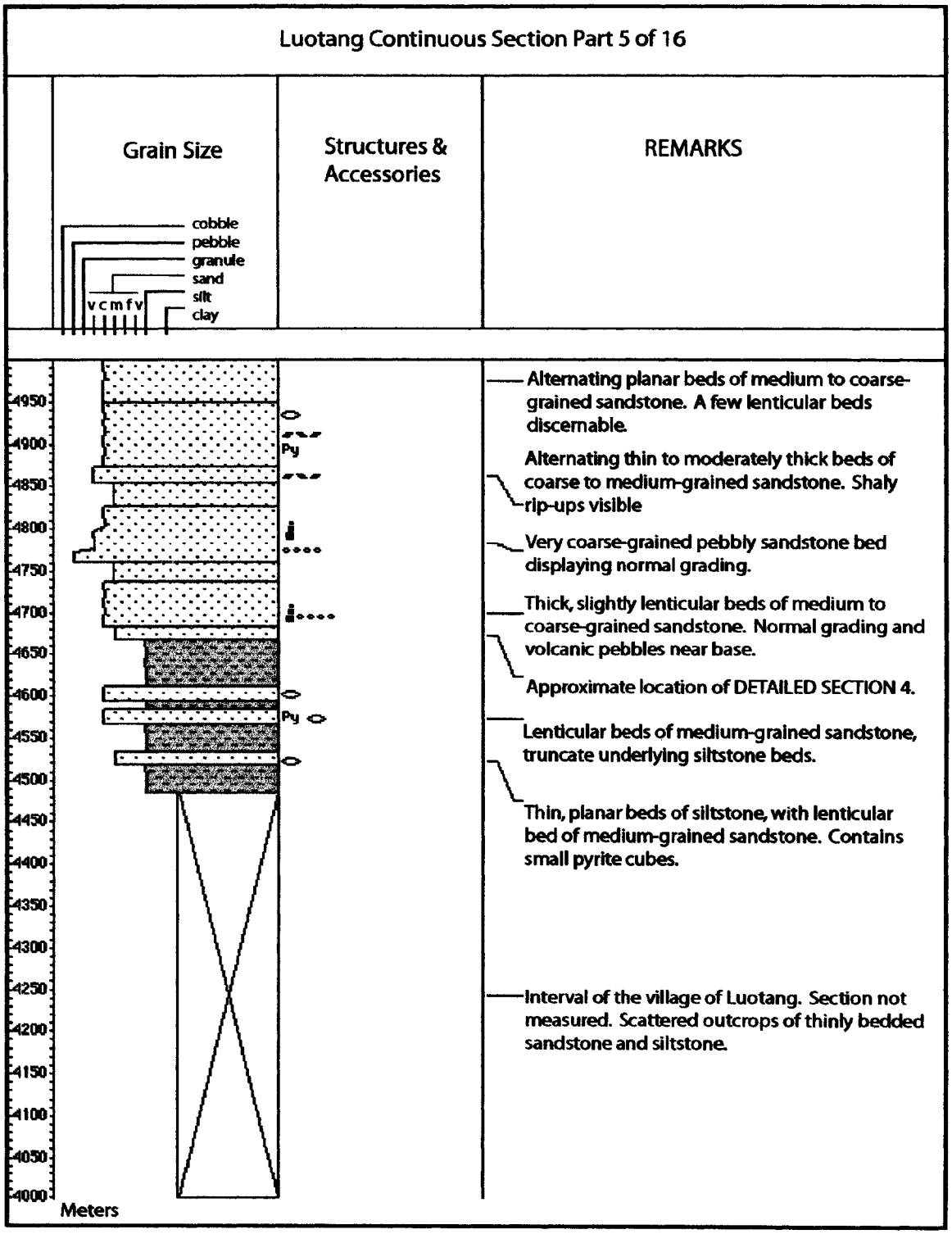

Appendix I

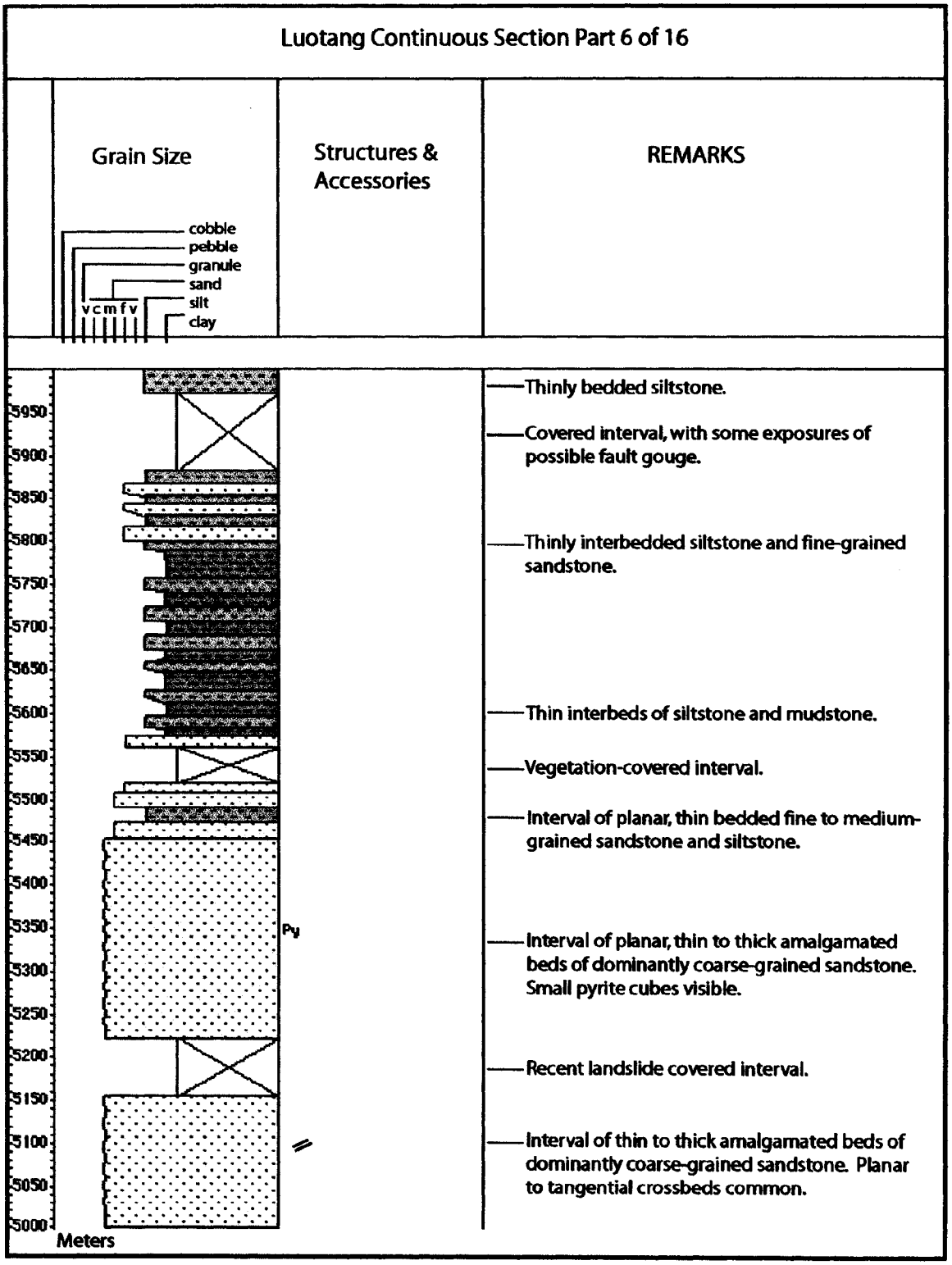

Appendix I

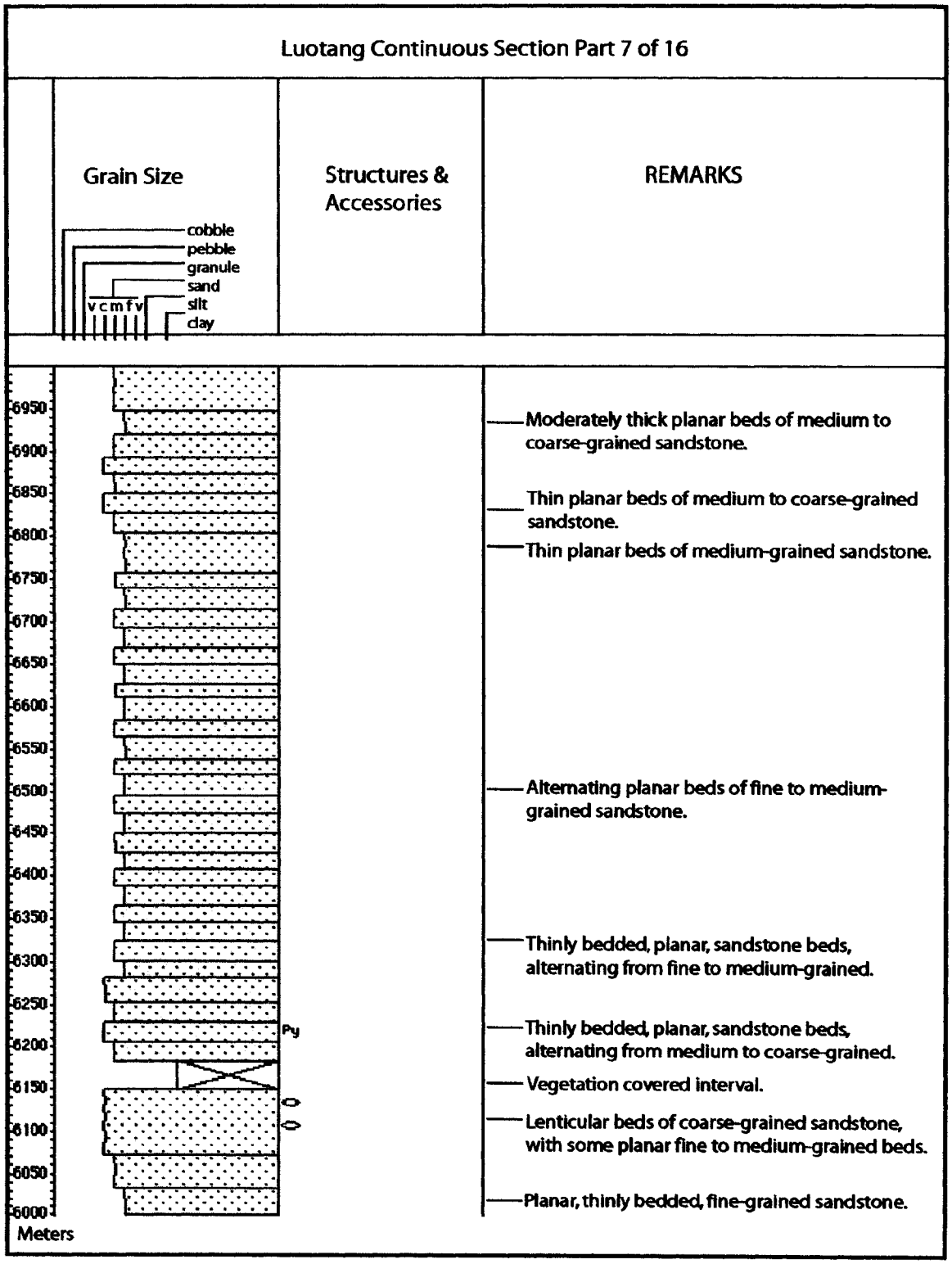

Appendix I

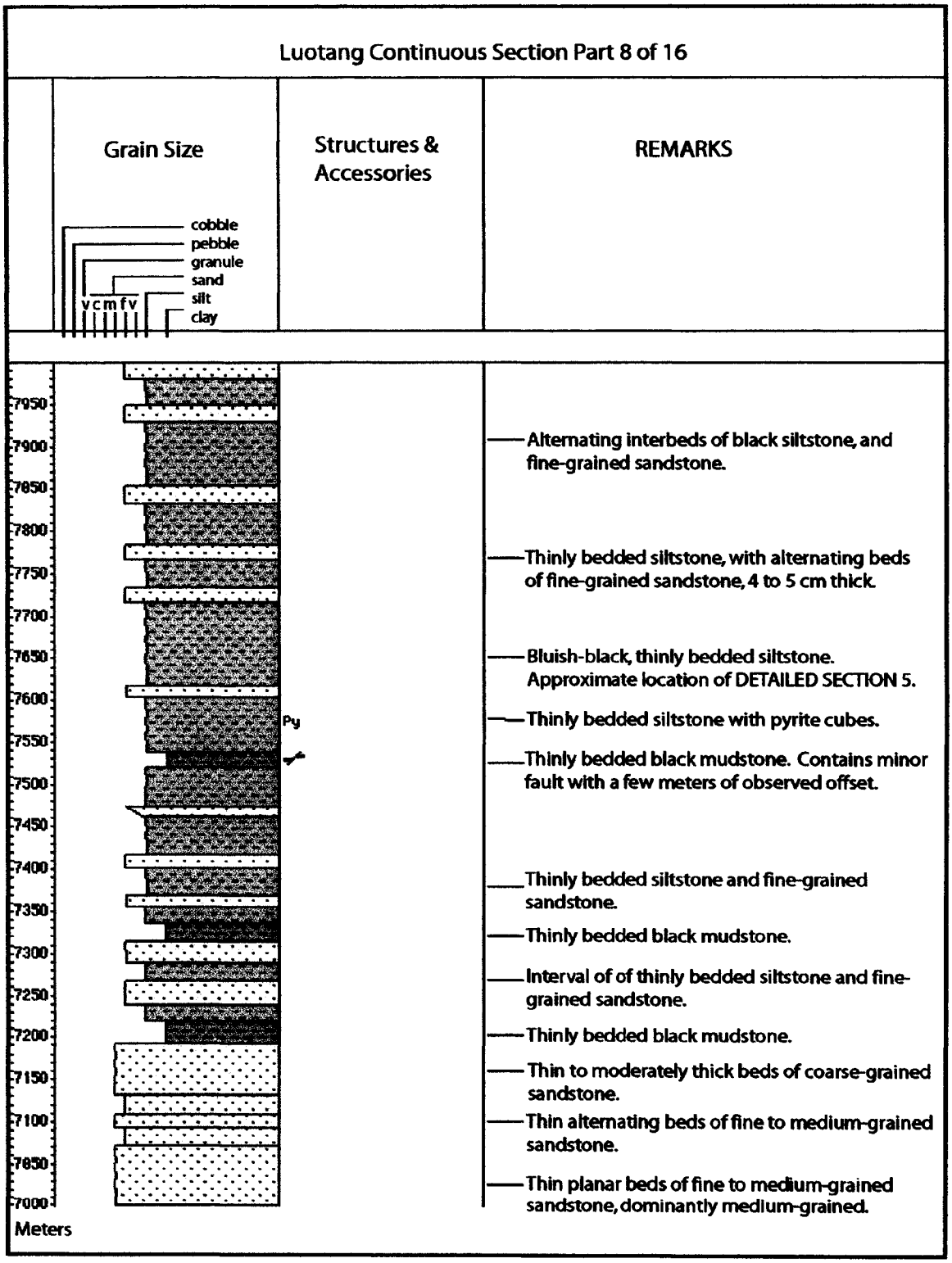

Appendix I

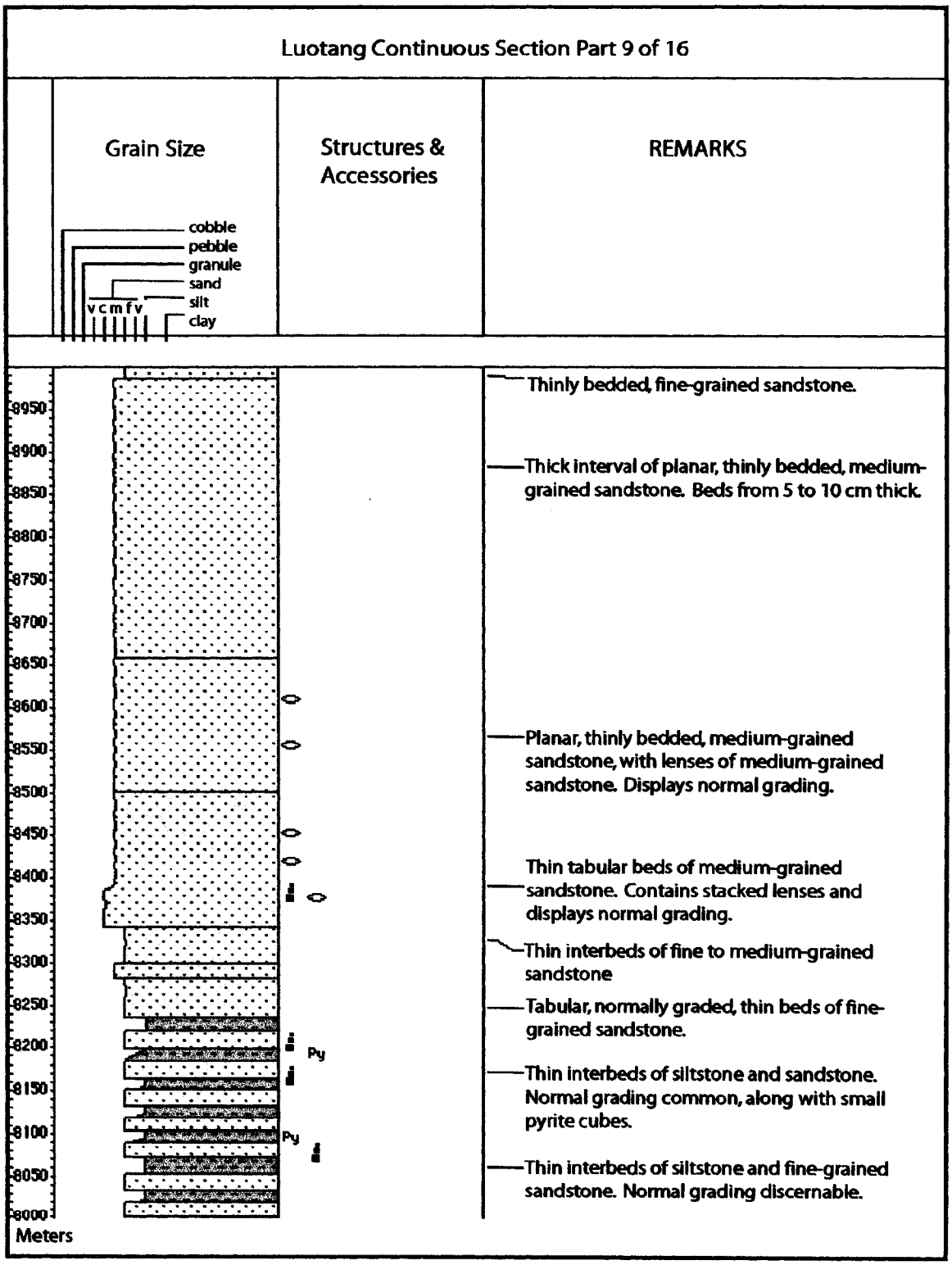

Appendix I

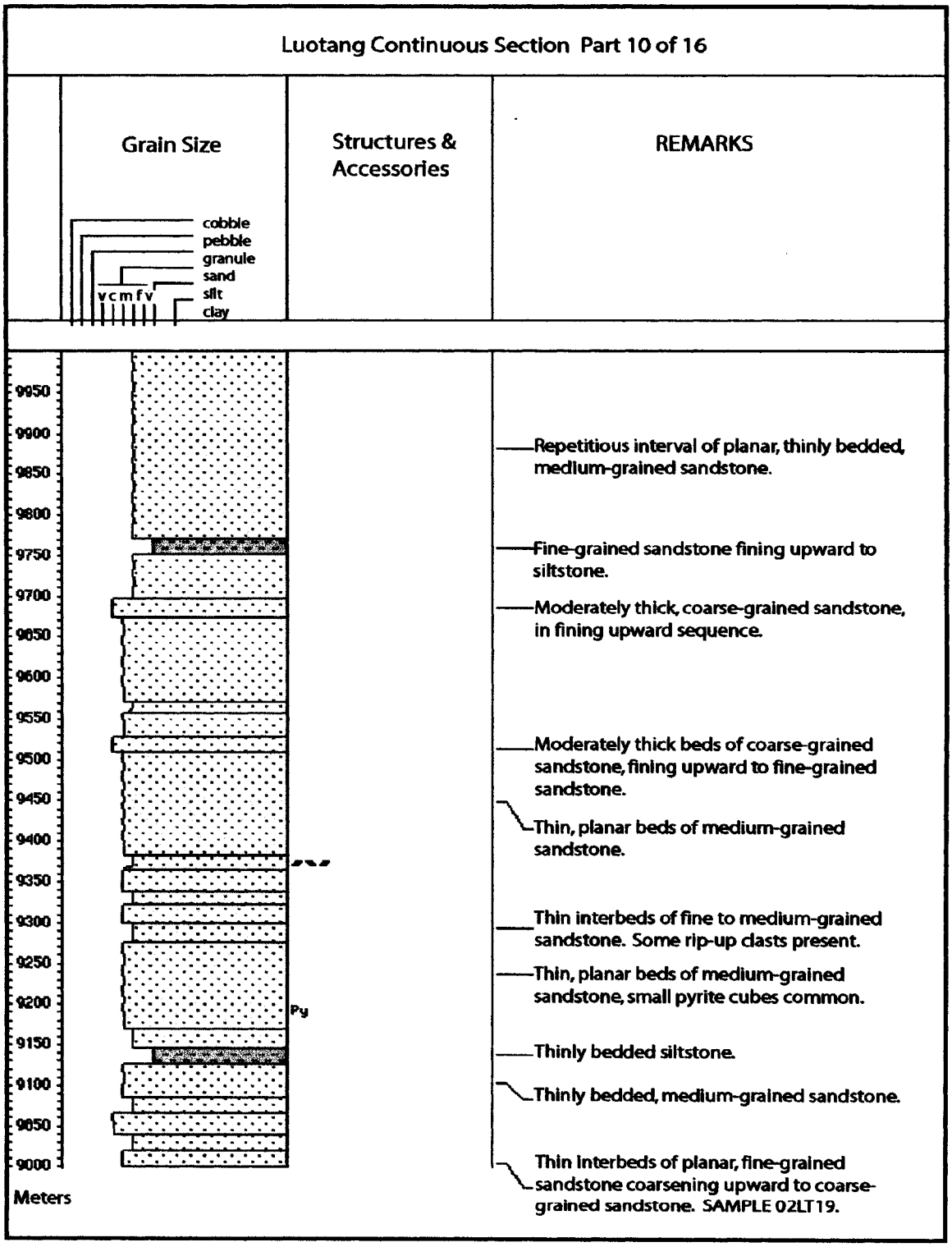

Appendix I

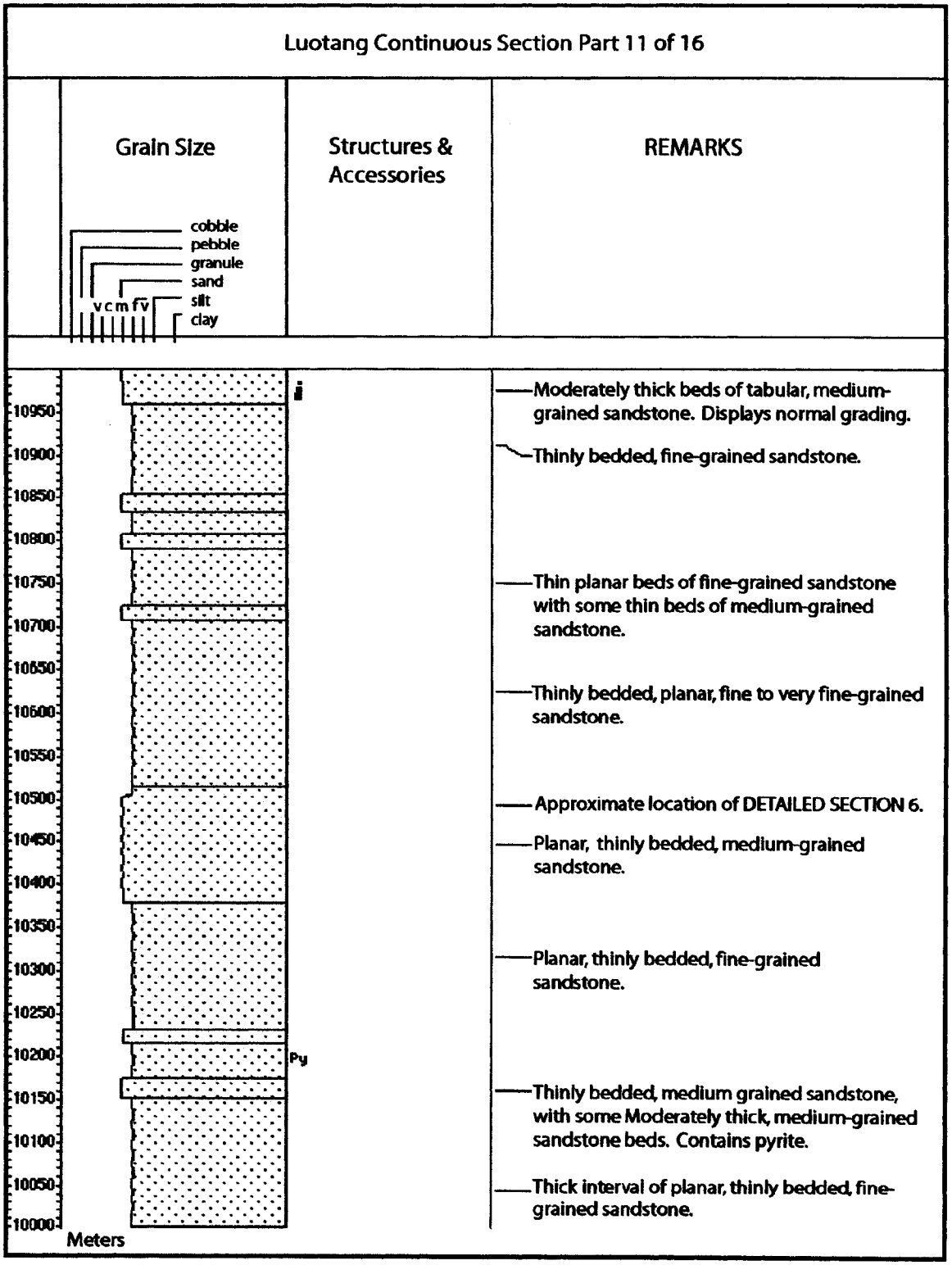

Appendix I

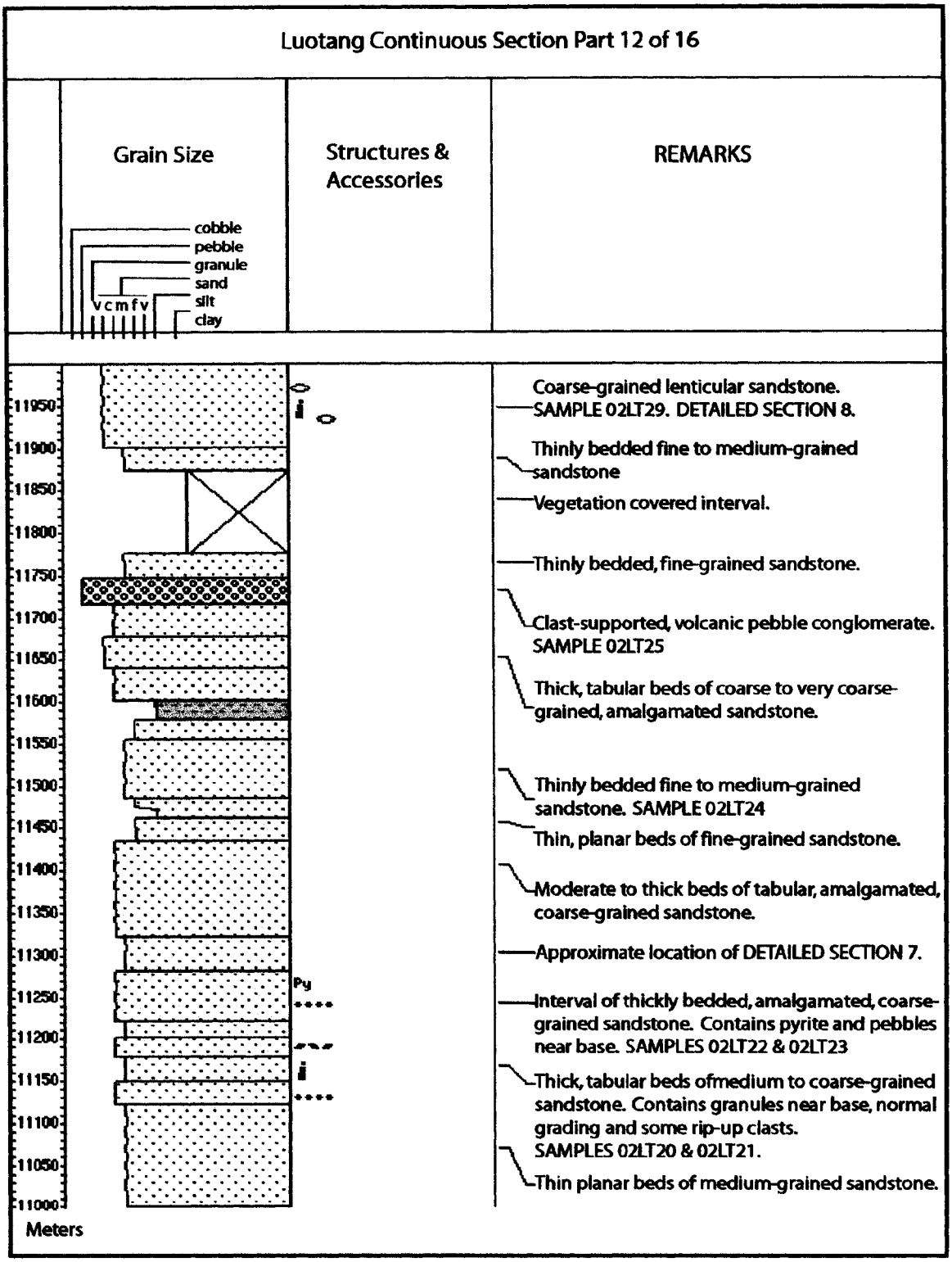

Appendix I

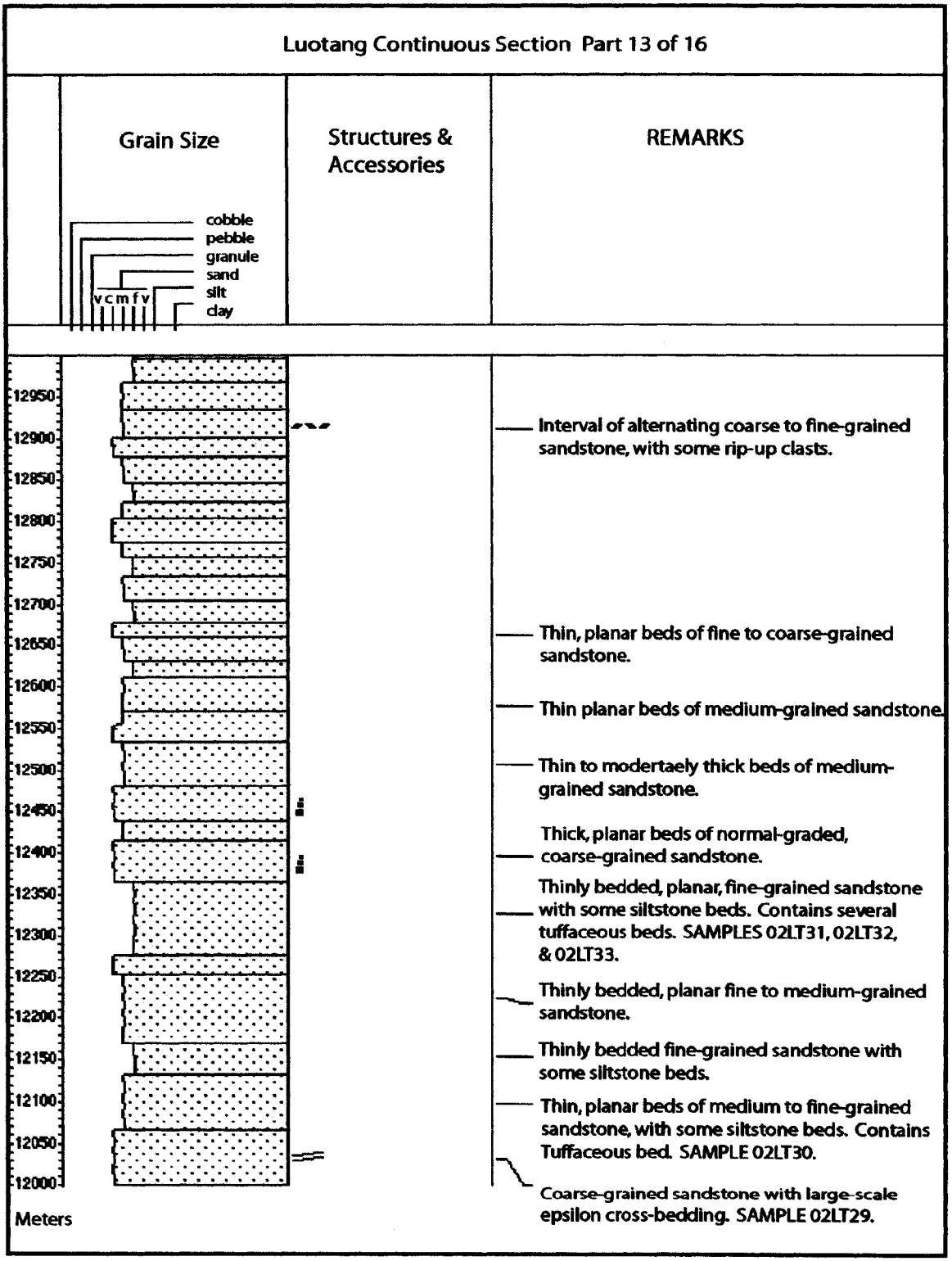

Appendix I

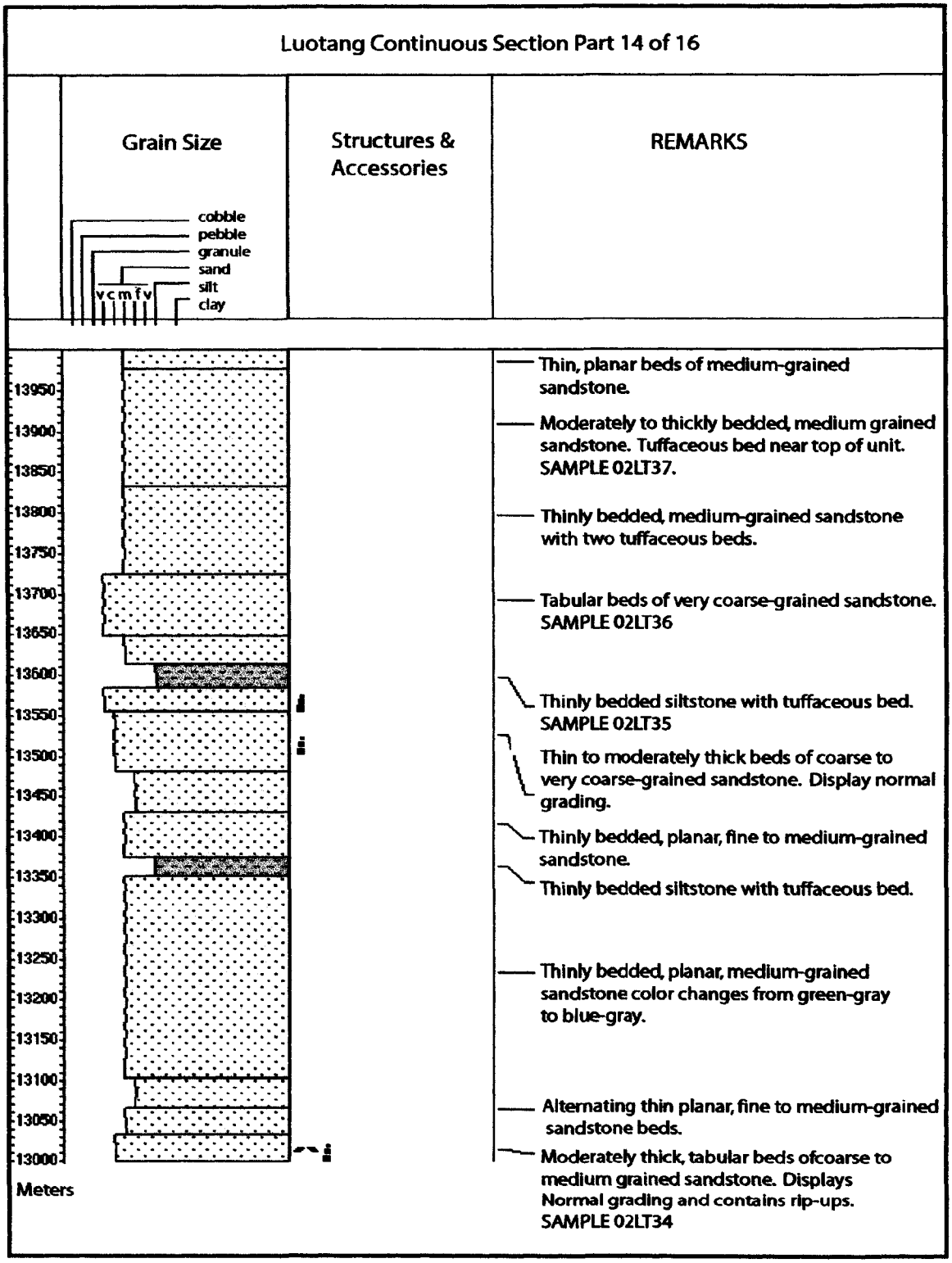

Appendix I

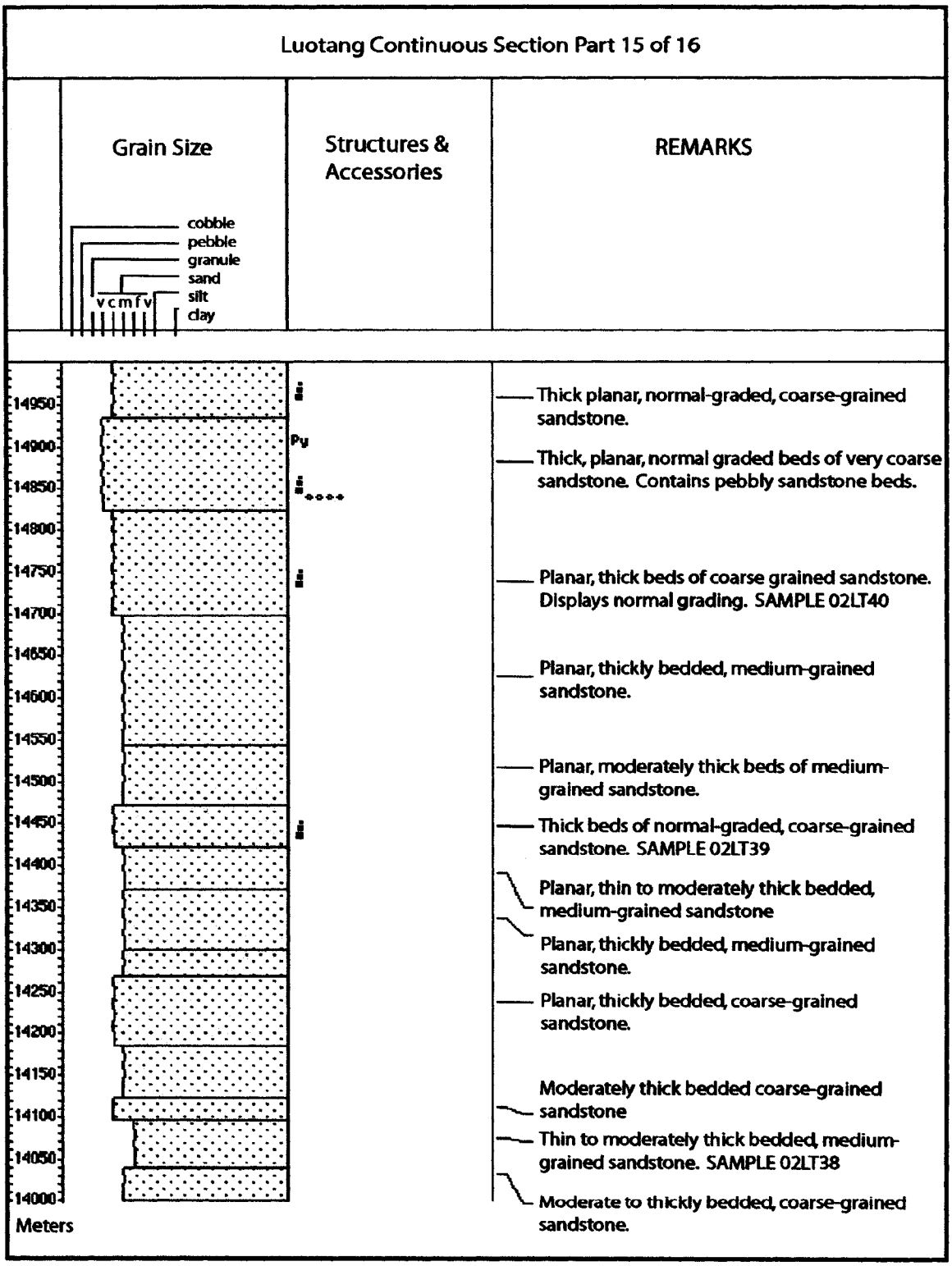

Appendix I

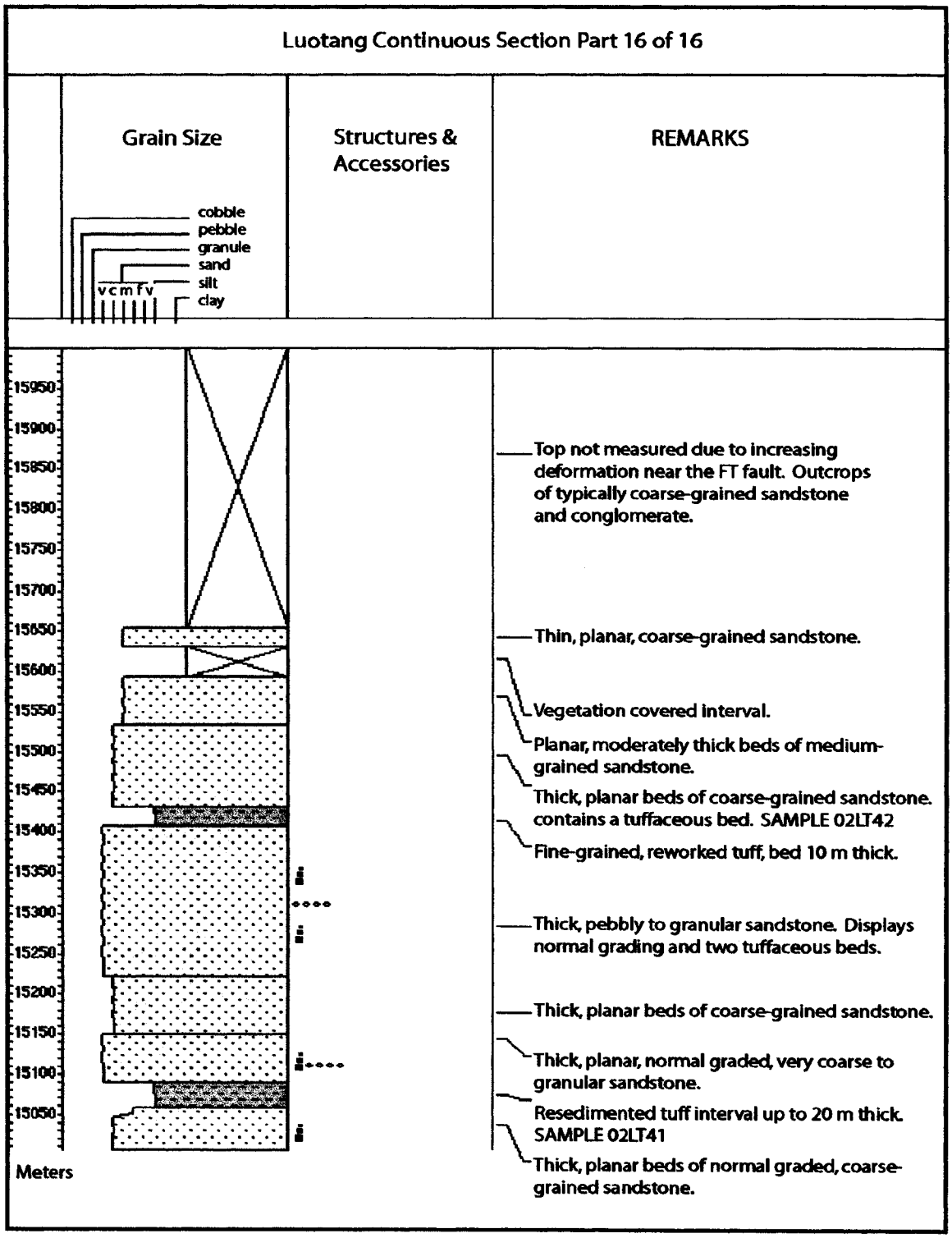

Appendix I

APPENDIX II

WENXIE CONTINUOUS SECTION PART 1-4

Appendix II contains the complete 3.2 km thick Wenxie continuous section. The purpose of the continuous sections is to depict variation in gross grain size of siliciclastic sediment within the basin, provide thickness estimates for the basin, show stratigraphic trends, and to show the locations of key sedimentologic or tectonic structures and samples. Symbols, patterns, and colors used to depict lithology are keyed to the legend provided in Appendix I.

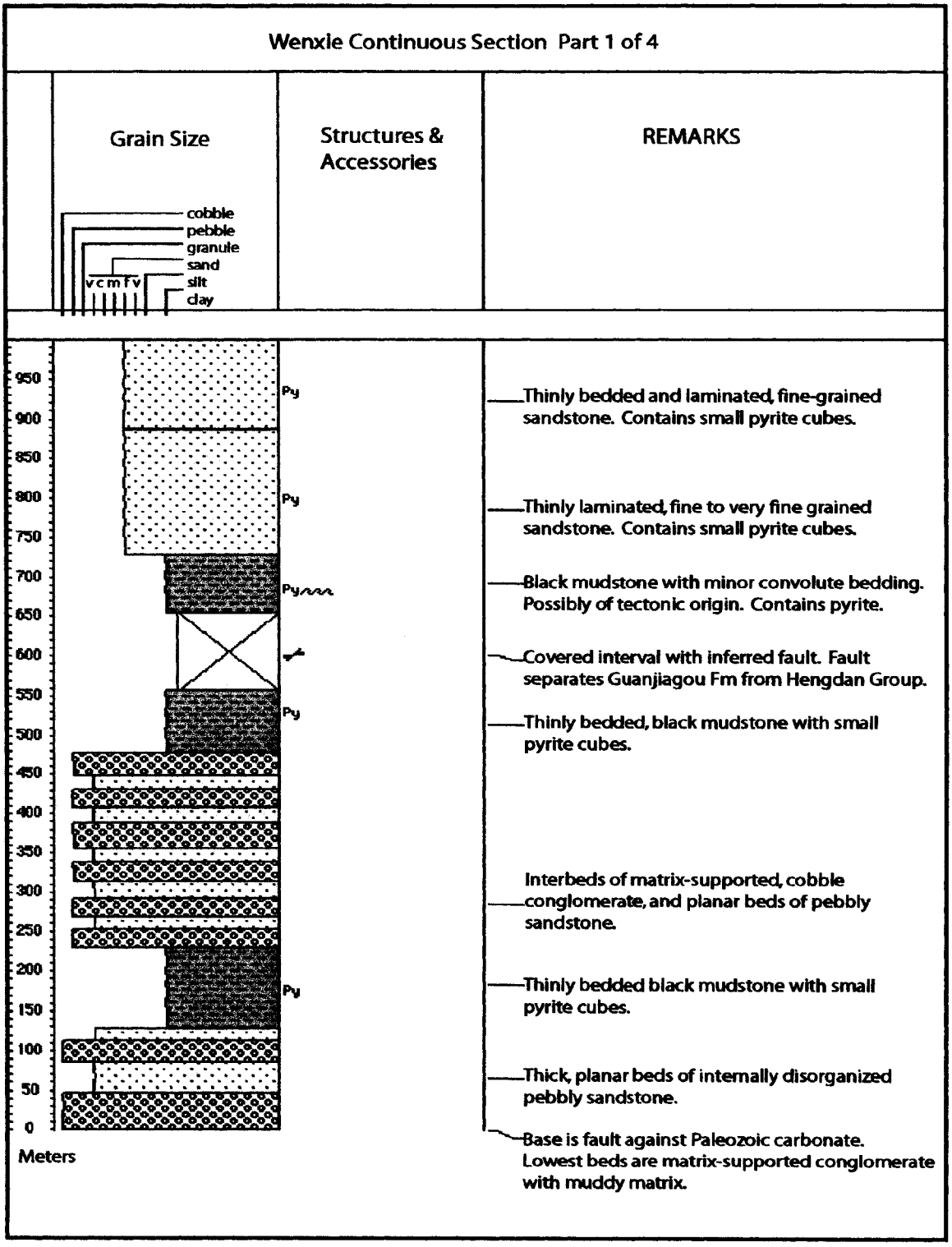

Appendix II

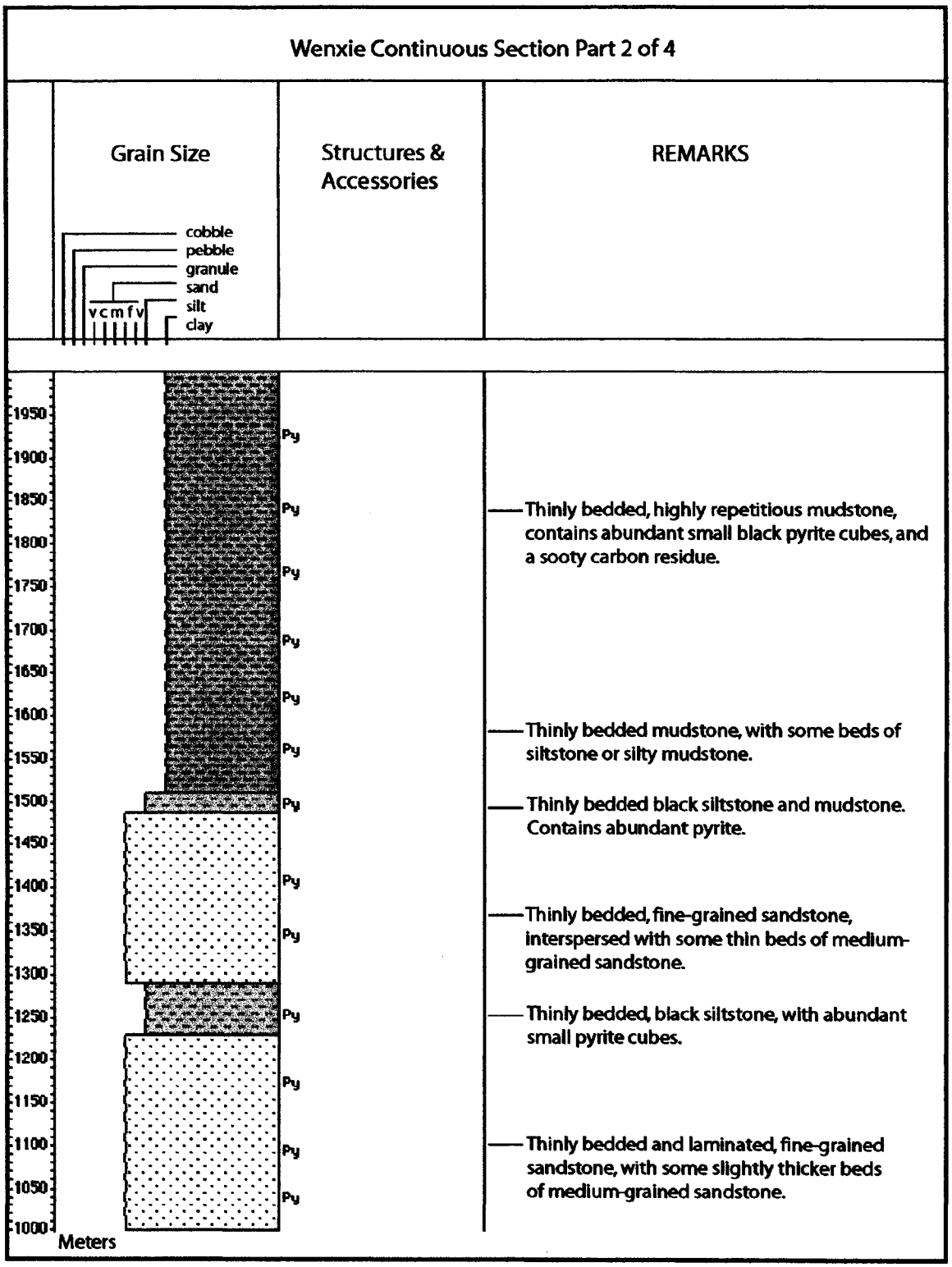

Appendix II

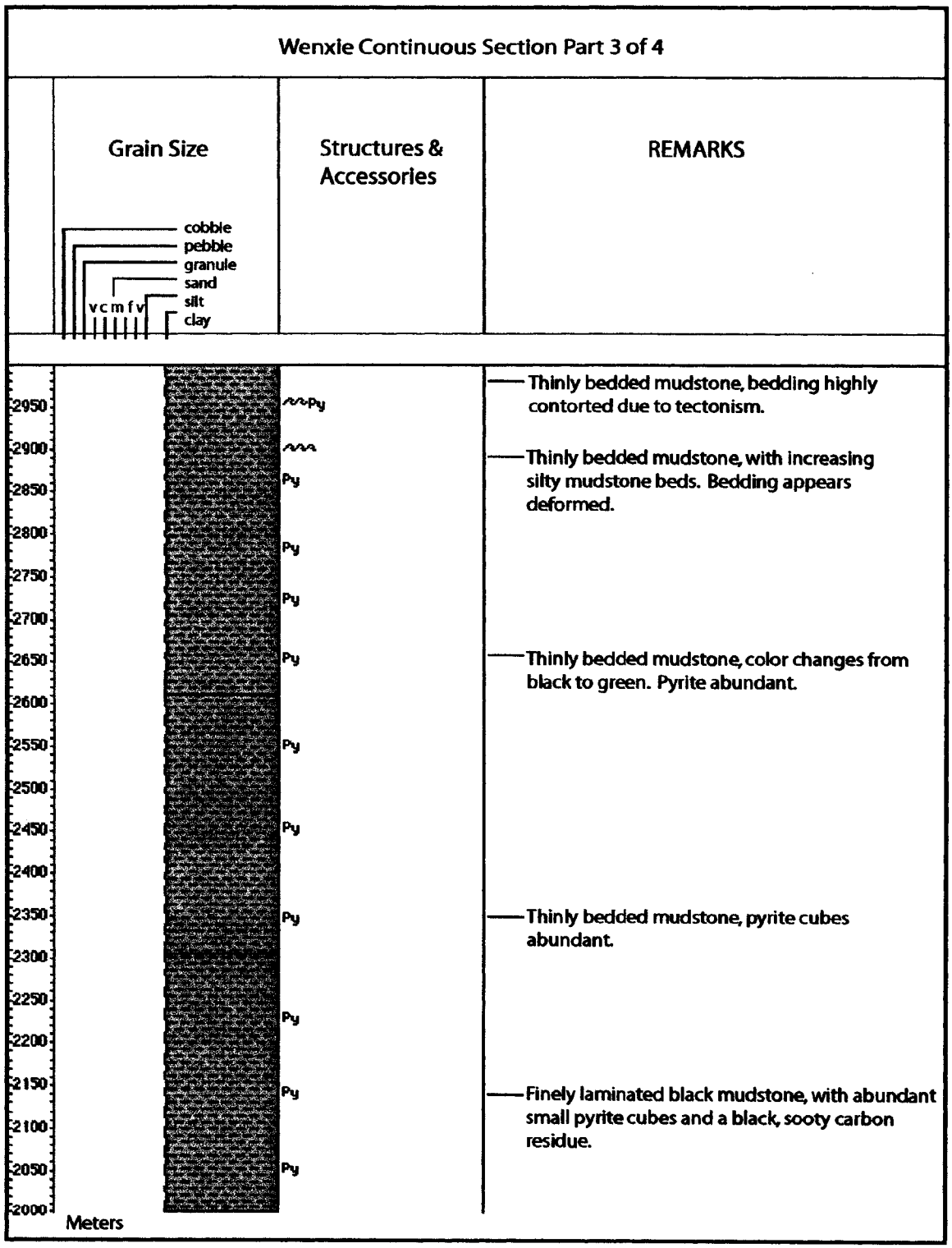

Appendix II

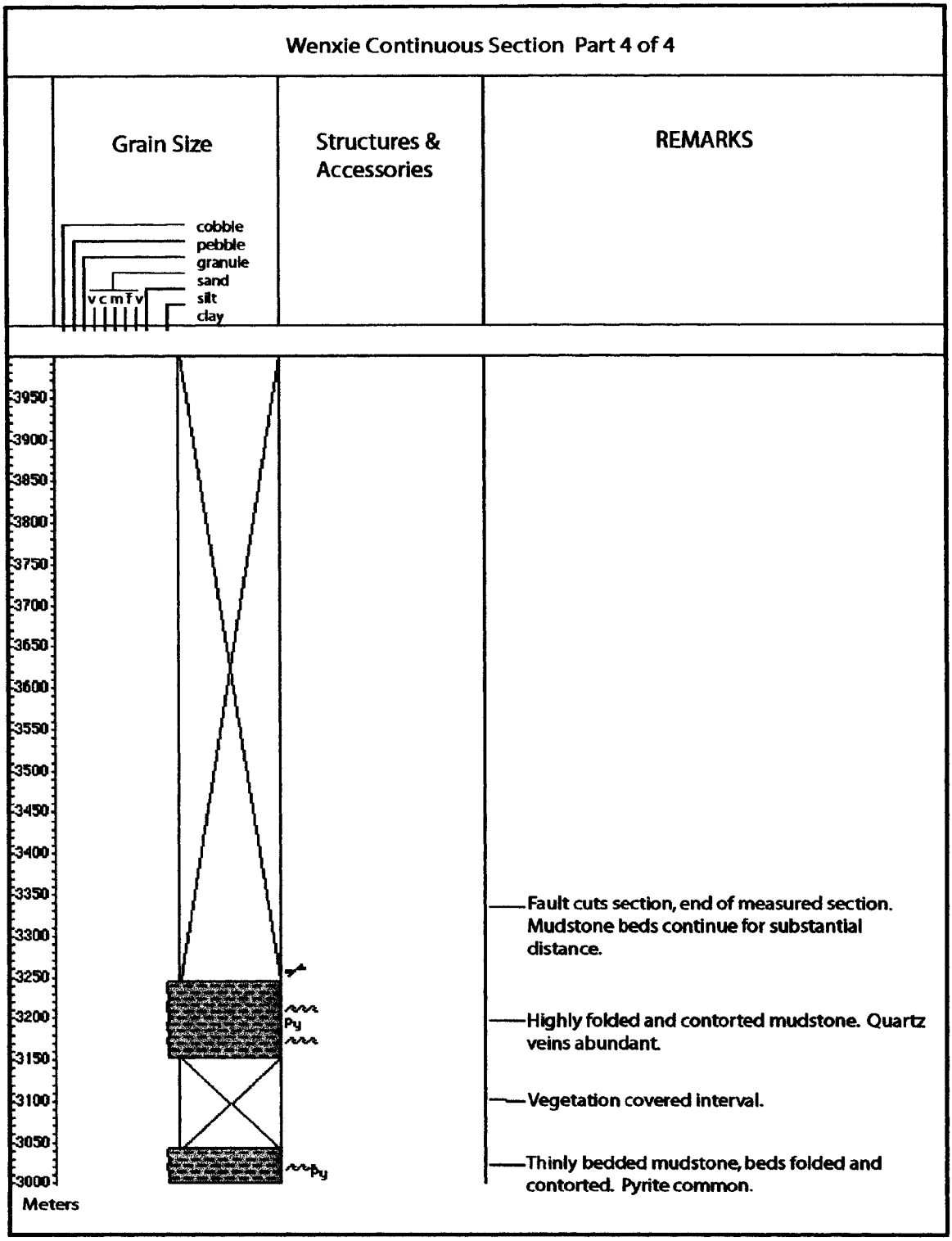

Appendix II

APPENDIX III

GEOCHRONOLOGIC DATA

Appendix III contains additional data used to calculate the detrital zircons ages presented in Chapter 4. Ion microprobe data was obtained at the Stanford/USGS SHRIMP-RG laboratory in Stanford, California. All reported ages have been adjusted by a $^{207}Pb/^{206}Pb$ correction factor.

APPENDIX III. U/Pb SHRIMP data

Sample	U (ppm)	Th (ppm)	$^{238}U/^{206}Pb$	error	$^{207}Pb/^{206}Pb$	error	$^{207}Pb/^{235}U$	error	$^{206}Pb/^{238}U$ Age	1σ error
02LT41-1	234.20	152.58	7.1389	0.0397	0.0664	0.0009	1.2837	0.0195	845.2	4.4
02LT41-2	84.75	154.76	7.6338	0.0696	0.0661	0.0015	1.2041	0.0304	794.0	6.8
02LT41-3	70.35	39.63	7.1586	0.0747	0.0672	0.0018	1.3381	0.0380	845.0	8.3
02LT41-4	79.99	97.80	7.3311	0.0816	0.0670	0.0016	1.2007	0.0400	821.5	8.7
02LT41-5	271.12	180.21	8.2470	0.0629	0.0658	0.0010	1.0974	0.0191	737.7	5.3
02LT41-6	44.48	23.56	7.4358	0.0994	0.0711	0.0024	1.2781	0.0524	811.5	10.3
02LT41-7	101.12	88.58	7.6226	0.1010	0.0648	0.0014	1.2420	0.0602	798.0	10.3
02LT41-8	154.15	141.16	8.3869	0.1039	0.0638	0.0012	1.0793	0.0341	727.6	8.6
02LT41-9	201.41	363.57	8.2519	0.0983	0.0648	0.0011	1.0631	0.0225	736.5	8.3
02LT41-10	68.23	67.55	8.1262	0.1186	0.0650	0.0018	1.1426	0.0350	750.0	10.3
02LT41-11	92.26	89.76	7.4742	0.1009	0.0673	0.0015	1.1792	0.0341	806.5	10.2
02LT41-12	253.72	289.58	8.1854	0.0944	0.0664	0.0009	1.1293	0.0206	743.6	8.1
02LT41-13	125.54	125.14	7.7182	0.0989	0.0645	0.0017	1.1451	0.0336	785.0	9.5
02LT41-14	64.04	72.48	7.3014	0.1077	0.0675	0.0022	1.2547	0.0465	826.5	11.4
02LT41-15	58.77	94.21	7.8742	0.1189	0.0708	0.0020	0.9813	0.0913	758.3	11.5
02LT41-16	81.66	124.14	7.9104	0.1105	0.0651	0.0016	1.0688	0.0370	764.2	10.1
02LT41-17	120.29	164.36	7.7246	0.1056	0.0661	0.0014	1.1626	0.0303	783.9	10.1
02LT41-18	97.86	84.37	6.8425	0.0907	0.0678	0.0014	1.3625	0.0343	879.2	10.9
02LT41-19	50.74	59.18	7.7995	0.1230	0.0674	0.0022	1.2138	0.0455	778.7	11.6
02LT41-20	74.07	70.36	7.9310	0.1131	0.0662	0.0017	1.1887	0.0348	767.3	10.3
02LT41-21	68.88	74.87	7.6787	0.1117	0.0643	0.0017	1.1609	0.0357	789.5	10.8
02LT41-22	110.47	85.16	7.6708	0.1000	0.0651	0.0014	1.1645	0.0292	789.7	9.7
02LT41-23	181.77	112.06	7.8542	0.0943	0.0666	0.0011	1.1482	0.0247	771.5	8.7
02LT41-24	101.80	74.63	8.2778	0.1187	0.0669	0.0015	1.1948	0.0540	739.1	10.3
02LT41-25	55.60	92.01	7.4020	0.1149	0.0668	0.0020	1.1766	0.0509	813.7	11.9

Sample	U (ppm)	Th (ppm)	$^{238}U/^{206}Pb$	error	$^{207}Pb/^{206}Pb$	error	$^{207}Pb/^{235}U$	error	$^{206}Pb/^{238}U$ Age	1σ error
02LT41-26	292.49	202.57	7.8063	0.1021	0.0668	0.0009	1.1788	0.0218	777.0	9.6
02LT41-27	80.47	36.45	7.7850	0.1085	0.0658	0.0016	1.2702	0.0594	784.1	10.6
02LT41-28	90.29	126.42	7.8839	0.1085	0.0648	0.0016	1.1164	0.0337	769.0	10.0
02LT41-29	57.29	45.29	7.6652	0.1243	0.0776	0.0023	0.9197	0.1450	767.7	13.4
02LT41-30	73.61	128.86	8.0800	0.1146	0.0617	0.0016	1.0140	0.0348	750.3	10.1
02LT41-31	137.78	78.29	7.6189	0.0941	0.0688	0.0012	1.1862	0.0335	792.2	9.3
02LT41-32	28.76	27.43	7.7417	0.1437	0.0728	0.0028	1.0362	0.1074	770.6	14.2

Sample	U (ppm)	Th (ppm)	$^{238}U/^{206}Pb$	error	$^{207}Pb/^{206}Pb$	error	$^{207}Pb/^{235}U$	error	$^{206}Pb/^{238}U$ Age	1σ error
02LT37-1	173.24	114.51	7.6881	0.0928	0.0654	0.0011	1.1234	0.0267	785.9338	8.9463
02LT37-2	206.12	267.10	8.3807	0.1000	0.0739	0.0012	1.0487	0.0474	718.5850	8.3316
02LT37-3	111.38	132.84	8.2845	0.1091	0.0653	0.0014	1.0599	0.0298	733.3409	9.1473
02LT37-4	58.31	59.47	7.6092	0.1170	0.0649	0.0020	1.1014	0.0435	792.4136	11.4908
02LT37-5	206.10	193.23	7.7969	0.0920	0.0668	0.0010	1.1764	0.0229	777.6355	8.6413
02LT37-6	148.44	124.98	7.8098	0.0975	0.0660	0.0013	1.1586	0.0268	776.3541	9.1300
02LT37-7	96.75	91.69	7.5613	0.1001	0.0652	0.0014	1.1535	0.0353	798.9715	9.9910
02LT37-8	153.80	122.18	8.5273	0.1053	0.0656	0.0012	1.0674	0.0241	715.1496	8.3612
02LT37-9	287.60	302.41	8.6524	0.1023	0.0654	0.0009	1.0289	0.0202	704.3717	7.8993
02LT37-10	127.92	138.84	7.9420	0.1004	0.0689	0.0013	1.2167	0.0278	765.5015	9.1272
02LT37-11	111.08	92.21	8.2133	0.1057	0.0646	0.0013	1.0890	0.0265	740.8268	9.0060
02LT37-12	54.64	47.60	7.9877	0.1219	0.0665	0.0020	1.1951	0.0390	762.6715	10.9779
02LT37-13	60.05	57.31	8.3761	0.1260	0.0649	0.0019	1.0232	0.0461	724.8150	10.4272
02LT37-14	152.55	136.98	8.1380	0.1002	0.0670	0.0015	1.1360	0.0285	747.1436	8.6904
02LT37-15	64.21	60.24	8.6229	0.1281	0.0661	0.0019	1.0492	0.0340	706.9348	9.9489
02LT37-16	56.77	67.87	8.4961	0.1297	0.0671	0.0020	1.0798	0.0359	716.8369	10.3603
02LT37-17	67.88	99.40	8.3053	0.1220	0.0660	0.0018	1.1112	0.0358	733.6630	10.1980

Appendix III

Sample	U (ppm)	Th (ppm)	$^{238}U/^{206}Pb$	error	$^{207}Pb/^{206}Pb$	error	$^{207}Pb/^{235}U$	error	$^{206}Pb/^{238}U$ Age	1σ error
02LT37-18	332.85	163.07	7.5815	0.0879	0.0681	0.0008	1.2403	0.0209	798.7605	8.7074
02LT37-19	107.87	84.24	7.5943	0.0983	0.0661	0.0014	1.1363	0.0347	794.3646	9.7203
02LT37-20	100.34	113.42	8.0808	0.1065	0.0651	0.0021	1.0394	0.0473	748.7052	9.4202
02LT37-21	349.24	253.39	34.4460	2.0751	0.9704	0.0631	4.0169	0.3583	191.4432	11.8957
02LT37-22	788.90	1364.25	8.8461	0.0951	0.0667	0.0005	0.9815	0.0181	687.5869	7.0295
02LT37-23	205.71	146.61	7.9624	0.0943	0.0663	0.0011	1.0962	0.0301	760.1856	8.5471
02LT37-24	207.77	260.53	8.1029	0.0957	0.0643	0.0010	1.0761	0.0220	749.2704	8.3591
02LT37-25	78.69	60.30	7.7957	0.1172	0.0686	0.0017	1.2072	0.0346	777.7199	11.0181
02LT37-26	89.83	98.36	7.9836	0.1170	0.0686	0.0017	1.1325	0.0363	758.2739	10.5063
02LT37-27	236.83	185.83	8.2653	0.1006	0.0676	0.0010	1.0169	0.0347	730.9283	8.5102
02LT37-28	90.51	92.44	7.8067	0.1050	0.0669	0.0015	1.1055	0.0383	773.3384	9.8652
02LT37-29	579.38	167.57	7.7869	0.0871	0.0734	0.0007	1.1067	0.0398	769.6168	8.2423
02LT37-30	98.68	77.01	7.9787	0.1076	0.0672	0.0015	1.0976	0.0337	758.1673	9.6645

Appendix III

VITA

Graduate College
University of Nevada, Las Vegas

Peter Alexander Druschke

Home Address:
1701 East Katie Avenue #40
Las Vegas, Nevada 89119

Degrees:
Bachelor of Science, Geology, 1999
California State University Sonoma, Rohnert Park

Publications:

Druschke, P., Hanson, A. D., Yan, Q., and Wang, Z., 2002, Recognition of a Late Paleozoic arc/forearc developed on the north margin of the South China Plate, Southwestern Qinling Mountains, China: Geological Society of America Abstracts with Programs, v. 34, p. 376-377.

Druschke, P., Hanson, A. D., Yan, Q., and Wang, Z., 2003, Is the Bikou terrane of the Southwest Qinling Mountains, Central China, the result of Late Proterozoic subduction along the north margin of the Yangtze Plate?: Geological Society of America Abstracts with Programs, v. 35, p. 343.

Hanson, A. D., Yan, Q., Druschke, P., and Wang, Z., 2002, The southwestern Qinling Shan of Central China: a Late Paleozoic subduction/accretionary system and a continental arc/forearc constructed upon the north-facing Devonian passive margin of the South China Block: Geological Society of America Abstracts with Programs, v. 34, p. 509.

Yan Q., Wang, Z., Hanson, A. D., Druschke, P., and Wang, T., 2002, Hengdan turbidite terrane: Filling in a Late Paleozoic forearc basin developed on the passive margin on the Yangtze Plate: Geological Bulletin of China (in Chinese with English abstract), v. 21, p. 495-500.

Yan, Q., Wang, Z., Hanson, A. D., Druschke, P., and Wang, T., 2004, The Guanjiagou Section of the South Qinling and its tectonic implications: Science in China (in press).

Thesis Title: The Age, Stratigraphy, and Tectonic Provenance of Clastic Deposits in the Western Bikou Terrane, Southwestern Qinling Mountains, China

Thesis Examination Committee:

Chairperson, Dr. Andrew Hanson, Ph.D.
Committee Member, Dr. Terry Spell, Ph.D.
Committee Member, Dr. Wanda Taylor, Ph.D.
Graduate Faculty Representative, Dr. Helen Neill, Ph.D.